RESPONSE OF A NONLINEAR AIRCRAFT TO RUNWAY INDUCED EXCITATIONS DURING VARIABLE VELOCITY RUNS

by

KAPADIA KAIKOBAD E.

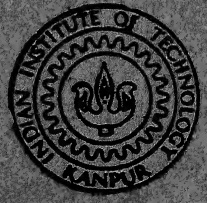

DEPARTMENT OF AEROSPACE ENGINEERING

INDIAN INSTITUTE OF TECHNOLOGY, KANPUR

MAY, 1989

RESPONSE OF A NONLINEAR AIRCRAFT TO RUNWAY INDUCED EXCITATIONS DURING VARIABLE VELOCITY RUNS

A Thesis Submitted
In Partial Fulfilment of the Requirements
for the Degree of
MASTER OF TECHNOLOGY

by
KAPADIA KAIKOBAD E.

to the
DEPARTMENT OF AEROSPACE ENGINEERING
INDIAN INSTITUTE OF TECHNOLOGY, KANPUR
MAY, 1989

CERTIFICATE

This is to certify that the work 'Response of a Nonlinear Aircraft To Runway Induced Excitations During Variable Velocity Runs' has been carried out under my supervision and has not been submitted elsewhere for a degree.

Dayanand yadav 5/5/89

(DR. DAYANAND YADAV)
Assistant Professor
Department of Aerospace Engineering
Indian Institute of Technology, Kanpur.

ACKNOWLEDGEMENT

I wish to express my deep sense of gratitude and thankfulness to Dr. Dayanand Yadav for his sustained efforts in the completion of this work in the present form. During the entire tenure of this work he has been a constant source of inspiration, guidance and encouragement to me.

I am grateful to my hall residents who made my stay at I.I.T.Kanpur a very memorable and pleasant one and above all to my friends Ramamoorthy, Gautam, Sanjay and Bohra in particular, who have helped me at various stages of my work.

I am thankful to Mr. A.K.Ganguly for his painstaking efforts in preparing the drawings and to Mr. G.R.Hoshing for his excellent typing of the manuscript.

Thanks are due to everybody in my department who provided a very warm and friendly enviornment to carry out this work.

(KAPADIA KAIKOBAD E.)

ABSTRACT

Response of an aircraft in variable velocity runs during landing, take-off and taxiing on runways, with non-zero mean and random unevenness, is studied. The aircraft is modelled as a rigid body and the runway is considered as a rigid pavement.The study incorporates the mathematical modelling of the aircraft including the landing gear and the runway.

The modelling of the landing gear includes non-linearity in the spring and the damper. It incorporates the polytropic compression of the air, compressibility of the hydraulic fluid and the internal frictional forces in the shock struts. The nonlinear tyre spring and the aerodynamic lift are also accounted for.The effect of inclination of the shock struts and the linkage dynamics is included in the analysis. For the present study, the model is limited to a rigid heave model with single point input from the track.

The track unevenness is prescribed as a random process in spatial coordinates over a mean level. The random unevenness is described by its power spectral density (p.s.d.). The mean level may include slopes, bumps, dips,ramps, bomb crater repair patches, step differences, etc., singly or in combination to simulate different possible faults in the runway.

Monte-Carlo simulation approach is used for the solution of the problem. The system dynamic equations have the initial conditions prescribed by the physical parameters.The track input

forms the forcing function. The input consists of random unevenness superimposed over deterministic mean.

The equations of motion along with the forcing function are integrated numerically to find the response of the system.

Response ensemble is generated by repeated solutions with different track input samples. The second order statistics of response is obtained by averaging across the sample sets in the ensemble.

Numerical data is presented for landing and take-off runs with parametric variation. The parameters studied are the roughness level of the track for landing and take-off and the sink velocity in landing.

CONTENTS

NOMENCLATURE

A_1	length of the drag linkage AE.
A_2	length of the part of the main linkage carrying the main shock strut.
A_3	length of the entire main linkage.
A_7	distance between the two points of the linkage hinged to the aircraft frame.
A_{10}	perpendicular projection of the main linkage.
A_a	pneumatic area.
A_h	hydraulic area.
A_n	orifice area.
C	roughness constant.
C_d	coefficient of discharge.
F_a	pneumatic force.
F_{f_j}	journal friction force.
F_{f_s}	seal friction force.
F_h	hydraulic force.
F_{h_a}	horizontal force on the wheel axle.
F_{h_g}	horizontal ground reaction.
F_{s_1}	axial force in the drag shock strut.
F_{s_2}	axial force in the main shock strut.

$F_{s_{1o}}$ preloading of the drag strut.

$F_{s_{2o}}$ preloading of the main strut.

F_{v_a} vertical force on the wheel axle.

F_{v_g} vertical ground reaction.

L lift force acting on the sprung mass.

ℓ_1 axial distance between the shock strut lower bearing and the lower end pin joint of the piston tube.

ℓ_2 axial distance between the upper and lower bearings on the extended shock strut.

n polytropic exponent for the air compression process.

p_{a_o} initial air pressure

S_1 stroke of the drag strut.

S_2 stroke of the main strut.

V_{a_o} initial air volume.

V_{o_o} initial oil volume.

W_1 weight of the sprung mass.

W_2 weight of the unsprung mass.

x_d horizontal relative displacement of the sprung and unsprung mass.

$Z(t)$ Gaussian Random state vector.

Z_1 vertical displacement of the sprung mass.

Z_2 vertical displacement of the unsprung mass.

Z_d relative vertical displacement of the sprung and unsprung mass.

β oil bulk modules.

θ angular position of the main linkage at any instance of time.

θ_o initial angular position of the main linkage.

μ coefficient of friction of the track.

μ_{j_1} coefficient of friction of upper bearing.

μ_{j_2} coefficient of friction of lower bearing.

μ_s coefficient of seal friction.

μ_x mean of a random process x.

ν correlation constant.

ρ mass density of the hydraulic fluid.

σ_x standard deviation of a random process x.

Φ power spectral density.

ϕ angular position of drag linkage at any instance of time.

ϕ_o initial angular position of the drag linkage.

Ω spatial frequency.

$\omega_1, \omega_2, \ldots$ Gaussian sequence.

$(\dot{})$ differentiation with respect to time.

List of Figures

List of Tables

CHAPTER I

Introduction

1.1 *Problem*

All conventional aircrafts spend a significantly large part of their useful life during taxiing, take-off and landing on runways. During these traversals on runways, the aircraft follows the ground profile. The ground unevenness, therefore acts as a base excitation to the aircraft during these motions. Besides the nature of the ground unevenness, the induced excitation also depends on the type of contact and the traversal velocity of the aircraft.

The vibration of the aircraft during its operation on the runway induces dynamic loads on the structure. This has become more and more important due to the increased need of reducing the time spent by an aircraft during landing, take-off and taxiing. As a consequence of this the aircraft traversal velocities have increased. These vibrational loads cannot be ignored, since their cumulative effects represent a considerable proportion of the total fatigue damage. The fatigue life of an undercarriage at its points of attachment with the airframe, and the associated structural components make up for an important design case.

Apart from the metal fatigue there are the equally important dynamic peak stresses that arise in a fully laden aircraft during its manoeuvres on rough runways. Thus it is important for designers to be aware of the vibrations induced due to runway

unevenness, so that an attempt can be made to reduce them.

The effects of these vibrations on passengers and the crew is very important. It is known [1] that cockpit vibration levels are roughly twice than those experienced at the aircraft mass centre, and thus pilots are more influenced than the passengers. In some cases high cockpit vibration levels in the vertical plane, can degrade the pilot's ability to read instrument panels accurately, and apply the correct amount of control required. It is also very important from the point of view of passenger comfort.

The dynamic displacements react through the oleo-pneumatic units and tyres with the runways which induce vibrations, thereby creating additional dynamic loading of runway surfaces. This results in their general deterioration, which would in turn again lead to an increased level of vibration causing a viscious derogatory cycle.

The rough ground can be treated either as a homogeneous (spatially stationary) or as a non-homogeneous random process depending on its statistical description. For the runway unevenness described by a stationary random process, the response of the aircraft can be predicted by classical stationary random vibration analysis, if the aircraft is moving at a constant velocity, as is the case commonly during taxiing. Contrary to this, during landing and take-off, when the aircraft accelerates or decelerates, the excitation becomes non-stationary even though the runway unevenness is stationary. Non-stationary excitation may also result with non-stationary ground profile.

For an accurate modelling the problem should take into account the following features :-

(a) nonhomogenity of the ground profile.

(b) nonlinearity of the aircraft dynamic characteristics.

(c) the aircraft traversal at both constant and variable velocities.

1.2 *Review of the Past Work*

This section briefly outlines work done by other researchers in the mathematical modelling of the landing gear and different approaches used for obtaining the response of the aircraft to runway induced excitations.

1.2.1 Mathematical Modelling

As early as 1948 Stowel, et. al. [2] investigated the effect of flexibility of the wing on the landing impact forces. The aircraft was modelled as a simplified structure consisting of a uniform bar for the wing, a concentrated mass for the fuselage and an undamped linear spring for the landing gear. It was found that for moderately flexible landing gears neglecting structural flexibility led to small conservative errors.

Later Cook and Milwitzky [3] studied the problem by considering several free-free modes of vibration of the aircraft and the non-linear characteristics of the landing gear. They indicated that the errors involved in neglecting the flexibility are not conservative.

Raghavan [4] also concluded that the maximum response after

landing impact is 5 to 29% less for a flexible system.

In view of the above mentioned investigations, it appears that the landing gear performance is relatively unaffected by the elastic deformations of the airplane structure. In addition, the proximity of the landing gear to the nodal points makes the conclusion all the more acceptable.

Milwitzky and Cook [5], probably for the first time, investigated the behaviour of the conventional type of oleo-pneumatic landing gear during landing impact. The basic analysis is presented in a general form and motions of the landing gear prior to and subsequent to the shock strut deflection were taken into account. The first phase of the impact was considered as a single degree of freedom system in order to find the initial conditions of motion at the instant of shock strut deflection, after which the landing gear was considered as a two degree of freedom system. The effects of the non-linearities of the landing gear parameters and that of the drag forces on the wheel were included. It was concluded that the orifice discharge coefficient has a marked effect on the behaviour of the landing gear, whereas the air compression was found to be relatively unimportant. Linear tyre characteristics gave good results during normal impact.

Refinements were added by Wahi [6,7] by including orifice function, hydraulic fluid compressibility and polytropic exponent of air during the compression stroke.

Jayarami Reddy, et. al. [8] carried out analysis on a semi-articulated gear with geometry included as a part of the analysis. They also included oil compressibility effects. To

identify the active parameters, they carried out a parametric study of various parameters like coefficient of friction of main orifice C_d, polytropic exponent of the air compression process n, coefficient of friction at lower and upper bearings μ_{j_1} & μ_{j_2} etc. The ground reaction factor F_L defined as the ratio of the ground reaction force F_{v_g} to the wieght of the aircraft to be supported by the landing gear W was taken as the objective function. The travel of the wheel axle was restricted to a value of 255 mm during landing.

It was shown that there is a value of C_d, for which the gound reaction factor is minimum. The ground reaction factor is not significantly affected by a variation in the polytropic exponent. The internal friction force in the shock strut remains nearly constant with changes in coefficient of friction.

1.2.2 Response Analysis

Traditionally undercarriages have been designed to absorb landing impact forces rather than vibratory forces caused by runway unevenness. For a relatively small aircraft, runway excited vibrations were considered unimportant. Thus despite the growth of the aircraft size little attempt has been made to design undercarriages from the vibration point of view, with the result that vibration levels have increased with aircraft size. Not much analytical work exists in the literature, may be because of the fact that the non-linear random vibration theory had not reached a stage so as to provide a tractable approach to consider inherent non-linearities of the aircraft.

It was only in the early sixties that Silsby [10] studied analytically the effects of aircraft and landing gear parameters on the airplane response to runway roughness. He considered a highly simplified linear model for the landing gear and a rigid airplane structure. The results of the study indicated that, within the limitations of the assumptions made, the parameter variations had little effect on the motion of the centre of gravity of the aircraft, whereas the motion of the pilots' compartment was strongly influenced by the speed.

Tung, et. al. [11] have computed the dynamic response of supersonic transport aircrafts to runway roughness during taxiing and take-off through a deterministic approach, in which the response is computed by numerically integrating the equations of motion of free-free aircraft. Nonlinearity of spring and damping forces have been taken into account. A statistical approach is also highlighted in which the runway unevenness is represented as a stationary random process. The major obstacle to applying a statistical analysis was that of the nonlinearities present in the oleo-pneumatic undercarriage, in the form of air spring stiffness, velocity squared damping and Coloumb friction. It was not possible to directly apply the theory to nonlinear systems and so two important approximate techniques are shown to apply. The methods are :

(a) The Perturbation Technique developed by S.H.Crandall.

(b) The equivalent linearization technique developed by T.K.Caughey.

Both mehtods assume that the input is a stationary random process and the nonlinearities are small. The perturbation theory

can only be applied to nonlinearities which can be represented as polynomials e.g., the air spring. But since the V|V| damping and the Coloumb friction cannot be represented by polynomials, perturbation theory cannot be thus employed. So it is suggested that first apply the linearization technique to obtain the equivalent linear damping coefficient for the nonlinear damping forces for the aircraft, considered as a single degree of freedom system, and then apply the perturbation method to a multi-degree of freedom system with an equivalent viscous damping coefficient, containing a polynomial representation for the nonlinear air spring force. The means for implementing such a scheme, however, was not given. But the paper applies the perturbation method to a two degree freedom rigid heave model. The nonlinear air spring was represented by a polynomial but only viscous damping was assumed. The paper concluded that although the equivalent linearization method was suitable for a single degree of freedom system with nonlinear damping, it appeared unlikely that it could be applied to a multi-degree of freedom system.

Kirk and Perry [12] have carried out the analysis of taxiing induced vibrations of a subsonic aircraft by the power spectral density (p.s.d.) method. They considered one elastic mode coupled with the rigid mode of the aircraft. They converted the nonlinear damping into an equivalent linear damping. In using this approach, one of the basic assumptions which is open to question, concerns the stationarity of runway profiles. Evidence regarding stationarity of runway profiles is given in reference [12], for relatively smooth surfaces (i.e., good quality runways in commercial use) having rms displacements less than about 0.018 m,

in which case the probability density function can be considered as Gaussian. For rougher surfaces, however, Gaussian distribution could not be assured without further investigations.

When the aircraft has a variable velocity, as is the case during landing and take-off runs the input excitation becomes nonstationary. Virchis, et. al. [13] and Sobczyk, et. al. [14] have used the time domain approach to determine the response statistics for a single degree of freedom model in constant velocity and constant acceleration runs.

Yadav and Nigam [15] use frequency domain formulation for response evaluation. The equations of motion are transformed to space coordinates, resulting in the governing equations having space dependent coefficients. The input process is spatially stationary. Due to this the solution admits an evolutionary spectral form of representation and for a particular velocity profile (viz., $S(t) = a_1 + a_2 t^b$), closed form solutions for response statistics are presented after some lengthy integration. Numerical mehtods could again be employed to handle more general situations.

Hammond, et. al. [16] computed the non-stationary response of a vehicle modelled by linear dynamics travelling over a homogeneous gound profile at variable velocities. The method uses linear state space technique and incorporates one important assumption, that the gound surface undulation may be described as the output of a white noise excited shaping filter (in the spatial domain). A set of first order equations are integrated numerically to obtain the zero lag response covariances

(correlations).

Later in another paper Harrison and Hammond [17] obtained the time varying mean and covariance of nonlinear systems excited by non-stationary random process, the non-stationarity arising out of the variable velocity of the vehicle. They used statistical linearization to overcome the nonlinear problem.

1.3 *Present Work*

For the present work, the response of an aircraft in variable velocity runs, as in taxiing, take-off and landing, is studied.

For a simplistic analysis, the weight of the aircraft to be carried by the landing gear is considered as a concentrated mass and the weight of the wheel unit is also assumed to be concentrated at the wheel axle. The input from the track unevenness is considered to be a single point input as only one landing gear is studied. These assumptions limit the aircraft model to a rigid heave model with a single point input from the track.

The landing gear is modelled as a telescopic landing gear with two shock struts, one the main strut and the other the drag strut. To make the model more general both, the main and the drag struts are inclined with the vertical and the geometry of the linkage is also included. The modelling includes nonlinearities in the spring and the damper. It also incorporates the polytropic compression of air, compressibility of hydraulic fluid and the internal friction forces in the wheel struts. Nonlinearity in the tyre spring and the aerodynamic lift is also accounted for.

The runway track is assumed to be a rigid pavement, so that in the absence of any flexibilities it does not interact dynamically with the response analysis.

The ground unevenness is prescribed as a random process in spatial coordinates superimposed over a mean level. The mean level includes slopes, bumps, dips, bomb crater repair patches, ramps etc., representative of the faults in the runway.

The random track profile is numerically simulated to fit the track description in the following steps :-

(a) Initially, an uniformally distributed, non-repeatable sequence of random numbers between zero and one is generated.

(b) A Gaussian white sequence, having zero mean and unit variance is generated by using the above numbers.

(c) This Gaussian sequence is operated upon by two differential operators in sequence to produce the required Gaussian random process.

After the simulation of the Gaussian process from the prescribed power spectral density (p.s.d.), a numerical scheme is used to obtain the p.s.d. of the simulated process to verify its closeness to the target. Monte-Carlo simulation approach is used for the solution of the problem. The system dynamic equations have the initial conditions prescribed by the physical parameters. The track input forms the forcing function. The equations of motion along with the forcing function are integrated numerically to find the response of the system. The response samples are generated to form an ensemble and then analysed to determine its statistical

parameters.

During the course of this work, response samples have been generated for analysis during landing and take-off, from a runway having a constant mean slope. For the study of the landing case, variation in the roughness of the runway track and variation in the sink velocity has been considered. For the take-off case variation in the roughess of the runway profile is studied.

1.4 *Structural Layout of the Thesis*

The second chapter embodies the system modelling, modelling of the runway track and the system equations of motion. In the third chapter, the approach used for the numerical solution is discussed. The fourth chapter constitutes the result and discussion part of the thesis and the fifth chapter concludes the present work with some suggestions for futuristic work.

CHAPTER II

Theory

2.1 *Introduction*

Whenever an aircraft lands, takes-off or taxiies on the runway, its dynamics response is mainly affected by the various landing gear parameters, because the ground input acting as a forcing function is interacted by the landing gear system.

In the present work only the vertical heave motion is considered. The combination of airplane and landing gear is idealized to constitute a two degree of freedom system. The landing gear used is of the articulated type with oleo-pneumatic shock struts. The equations of motion are developed to include the non-linearities of the landing gear parameters, the wing lift and the inclinations of the landing gear linkages carrying the oleo-pneumatic struts. In the analysis, the motion of the landing gear prior to and subsequent to the beginning of stock strut deflection is treated. Monte-Carlo simulation approach is used for generating the ground input. The solution for the equations of motion along with the input, is obtained by employing a numerical scheme of integration.

2.2 *System Modelling*

2.2.1 Representation of the aircraft

For an initial analysis, the airplane is considered as a rigid lumped mass with only heave degree of freedom. As the airplane is constrained to move only in the vertical direction, a

single landing gear with its share of the aircraft weight W1 can be considered for the purpose of the analysis. Thus the landing gear together with the airplane mass constitute a system shown in Figure 2.1. Assuming the weight of the lower portion of the landing gear and wheel, W2, to be concentrated at the wheel axle, the airplane reduces to a two degree of freedom system.

The present analysis is subjected to the following assumptions :

i) Airplane is a rigid mass.
ii) Mass of the landing gear and the wheel with its attachment or the unsprung mass, is concentrated at the wheel axle.
iii) Shock struts are infinitely rigid in bending.
iv) Only vertical motion of the aircraft is considered.

2.2.2 Mechanics of the Gear

Figure 2.1 shows the system model used for analysis in the present work. It consists of two linkages AE and BD carrying the drag and the main oleo-pneumatic struts. The drag linkage is hinged at both ends, one end to the aircraft frame, A; and the other to the hinge point E on the main linkage. The main linkage has its upper end B hinged to the aircraft frame and carries the wheel set at its lower end D. The arm CE is rigidly connected perpendicular to the main link. A_1 to A_9 are the geometrical parameters describing the gear.

The vertical travel of the aircraft is Z_1 and the vertical deflection of the tyre is Z_2, both measured positive

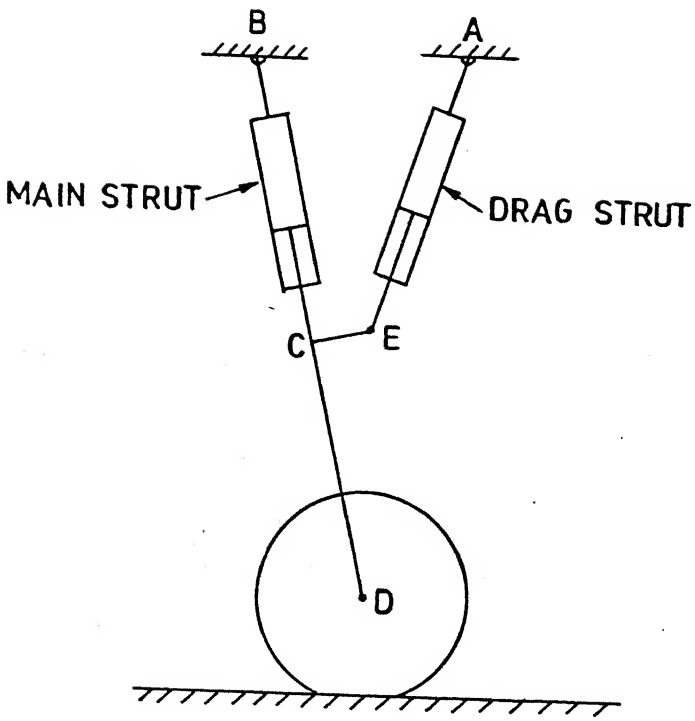

FIG. 2.1 SYSTEM MODEL

downwards from the unloaded fully extended condition of the gear.

2.2.3 Kinematics of the Gear

The kinematics of the telescopic gear is shown in Figure 2.2. At any time instant t, the linkages AE and BD move from their original position to the deflected position AE' and BD'. Z_d and x_d represent the differential travel of the wheel axle with respect to the main mass in the vertical and the horizontal directions respectively.

The kinematic relations for x_d , Z_d , main strut closer, S_z and their derivatives are established as presented below.

From geometry -

$$\begin{aligned} A_4 &= A_2 \cdot \cos\theta_o \\ A_5 &= A_3 \cdot \sin\theta_o \\ A_6 &= A_3 \cdot \cos\theta_o \\ A_8 &= A_1 \cdot \cos\phi_o \\ A_9 &= A_1 \cdot \sin\phi_o \end{aligned} \qquad (2.1)$$

As Z_d is the differential movement at the wheel axle point

$$\begin{aligned} Z_d &= Z_2 - Z_1 \\ \dot{Z}_d &= \dot{Z}_2 - \dot{Z}_1 \\ \ddot{Z}_d &= \ddot{Z}_2 - \ddot{Z}_1 \end{aligned} \qquad (2.2)$$

Also, let the new position of the wheel axle in the vertical plane be given by

$$u = A_6 + Z_d \qquad (2.3)$$

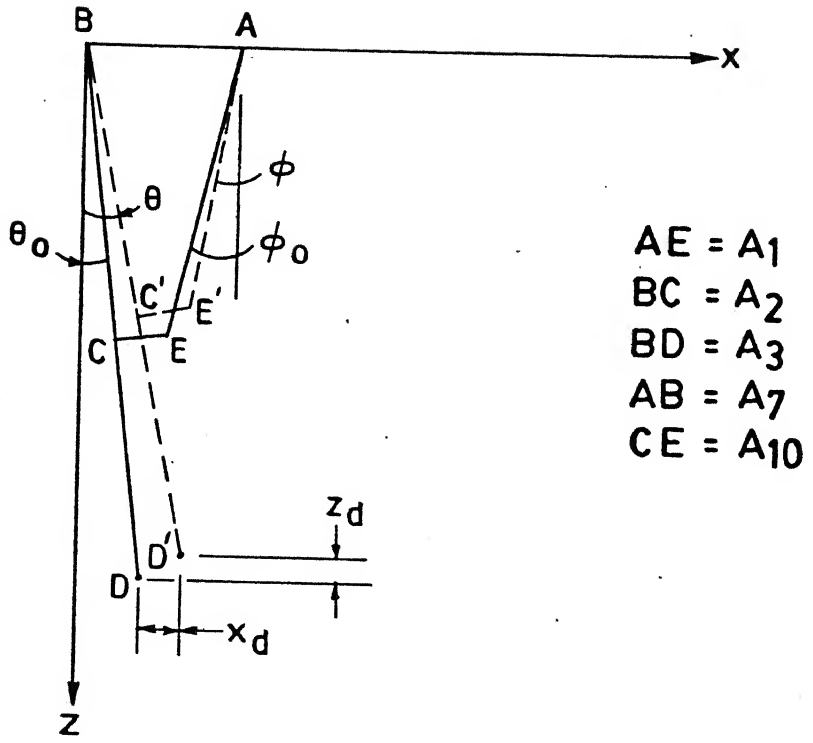

FIG.2.2 KINEMATICS OF THE LANDING GEAR

Then the shock strut stroke S_z and the strut telescoping velocity $\dot{S}_z$ are given as :

$$S_z = A_3 - \left[(x_d + A_5)^2 + u^2 \right]^{1/2} \qquad (2.4)$$

$$\dot{S}_z = - \frac{(x_d+A_5)\dot{x}_d + u\dot{u}}{\left[(x_d + A_5)^2 + u^2 \right]^{1/2}} \qquad (2.5)$$

and the acceleration of the strut $\ddot{S}_z$ can be written as

$$\ddot{S}_z = \frac{\left[(x_d+A_5)\dot{x}_d + u\dot{u}\right]^2}{\left[(x_d+A_5)^2 + u^2 \right]^{3/2}} - \frac{(x_d+A_5)\ddot{x}_d + (\dot{x}_d)^2 + u\ddot{u} + (\dot{u})^2}{\left[(x_d+A_5)^2 + u^2 \right]^{1/2}} \qquad (2.6)$$

From the gear geometry the angle of inclination of the main struct (θ) is expressed as

$$\theta = \cos^{-1} \left[\frac{u}{A_3 - S_z} \right] \qquad (2.7)$$

Also from the figure 2.2 it can be seen that

$$\sin \theta = \frac{\left[(A_3 - S_z)^2 - u^2 \right]^{1/2}}{(A_3 - S_z)} \qquad (2.8)$$

Differentiating equation (2.7) and substituting the value of $\sin \theta$ from equation (2.8) gives

$$\dot{\theta} = \frac{-u\dot{S}_2 - \dot{u}(A_3 - S_2)}{(A_3 - S_2)\left[(A_3 - S_2)^2 - u^2\right]^{1/2}} \tag{2.9}$$

Differentiating equation (2.9) once more yields

$$\ddot{\theta} = \frac{-u\ddot{S}_2 - \ddot{u}(A_3 - S_2)}{(A_3 - S_2)[(A_3 - S_2)^2 - u^2]^{1/2}} - \frac{\dot{S}_2[u\dot{S}_2 + \dot{u}(A_3 - S_2)]}{(A_3 - S_2)^2[(A_3 - S_2)^2 - u^2]^{1/2}}$$

$$- \frac{[(A_3 - S_2)\dot{S}_2 + u\dot{u}]\ [u\dot{S}_2 + \dot{u}(A_3 - S_2)]}{(A_3 - S_2)[(A_3 - S_2)^2 - u^2]^{3/2}} \tag{2.10}$$

The horizontal displacement of the wheel axle x_d is

$$\begin{aligned} x_d &= O'D' - OD \\ &= (A_3 - S_2)\sin\theta - A_3\sin\theta_o \\ &= (A_3 - S_2)\sin\theta - A_5 \end{aligned} \tag{2.11}$$

On differentiating it once, the velocity $\dot{x}_d$ is

$$\begin{aligned} \dot{x}_d &= (A_3 - S_2)\cos\theta.\dot{\theta} - \dot{S}_2\sin\theta \\ &= u\dot{\theta} - \dot{S}_2\sin\theta \end{aligned} \tag{2.12}$$

On differentiating euation (2.12), the corresponding acceleration $\ddot{x}_d$ is

$$\ddot{x}_d = \dot{u}\theta + u\ddot{\theta} - \dot{S}_2\cos\theta.\dot{\theta} - \ddot{S}_2\sin\theta \tag{2.13}$$

The kinematic relations for the stroke of the drag strut S_1 and its derivative is established as follows.

Looking at figure 2.2 it can be seen that

$$BD' = A_{3t} = A_3 - S_2 \tag{2.14}$$

$$BC' = A_{2t} = A_2 - S_2 \tag{2.15}$$

$$O'''C' = BC' \cdot \sin\theta$$

$$= (A_2 - S_2) \cdot \sin\theta \tag{2.16}$$

$$BO''' = \omega = (A_2 - S_2) \cdot \cos\theta \tag{2.17}$$

$$AP' = \omega - (A_{10} \cdot \sin\theta) \tag{2.18}$$

$$E'P' = A_7 - O'''C' - (A_{10} \cdot \cos\theta) \tag{2.19}$$

$$A_{1t} = [AP'^2 + E'P'^2]^{1/2} \tag{2.20}$$

$$\therefore S_1 = A_1 - A_{1t} \tag{2.21}$$

$$\text{Also } \tan\phi = E'P'/AP' \tag{2.22}$$

Differentiating equations (2.16), (2.17), (2.18) and (2.19) once each we have the following derivatives

$$\dot{O}'''C' = (\dot{A}_2 - \dot{S}_2) \cdot \cos\theta \cdot \dot{\theta} - (\dot{S}_2 \sin\theta) \tag{2.23}$$

$$\dot{\omega} = -(\dot{A}_2 - \dot{S}_2)\sin\theta \cdot \dot{\theta} - (\dot{S}_2 \cos\theta) \tag{2.24}$$

$$\dot{AP}' = \dot{\omega} - (\dot{A}_{10} \cdot \cos\theta \cdot \dot{\theta}) \tag{2.25}$$

$$\dot{E'P'} = -\dot{O}'''C' + (\dot{A}_{10} \cdot \sin\theta \cdot \dot{\theta}) \tag{2.26}$$

Differentiation of equations (2.21) and (2.20) subsequently yields

$$\dot{S}_1 = -\dot{A}_{1t} = -((AP' \cdot \dot{AP}') + (E'P' \cdot \dot{E'P'}))/A_{1t} \tag{2.27}$$

These expressions are used for calculating the shock strut forces required to solve the equations of motion.

2.2.4 Forces in the Shock Strut

It can be observed that the system under the present study consists of two oleo-pneumatic shock struts. One strut is located on link BC and is the main strut, the other one located on the link AE is the drag strut. During the compression stroke the hydraulic fluid is forced out of the hydraulic chamber through an orifice to a lower chamber, providing a nonlinear damping which is proportional to the square of the strut telescoping velocity $\dot{S}_z$. When the fluid enters the lower chamber, it pushes a seperator downwards in the pneumatic chamaber, thereby providing a nonlinear spring due to the polytropic air compression in the pneumatic chamber.

The shock strut axial force is a combination of the pneumatic force F_a, the hydraulic force F_h, the journal friction force F_{f_j} and the seal friction force F_{f_s} [8] and is expressed as

$$F_s = F_a + F_h + F_{f_j} + F_{f_s} \tag{2.28}$$

The pneumatic force F_a is

$$F_a = p_a A_a = p_{a_o} A_a \left[\frac{v_{a_o}}{v_{o_o}\left[\frac{p_a - p_{a_o}}{\beta} \right] + v_{a_o} - A_a . S} \right]^n \qquad (2.29)$$

where

v_{a_o} = initial air volume

v_{o_o} = initial oil volume

p_{a_o} = initial air pressure

p_a = instantaneous air pressure

β = oil bulk modulas

n = polytropic exponent for the air compression process.

while computing the pneumatic force F_a, the compressibility of oil has also been considered. [7]. The solution of the transcendental equation (2.29) is obtained by the method of successive approximation.

The hydraulic force F_a is given as [5]

$$F_h = \frac{\dot{S}}{|\dot{S}|} \frac{\rho A_h^3}{2(C_d \cdot A_n)^2} \cdot \dot{S}^2 \qquad (2.30)$$

where

ρ = mass density of the hydraulic fluid

A_h = hydraulic area

C_d = coefficient of discharge

A_n = orifice area

The journal friction force F_{f_j} in the strut is the sum of the journal friction forces contributed by each of the two bearings. It is obtained as [5]

$$F_{f_j} = \frac{\dot{S}}{|\dot{S}|} |F_n| \left[(\mu_{j_1} + \mu_{j_2}) \frac{\ell_2 - S}{\ell_1 + S} + \mu_{j_2} \right] \qquad (2.31)$$

where

F_n = normal load on the shock strut

μ_{j_1} & μ_{j_2} = coefficient of friction of upper and lower bearings on the shock strut

ℓ_1 = axial distance between the upper and lower bearings on the extended shock strut

ℓ_2 = axial distance between the shock strut lower bearing and the lower end pin joint of the piston tube.

A consideration of the system shown in figure 2.1 will show that the drag strut on the link AE is always axially loaded and so for this strut, the journal friction force does not come into picture.

Also, it can be observed that the normal force on the main shock strut is given as

$$F_n = F_s \cos\theta \sin\theta \qquad (2.32)$$

Substituting equation (2.32) in (2.31), the journal friction force is

$$F_{f_j} = \mu_e \cdot F_s \qquad (2.33)$$

where

$$\mu_e = \frac{\dot{S}}{|\dot{S}|} \; |\cos\theta . \sin\theta| \left[(\mu_{j_1} + \mu_{j_2}) \frac{\ell_2 - S}{\ell_1 + S} + \mu_{j_2} \right]$$

The seal friction force F_{f_s} is assumed to be proportional to the pneumatic force [8] as

$$F_{f_s} = \frac{\dot{S}}{|\dot{S}|} \mu_s \cdot F_a \qquad (2.34)$$

where

μ_s = coefficient of seal friction

By substituting equation (2.33) in equation (2.28) and rearranging, the shock strut axial force is obtained as

$$F_s = (F_a + F_n + F_{f_s}) \; / \; (1-\mu_e) \qquad (2.35)$$

2.2.5 Forces on Tyre

The force transmitted from the ground to the tyre, F_{v_g} can be expressed as a polynomial in tyre deflection with the coefficients obtained to fit the experimental curve provided by the tyre manufacturers.

$$F_{v_g} = a_1 (Z_2+h) + a_2 (Z_2+h)^2 + a_3 (Z_2+h)^3 + a_4 (Z_2+h)^4 + a_5 (Z_2+h)^5 + a_6 (Z_2+h)^6 + a_7 (Z_2+h)^7 + a_8 (Z_2+h)^8 + a_9 (Z_2+h)^9 + a_{10} (Z_2+h)^{10} \quad (2.36)$$

where,

h = profile of the ground surface

Z_2 = displacement of the unsprung mass

$a_1, a_2, \ldots, a_{10}$ = constants

The instantaneous drag force between the tyre and the ground F_{h_g} is assumed to be equal to the vertical ground reaction F_{v_g} multiplied by a suitable coefficient of ground friction μ_g

$$F_{h_g} = \mu_g \cdot F_{v_g} \quad (2.37)$$

Thus the vertical and horizontal forces on the tyre at the place of ground contact are determined from equations (2.36) and (2.37).

2.2.6 Equations of Motion

The dynamic system considered in the analysis is shown in figure 2.3. The portion of the aircraft weight acting on the gear or the sprung mass is W1. The various forces acting on it in the vertical direction are shown in this figure. The mass of the shock strut pistons and linkages is transferred to the unsprung mass, which also consists of the mass of the wheel unit assembly.

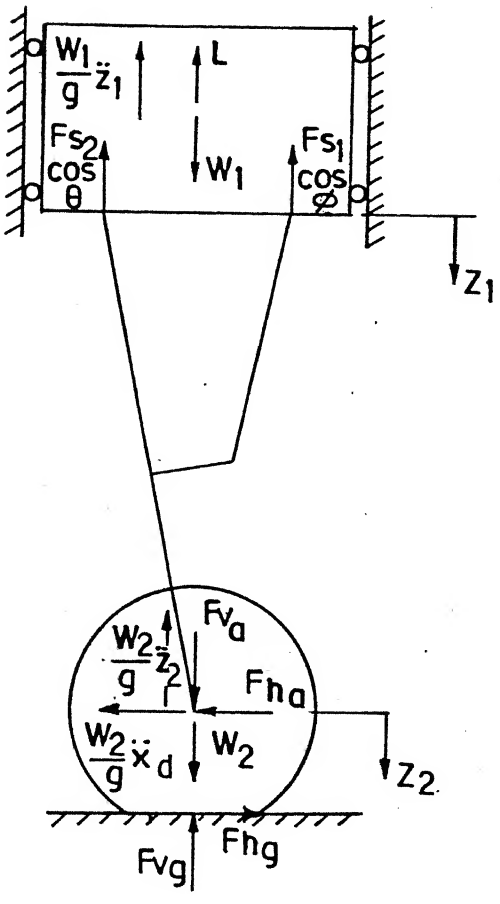

FIG. 2.3 DYNAMIC SYSTEM OF THE LANDING GEAR

e various forces acting on the unsprung mass are also shown in e figure 2.3.

The shock struts on both the main and drag linkages have eloads $F_{s_{20}}$ and $F_{s_{10}}$ respectively due to the extended or initial r pressures pa_{o_2} and pa_{o_1} respectively. Until the preload of the rut is exceeded the strut acts as a rigid member.

Initially, until the preloads of the two struts are exceeded, ly the tyre deflects, and the system acts as a single degree of eedom system with $Z_1 = Z_2 = Z$. The equilibrium equation of the stem is

$$\frac{W}{g}\ddot{Z} + L - W + F_{v_g} = 0 \qquad (2.38)$$

After the preload in either the main or the drag shock strut exceeded, the system starts behaving as a two degree of freedom stem with either the main or the drag or both the struts lescoping. The vertical force equilibrium of the unsprung mass

$$\frac{W_2}{g}\ddot{Z}_2 + F_{v_g} - F_{v_a} - W_2 = 0 \qquad (2.39)$$

l the vertical force equilibrium of the sprung mass is

$$\frac{W_1}{g}\ddot{Z}_1 + L - W_1 + (F_{s_1}.\cos\phi) + (F_{s_2}.\cos\theta) = 0 \qquad (2.40)$$

The horizontal equilibrium of the unsprung mass gives

$$\frac{W_2}{g} \ddot{x}_d + F_{h_a} - F_{h_g} = 0 \qquad (2.41)$$

where,

F_{h_a} = horizontal force on the wheel axle.

2.2.7 Initial Conditions

To establish the point at which the transition from one degree of freedom system to the two degree of freedom system takes place, it is necessary to solve equation (2.38) for the single degree of freedom system.

Equation (2.38) can be rewritten as

$$\ddot{Z} = (W-L-F_{v_g}) \; / \; (W/g) \qquad (2.42)$$

The vertical force equilibrium of the linkage system can be written as

$$F_{v_a} = F_{s_1} \cos \phi + F_{s_2} \cos \theta \qquad (2.43)$$

Substituting equations (2.42) and (2.43) in (2.40) yields

$$F_{v_a} = F_{v_g} \qquad (2.44)$$

The horizontal force equilibrium of the linkage gives

$$F_{s_2} \sin \theta + F_{h_a} - F_{s_1} \sin \phi = 0 \qquad (2.45)$$

Equation (2.41), after substituting equation (2.37) and neglecting the inertia force acting on the unsprung mass, yields

$$F_{h_a} = \mu_g F_{v_g} \tag{2.46}$$

Substituting equation (2.46) in (2.45) gives a relationship between F_{s_1} and F_{s_2} as

$$F_{s_2} = (F_{s_1} \sin \phi - \mu_g F_{v_g})/\sin \theta \tag{2.47}$$

Substituting equation (2.47) in (2.43) we have

$$F_{s_1} = \frac{(F_{v_a} + (\mu_g F_{v_g}) \cos \theta / \sin \theta)}{\left[\cos \phi + \frac{\sin \phi}{\sin \theta} \cos \theta \right]} \tag{2.48}$$

The calculated values of F_{s_2} and F_{s_1} in the one degree case are compared with their corresponding preloads at each step. The instance at which any one of these exceeds the preloading transition takes place from the one degree system case to the two degree case.

2.3 *Modelling of the Runway Profile*

As has been stated before, the input to the landing gear system arises due to the motion of the aircraft on the runway, which inherently has roughness to a greater or a lesser extent. It is this undulating ground profile which acts as a forcing function for the undercarriage system. During the present work, the ground profile is numerically simulated as a Nonstationary

Gaussian random process. The profile h(s) in space coordinates is expressed as the sum of a deterministic and a random part.

The deterministic part may arise due to a variation in the mean of the track level because of faults such as aclivity, declivity, bumps, dips, step-ups, step-downs, ramps and repair patches resulting due to improper leveling, differential settlement of slabs, repair at joints and bomb craters. Some of these faults are shown in figure 2.4 and can be used singly or in combination to model the various faults in the runway.

The random profile generated represents the ground undulations. The runway unevenness is considered to be a Gaussian Random process with a power spectral density as

$$\Phi(\Omega) = \frac{C}{\Omega^2 + \nu^2} \qquad (2.49)$$

where,

Ω = spatial frequency

C = roughness constant

ν = correlation constant

The algebraic sum of the determinstic profile and the random profile gives the nonstationary runway profile.

2.4 *Response Statistics*

Repeated solution of the system equations can be resorted to generate an ensemble of the system response. The second order

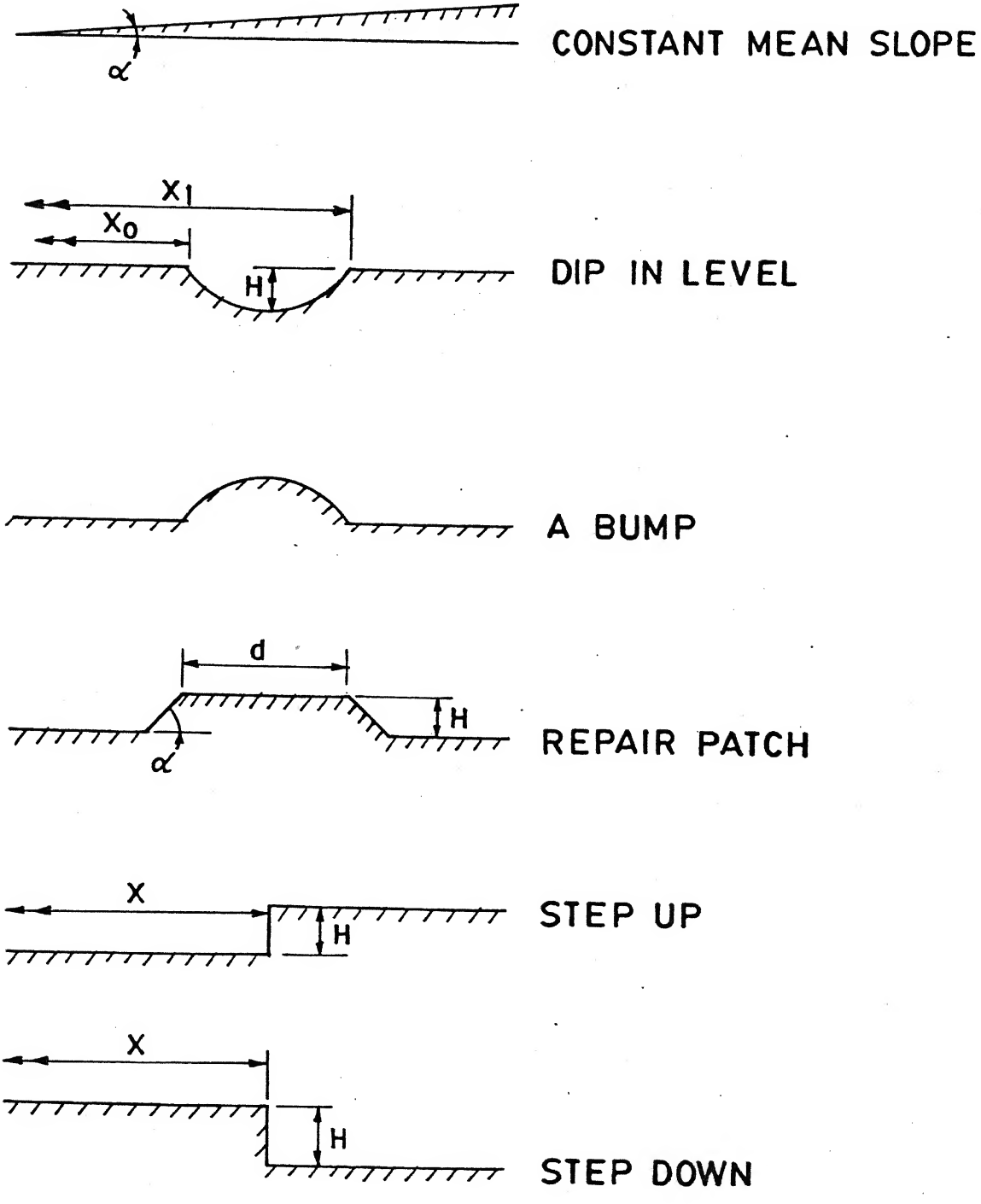

FIG. 2.4 FAULTS IN THE RUNWAY TRACK

statistics of the response can then be obtained by averaging across the ensemble as [19]

$$\mu_x(t) = \frac{1}{N} \sum_{i=1}^{N} X_i(t) \qquad (2.50)$$

$$\sigma_x^2(t) = \frac{1}{N-1} \sum_{i=1}^{N} [X_i(t) - \mu_x(t)]^2 \qquad (2.51)$$

where, μ_x and σ_x denote the mean and the standard deviation of a random process X with N as the number of samples in the ensemble.

CHAPTER III

Numerical Solution Approach

3.1 *Introduction*

To obtain the response of the aircraft during its runs on the runway, as during taxii, take-off and landing, it is required to solve the vertical force equilibrium equations (2.39) and (2.40). Since, it is difficult to obtain a closed form solution for these coupled nonlinear differential equations in the general case, some numerical approach has to be adopted. For this a standard library routine using variable order, variable step size Adam's method is selected.

The initial conditions of state required for any numerical integration scheme to start, are known at the start of the run. At this instance the system is assumed to behave as a single degree of freedom system. When transition takes place to two degrees of freedom the number of variables increase and the appropriate initial conditions have to be set up to reinitiate the integration scheme. An iterative approach is developed for this purpose which is described later in this chapter.

Besides this, a numerical scheme is also needed for the simulation of the mean and the random profile of the runway track as this information is required at each step for the integration of the system equations.

3.2 *Initial conditions for the two degree case*

When the aircraft commences to move on the runway the modelled system is in the one degree of freedom case in which the shock struts do not telescope and both the sprung and the unsprung mass move as a single mass. The system functions as a single degree of freedom system until the forces in the shock strut as calculated by equations (2.47) and (2.48) exceed the preloads in the shock struts.

The moment the preloads are exceeded the system starts behaving as a two degree of freedom system. At this point of time, it is necessary to establish the movements of the shock struts and consequently the displacements and velocities of the sprung and the unsprung mass. This can be posed as a problem of obtaining the root of a transcendental equation. An iterative scheme developed to obtain the displacements of the shock struts is presented below.

Initially, a very small displacement is set in the strut, from which the strut telescoping velocity is obtained, based on the impact considerations discussed in the following section 3.3. Then these values of the displacement and velocity of the strut are used to find the force in the shock strut as shown in equation (2.35). The value of the force calculated is then compared to the force at which the system had transited from the one degree of freedom case to the two degree case. This process is repeated until the calculated force equals the force at transition.

Various possibilities exists, sometimes the calculated force is less than the force at transition and then the values of the

stroke and velocity of the strut are increased and the reverse is true when the calculated force is larger than the force at transition. But it may also happen that the calculated force initially is less but after some particular step it becomes larger than the force at transition. When this happens then linear interpolation is done to obtain the value of the stroke of the strut and the force is then calculated at that point. The process is repeated until the correct value of the stroke and velocity of the strut, corresponding to the force at transition is obtained.

Once the strut telescoping velocities are determined then the angular velocity of the linkage is established and this is used to obtain the velocity of the differential motion of the two masses.

Then using equation set (2.2) the initial conditions for the two degree case are established.

3.3 *Impact Consideration for determining the Strut Telescoping Velocity*

As seen in the previous section, a method has to be developed for obtaining the strut telescoping velocity because it is required to evaluate the force in the shock strut.

Usually as the transition takes place very early during the motion of the aircraft and must happen in a very small interval of time, it could be considered to be occuring during an impact phase. During impact the shock struct force will vary with the strut movement causing a variable acceleration of strut closer. Assuming the acceleration to change linearly with time

$$\ddot{S} = a_n t \qquad (3.1)$$

where a_n is a constant to be determined and t is the time instance measured from the instance of the strut unlocking.

Integrating equation (3.1) yields

$$\dot{S} = \frac{a_n t^2}{2} + \dot{S}_o \qquad (3.2)$$

where $\dot{S}_o$ = initial velocity

= 0 (as it has just started from rest)

Integrating once more

$$S = \frac{a_n t^3}{6} + S_o \qquad (3.3)$$

$$\therefore \quad a_n = \frac{6\,(S-S_o)}{t^3} \qquad (3.4)$$

Substituting equation (3.4) in (3.2) gives

$$\dot{S} = \frac{3(S-S_o)}{t} \qquad (3.5)$$

Equation (3.5) is used to obtain the strut telescoping velocity during the iterative scheme, used for transition.

3.4 *Numerical Simulation of the Random Profile*

The ground unevenness acts as a base excitation to the modelled system. The random part of the runway profile is simulated based on a method developed by Joel N Franklin [18],

which confirms to the power spectral density of the runway track.

The simulation is carried out in the following steps :

First a sequence (x_n) of independent samples from the uniform distribution on $0 \leq x < 1$ is generated using a standard library routine.

Using these, a sequence (ω_n) of independent sample from the Gaussian distribution with mean zero and unit variance is constructed by using the method of Box and Muller [20].

The sequence $\omega_1, \omega_2, \omega_3, \ldots$ is obtained from the formulas

$$\left.\begin{aligned} \omega_{2n-1} &= (-2.\ \ell n\ x_{2n-1})^{1/2}\ \text{Cos}\ 2\pi\ x_{2n}, \quad n = 1, 2.... \\ \omega_{2n} &= (-2.\ \ell n\ x_{2n-1})^{1/2}\ \text{Sin}\ 2\pi\ x_{2n}, \quad n = 1, 2.... \end{aligned}\right\} \quad (3.6)$$

This one dimensional sequence $\omega_1, \omega_2, \ldots$ can be used to simulate samples from the n-dimensional Gaussian distribution by defining vectors

$$\omega^{(0)} = \begin{Bmatrix} \omega_1 \\ \vdots \\ \omega_n \end{Bmatrix}, \quad \omega^{(1)} = \begin{Bmatrix} \omega_{n+1} \\ \vdots \\ \omega_{2n} \end{Bmatrix}, \ldots \qquad (3.7)$$

These will be used to determine the Gaussian random vector.

Assuming that the given power spectral density $\Phi(\Omega)$ can be represented with sufficient accuracy by a rational function, we can represent $\Phi(\Omega)$ as the ratio of two polynomials in Ω as

$$\Phi(\Omega) = \left| \frac{P(i\Omega)}{Q(i\Omega)} \right|^2 \qquad (3.8)$$

where the degree of P is one less than the degree of Q.

The output x(t) is related to the input $\omega(t)$ by

$$x(t) = \frac{P(i\Omega)}{Q(i\Omega)} \cdot \omega(t) \qquad (3.9)$$

or equivalently, if D = d/dt

$$x(t) = \frac{P(D)}{Q(D)} \cdot \omega(t) \qquad (3.10)$$

The last equation is to be understood in the sense that we first solve the differential equation

$$Q(D) \cdot \Phi(t) = \omega(t) \qquad (3.11)$$

for the steady state solution $\Phi(t)$, and then obtain the required signal

$$x(t) = P(D).\Phi(t) \qquad (3.12)$$

Let equation (3.11) in general have the form

$$\Phi^{(n)}(t) + a_1\Phi^{(n-1)}(t) + \ldots + a_n\Phi(t) = \omega(t) \qquad (3.13)$$

where $\omega(t)$ is white noise

In order to compute equation (3.12) we will require samples of the state vector

$$Z(t) = \begin{Bmatrix} \Phi(t) \\ \Phi'(t) \\ \vdots \\ \Phi^{(n-1)}(t) \end{Bmatrix} \tag{3.14}$$

The vector z(t) satisfies the stochastic differential equation

$$\frac{dZ(t)}{dt} = A.Z(t) + f(t) \tag{3.15}$$

where,

$$A = \begin{bmatrix} 0 & 1 & 0 & 0 \\ 0 & 0 & 1 & 0 \\ \vdots & \vdots & \vdots & \vdots \\ 0 & 0 & 0 & 1 \\ -a_n & -a_{n-1} & -a_{n-2} & -a_1 \end{bmatrix}, \quad f(t) = \begin{Bmatrix} 0 \\ 0 \\ \vdots \\ 0 \\ \omega(t) \end{Bmatrix} \tag{3.16}$$

The vector Z(t) is a Gaussian Random Vector with a positive definite moment matrix

$$M = E\,[Z(t).\ Z^{*}(t)] \tag{3.17}$$

The moment matrix M can be computed without a knowledge of the eigen values of A. The matrix M has components of the form

$$M_{ij} = \begin{cases} 0 & , \ i+j \text{ odd} \\ (-1)^{(j-i)/2} \cdot m_{((j+i)/2)-1)} & , \ i+j \text{ even} \end{cases} \tag{3.18}$$

where the numbers $m_o, m_1, \ldots, m_{n-1}$ can be computed by solving the n linear equations

$$(-1)^k \sum_{k/2 \le q \le (n+k)/2} (-1)^q \, a_{n-2q+k} \cdot m_q = \begin{cases} 0 & , k=0,\ldots,n-2 \\ 1/2 & , k=n-1 \end{cases} \qquad (3.19)$$

where we define $a_o = 1$

When M has been computed it can be factored by the Crout factorization

$$M = TT^* \qquad (3.20)$$

The required initial vector $Z(0) = Z^{(o)}$ can be computed as

$$Z(0) = T.\omega^{(o)} \qquad (3.21)$$

Suppose Z(t) has been computed for any $t \geq 0$, we will have to compute the succeeding state vector $Z(t+\Delta t)$.

Let $$X(t) = e^{At} = \exp At \qquad (3.22)$$

be the solution of the initial-value problem

$$\frac{dx(t)}{dt} = A.\ X(t)$$
$$X(0) = I \qquad (3.23)$$

We need to know the values of the matrix exp(At) for the single value of time $t = \Delta t$. The solution of the differential equation gives the values of the matrix exp (At), at a particular time $t = \Delta t$

$$e^{A\Delta t}.C.[\,e^{A\Delta t}]^{*} - C = AM_r + M_r A^{*} \qquad (3.24)$$

where C is a positive semidefinite matrix

$$C = \begin{bmatrix} 0 & 0 & \ldots. & 0 \\ 0 & 0 & \ldots. & 0 \\ \vdots & \vdots & \ldots. & \vdots \\ 0 & 0 & \ldots. & 1 \end{bmatrix} \qquad (3.25)$$

Once $[\,e^{A\Delta t}]$ is known the Ljapunov equation (3.24) can be solved to obtain the moment matrix M_r.

Having computed the matrix M_r, we factor it by the Crout factorization.

We are now ready to compute a sample for r.

Let $$t + \Delta t = \nu.\Delta t \qquad (3.26)$$

Let $\omega^{(\nu)}$ be one of the vectors defined in equation (3.7). We then compute

$$Z(t+\Delta t) = e^{A\Delta t}.\ Z(t) + r \qquad (3.27)$$

If the polynomial P has the form

$$P(\rho) = b_o.\rho^{m} + b_1\rho^{m-1} + \ldots + b_m,\ b_o \neq 0,\ m < n \qquad (3.28)$$

then the required scalar function x(t) with p.s.d. $\Phi(\Omega)$ is computed as a linear combination

$$x(t) = b_o\, Z_{m+1}(t) + b_1\, Z_m(t) + \ldots + b_m\, Z_1(t) \qquad (3.29)$$

Equation (3.29) is equivalent to equation (3.12)

CHAPTER IV

Results and Discussions

4.1 *Introduction*

Response of a non-linear aircraft to the ground induced excitation has been considered during variable velocity runs - landing and take-off.

The various numerical data used for the system in generating the response values are provided in the Appendix. As a first study, the main shock strut is always considered locked and only the drag strut is allowed to telescope.

The response obtained constitutes the mean values and the standard deviations for the displacement, velocity and acceleration of the sprung and the unsprung mass. Due to the physical constraints of time, the sample size used for obtaining the mean and standard deviation is restricted to fifteen in number. To smoothen out the irregularities in the response due to the small size of the ensemble, a ten point moving average is carried out over the generated response. Most of the times to obtain a more clear and vivid picture of the variations in the response for the presentation of graphs, the duration of the landing or take-off run is broken down into more than one interval of time.

The duration of the landing run is taken as fifteen seconds and that of the take-off run as seventeen seconds.

For the landing case, variation in the values of the roughness constant of the runway track and the variations in the sink velocity of the aircraft at touchdown has been studied. For the take off runs the effect of variations in the roughness constant of the runway track or the response behaviour is studied.

4.2 *Landing Run with variation in Track Roughness*

During the course of study the value of the sink velocity of the aircraft at touchdown was held constant at 350 cm/s. The value of the ground mean slope was also held constant at 1 in 1000. The roughness costant C has been taken as 0.0001, 0.0005 and 0.00002 in ft units.

4.2.1 Mean Displacement of Unsprung mass

The mean displacement response of the unsprung mass is presented in Figures 4.1a and 4.1b. The following observations are made:

i) The track roughness has a very small effect on the mean response.

ii) As time progresses during the landing run, the heaving of the unsprung mass ceases considerably beyond one second after touchdown and only a slight heave movement is discernible.

iii) For the landing gear data used the aircraft does not 'balloon' after touchdown.

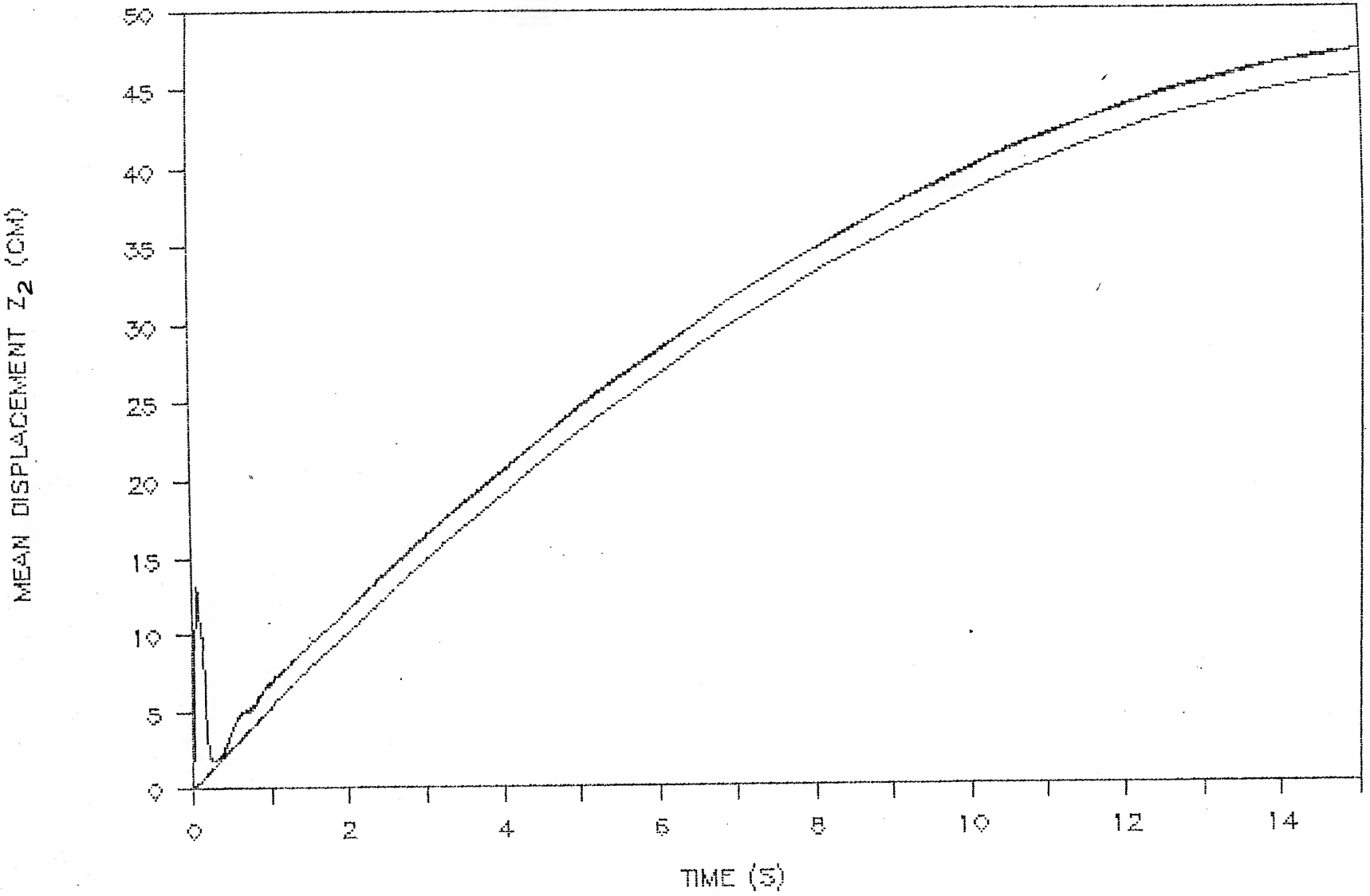

Fig. 4.1a Landing run, Roughness variation; Mean Displacement Response.

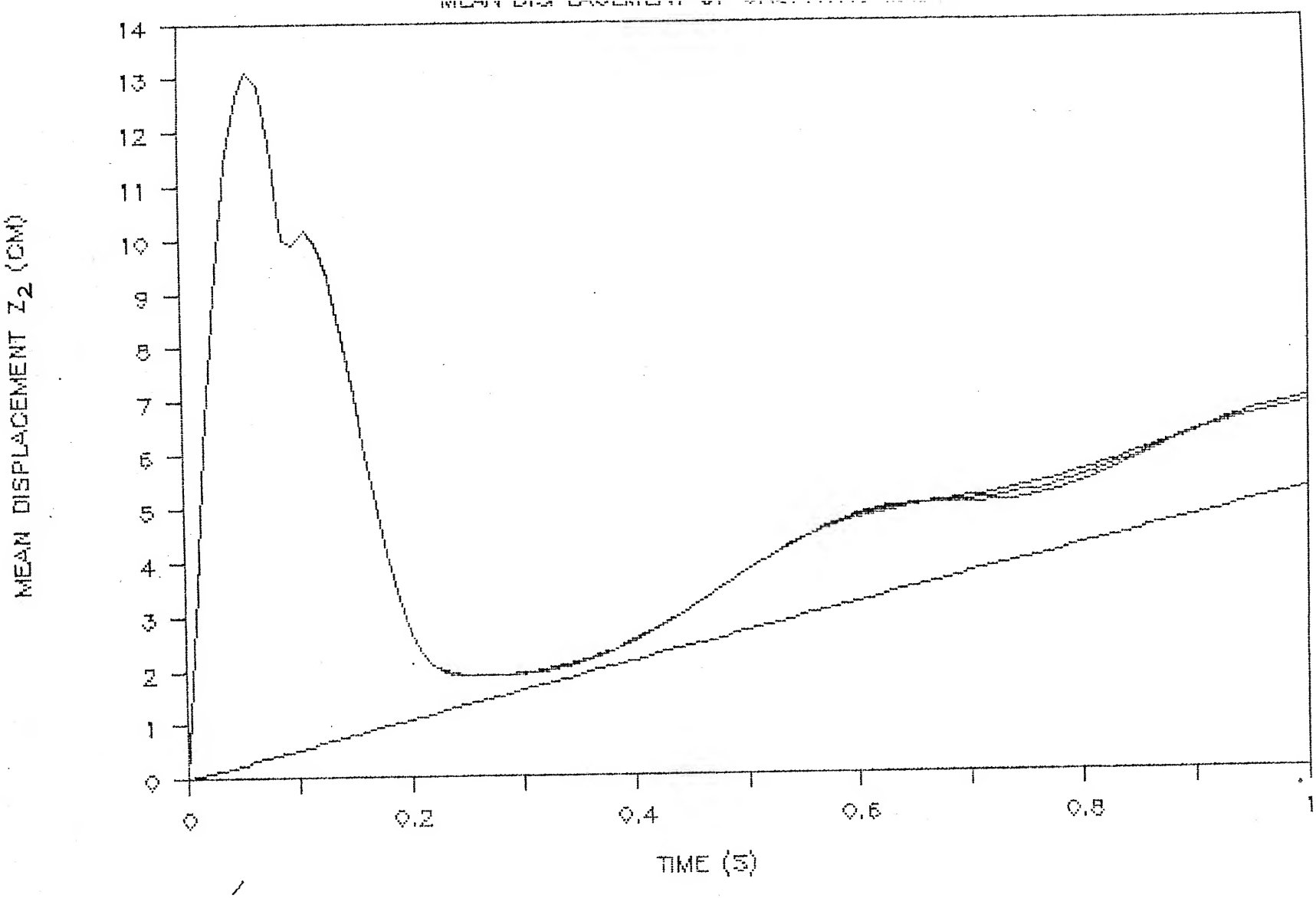

Fig. 4.1b Landing run, Roughness variation; Mean Displacement Response.

4.2.2 Mean Displacement of the Sprung mass

The mean displacement response of the sprung mass is shown in Figures 4.1c and 4.1d. Some observations are :

i) The track roughness has a very minor effect on the mean response.

ii) At around 0.15 seconds after touchdown a resonance is observed.

iii) Just after or very near to the time of impact, fluctuations are observed but with the passage of time these gradually decrease.

iv) There is a steady increase in the response due to the motion of the aircraft over the mean slope.

4.2.3 Standard Deviation of Displacement of Unsprung mass

The standard deviation of displacement response of the unsprung mass is portrayed in Figures 4.2a and 4.2b. The observations are :

i) The influence of the variation in the track roughness is more easily noticeable than in the case of the mean displacement.

ii) The graph for the time duration of 0 to 1 second shows two resonances occuring at around 0.2 and 0.8 seconds from touchdown.

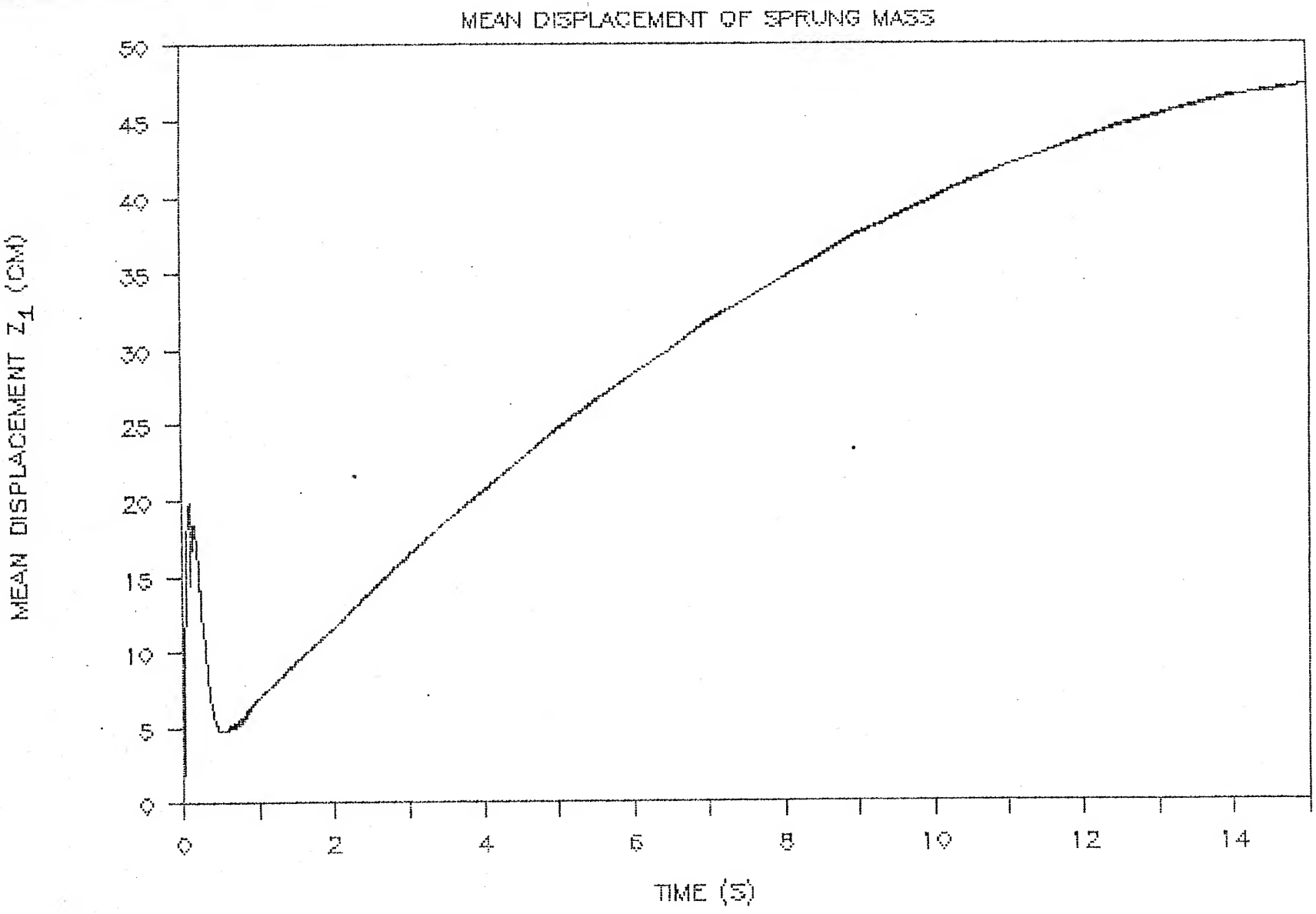

Fig. 4.1c Landing run, Roughness variation; Mean Displacement Response.

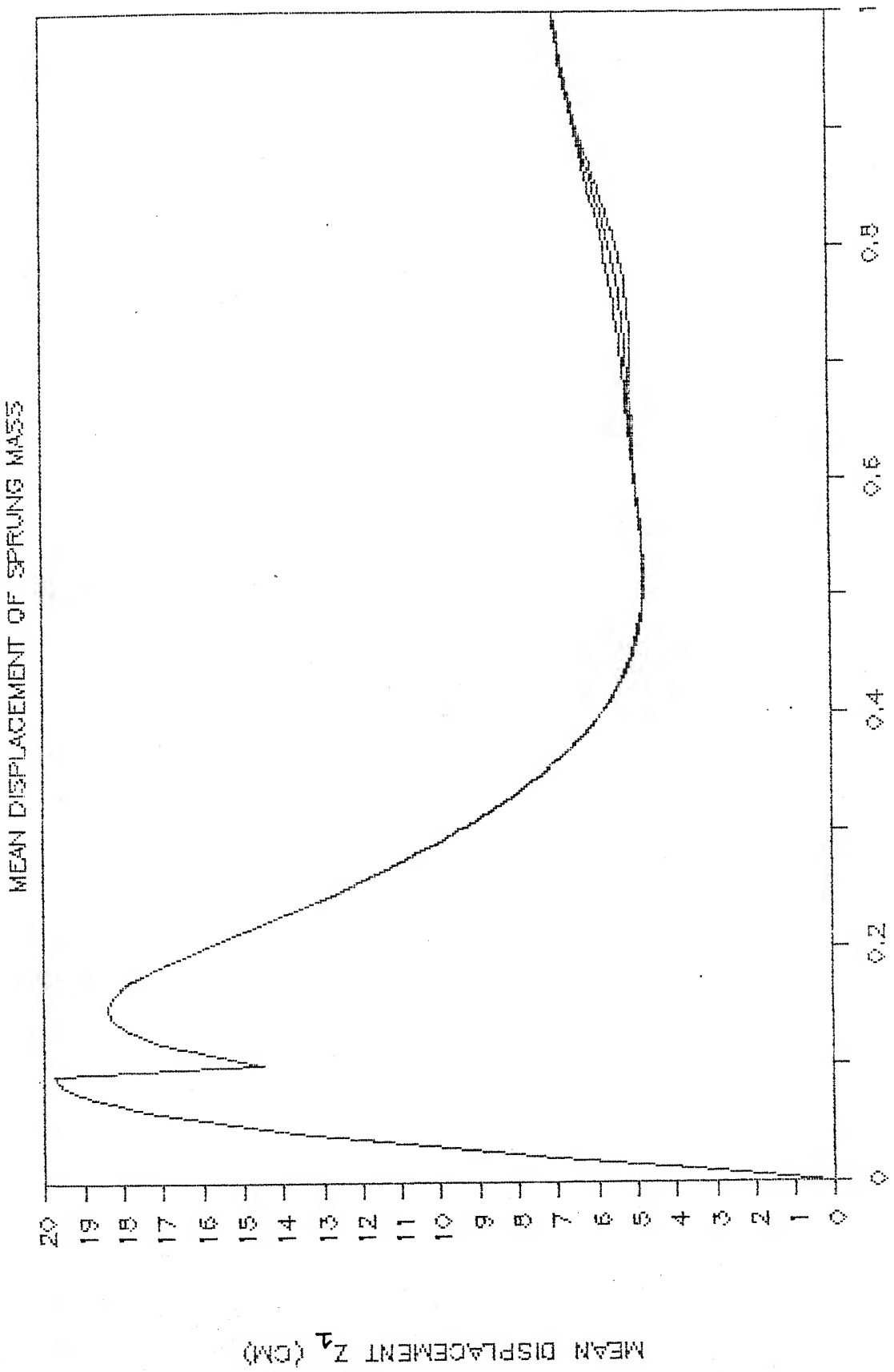

Fig. 4.1d Landing run, Roughness variation; Mean Displacement Response.

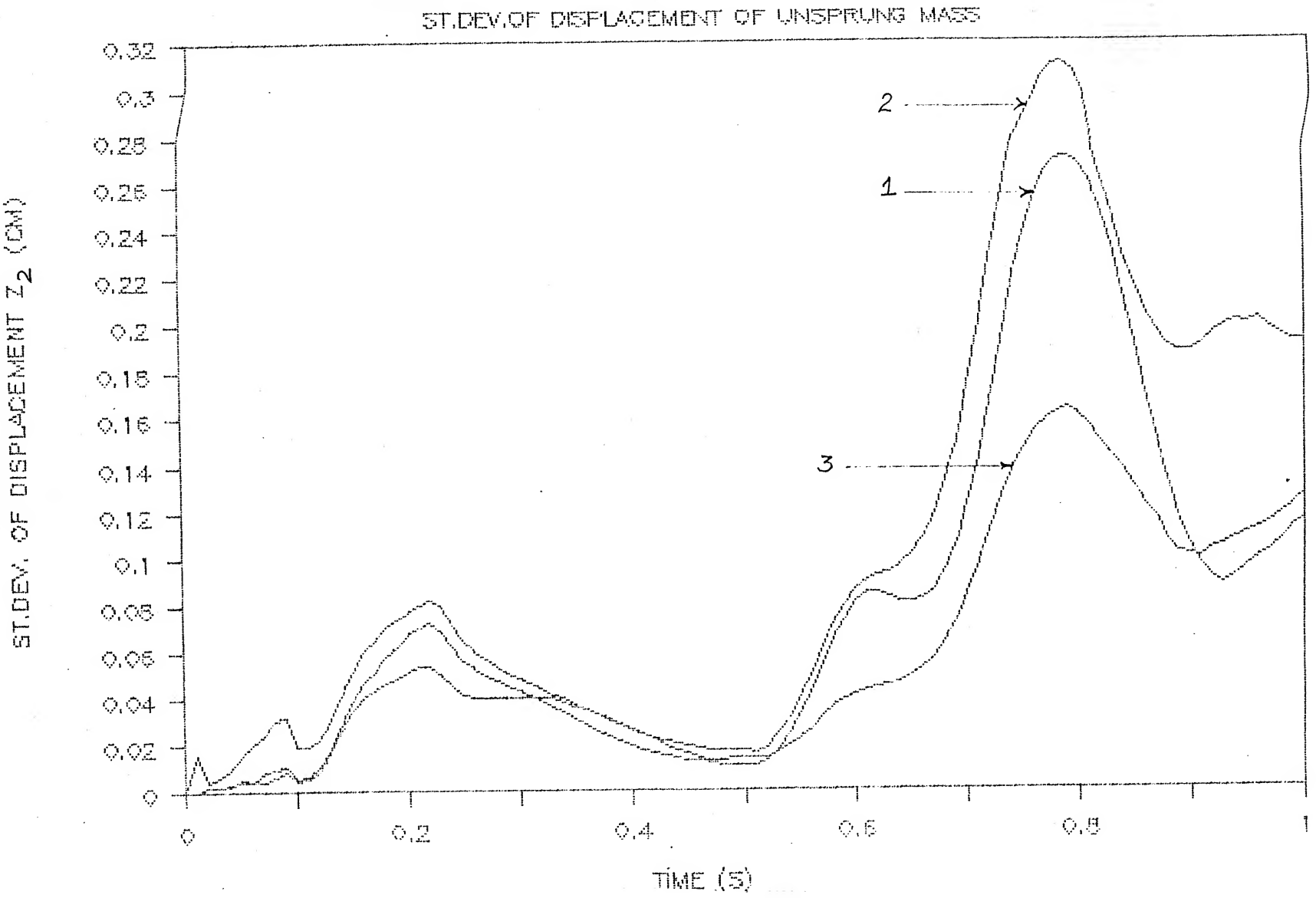

Fig. 4.2a Landing run,Roughness variation; Standard Deviation of Displacement Response.

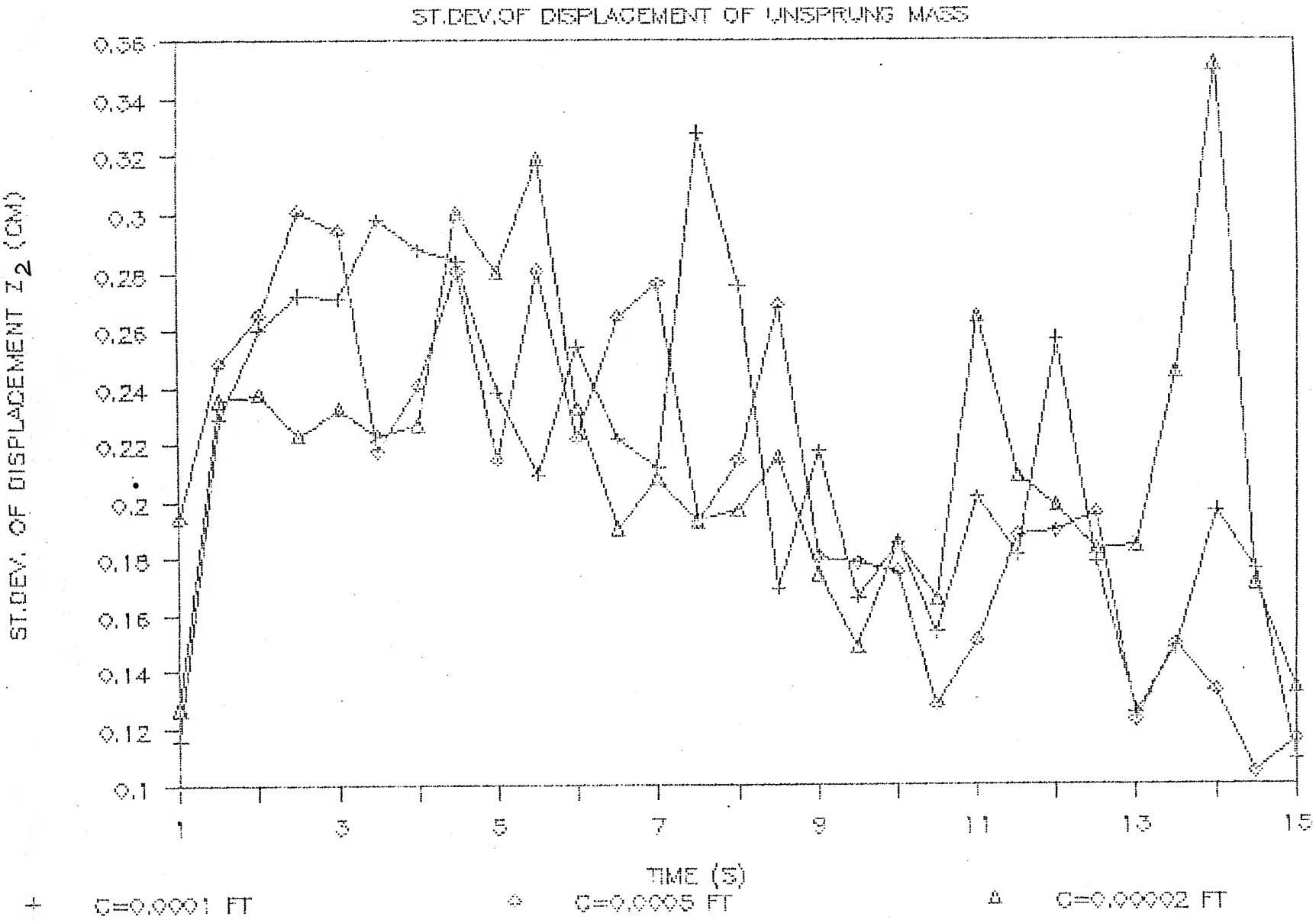

Fig. 4.2b Landing run,Roughness variation; Standard Deviation of Displacement Response.

iii) The overall trend of the graph shows a decreasing pattern of the standard deviation as time progresses during the landing run. This holds true for the different roughness levels considered. At around 15 seconds the value of standard deviation is as small as 1 to 1.5 mm.

4.2.4 Standard Deviation of Displacement of Sprung mass

The response is shown in Figures 4.2c and 4.2d. The inferences made are :

i) As in the case of the unsprung mass, here also the effect of variations in the roughness levels of the track is easily seen.

ii) Resonance is observed at around 0.35 seconds and 0.8 seconds after touchdown.

iii) At around 9.0 seconds also a large peak response is seen for a particular value of roughness constant, C = 0.0001 ft.

iv) The trend of standard deviation of the displacement shows a dropping pattern and at 15 seconds it has a value of about 1 to 1.5 mm.

4.2.5 Mean Velocity of the Unsprung mass

The mean velocity response of the unsprung mass is shown in Figures 4.3a and 4.3b. The salient points noted from the graphs are :

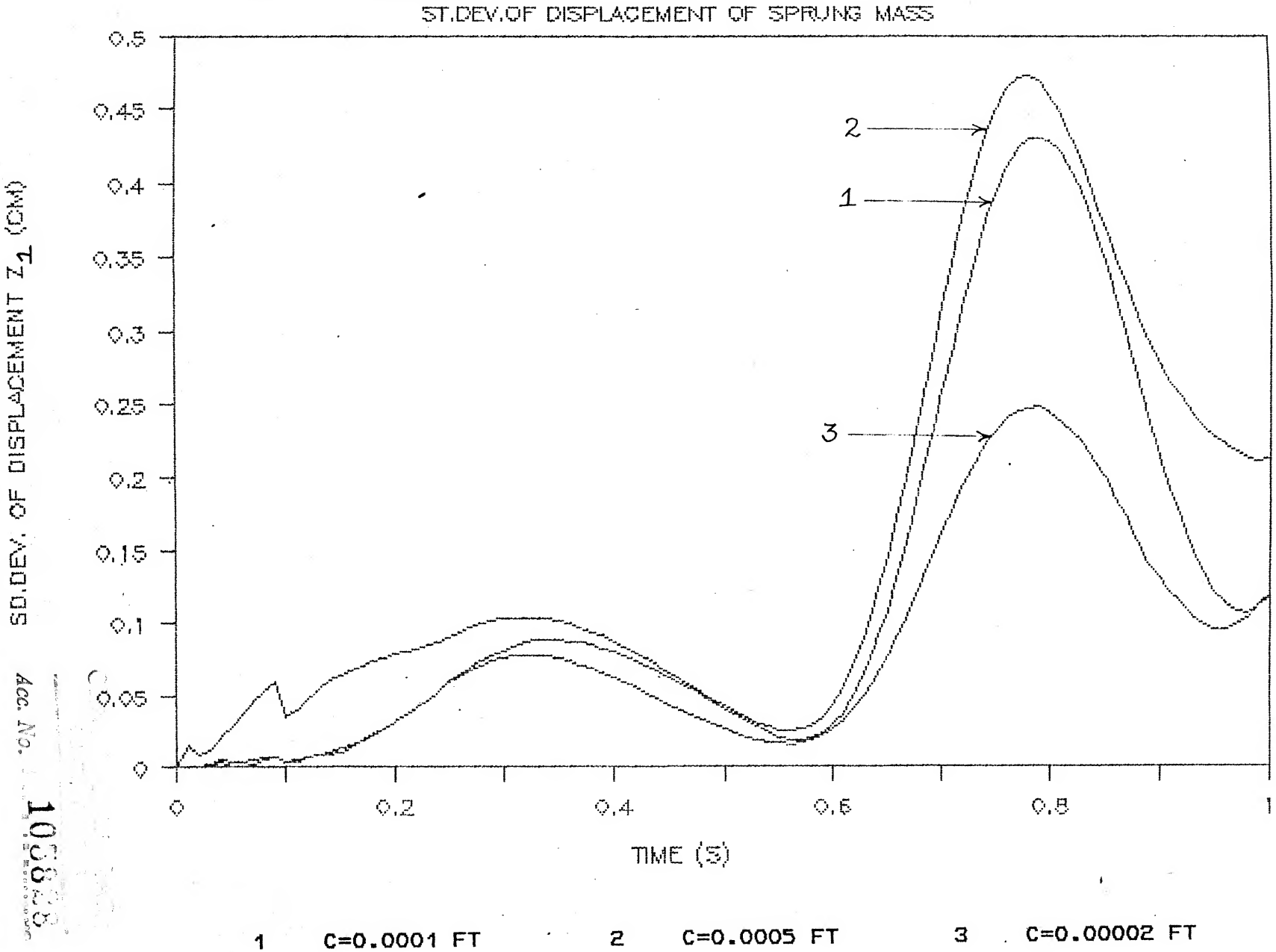

1 C=0.0001 FT 2 C=0.0005 FT 3 C=0.00002 FT

Fig. 4.2c Landing run,Roughness variation; Standard Deviation of Displacement Response.

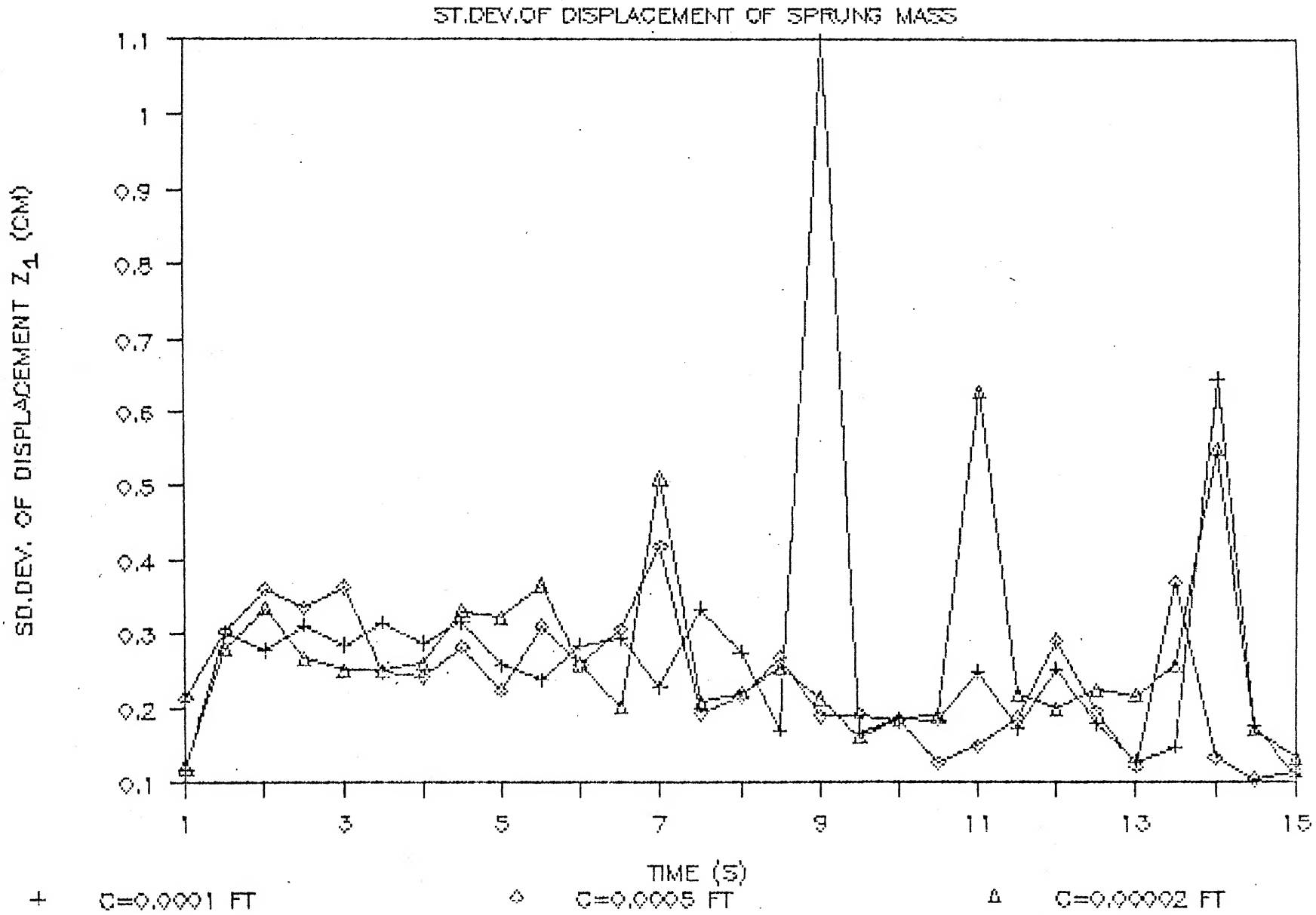

Fig. 4.2d Landing run,Roughness variation; Standard Deviation of Displacement Response.

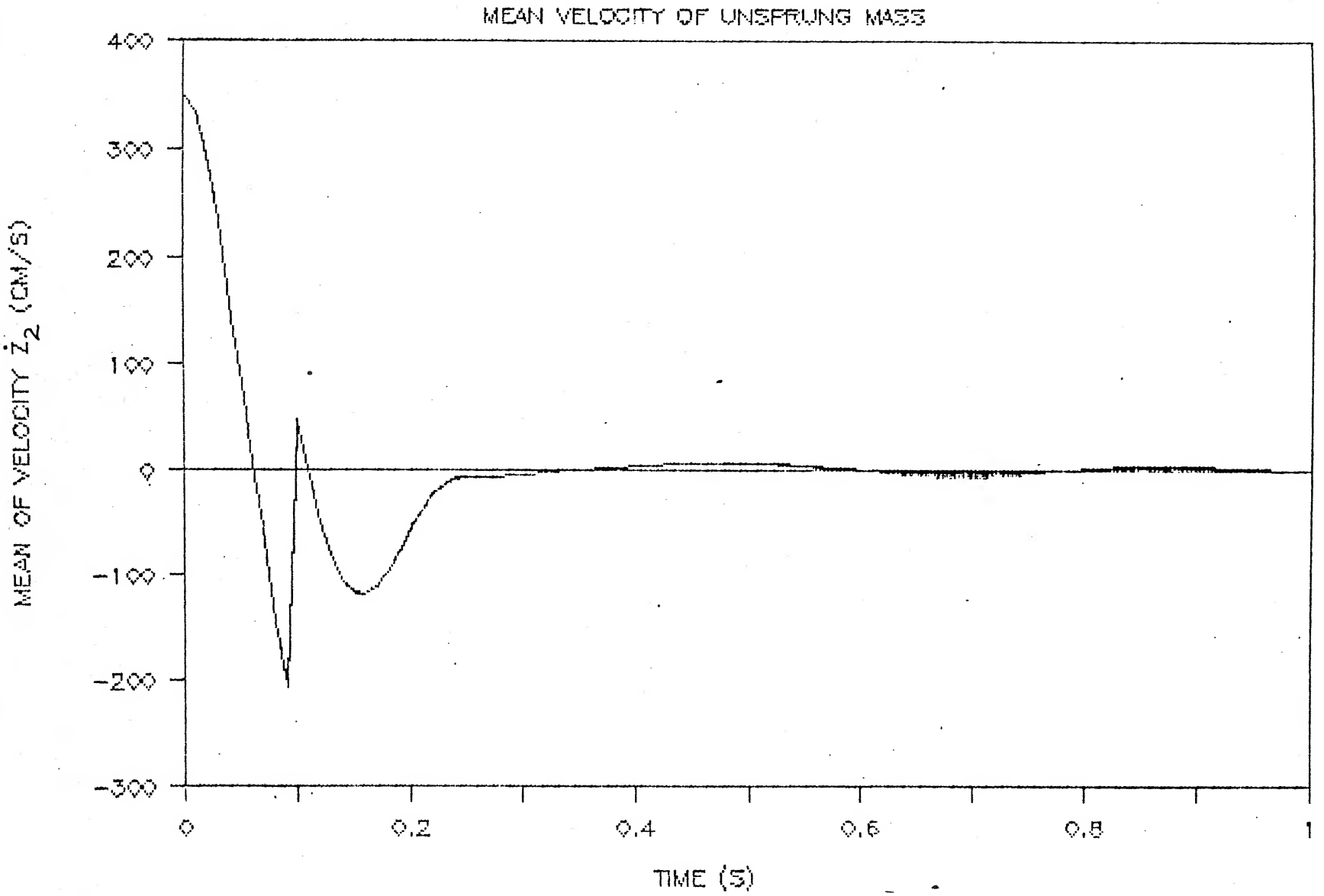

Fig. 4.3a Landing run, Roughness variation; Mean Velocity Response.

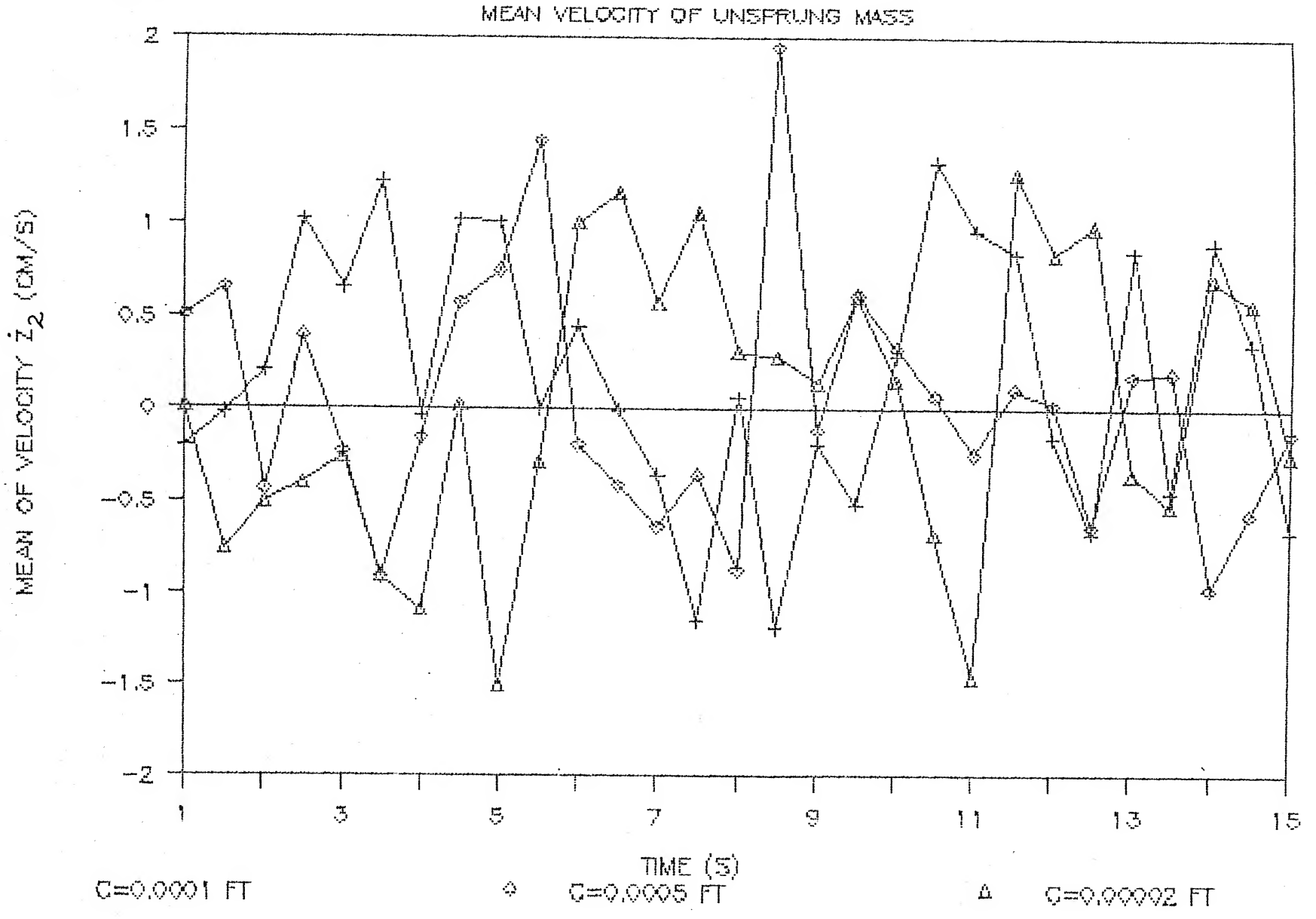

Fig. 4.3b Landing run, Roughness variation; Mean Velocity Response.

i) At different roughness levels the effect of the variations in the roughness levels of the track is not very significant, giving a maximum value of the mean velocity of only about 2 cm/s.

ii) After the initial impact phase, beyond 0.25 seconds the mean value of velocity is maintained at a very low value. The maximum value during the phase is approximately 2 cm/s.

4.2.6 Mean Velocity of the Sprung mass

The mean velocity of the sprung mass response is presented in Figures 4.3c and 4..3d. The noteworthy points observed are :

i) As before in the case of unsprung mass, the effect of roughness variation is not appreciable.

ii) After an initial drop in the mean velocity a second peak is observed at around 0.1 seconds from touchdown.

4.2.7. Standard Deviation of the Velocity of the Unsprung mass

The response is shown in Figures 4.4a and 4.4b. The points of interest observed are :

i) Effect of roughness variation is more marked in the first one second of the run than during the later period of time.

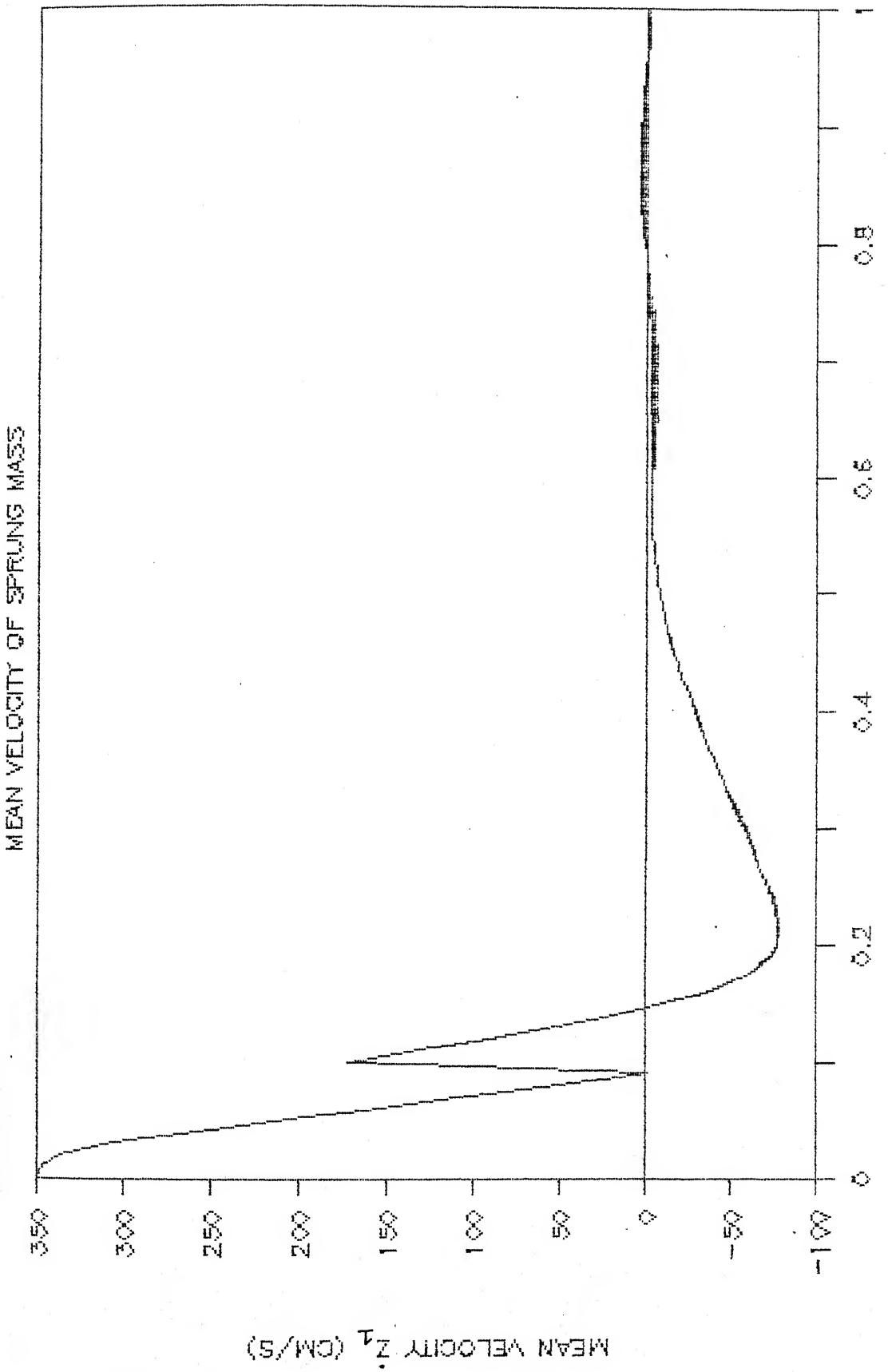

Fig. 4.3c Landing run, Roughness variation; Mean Velocity Response.

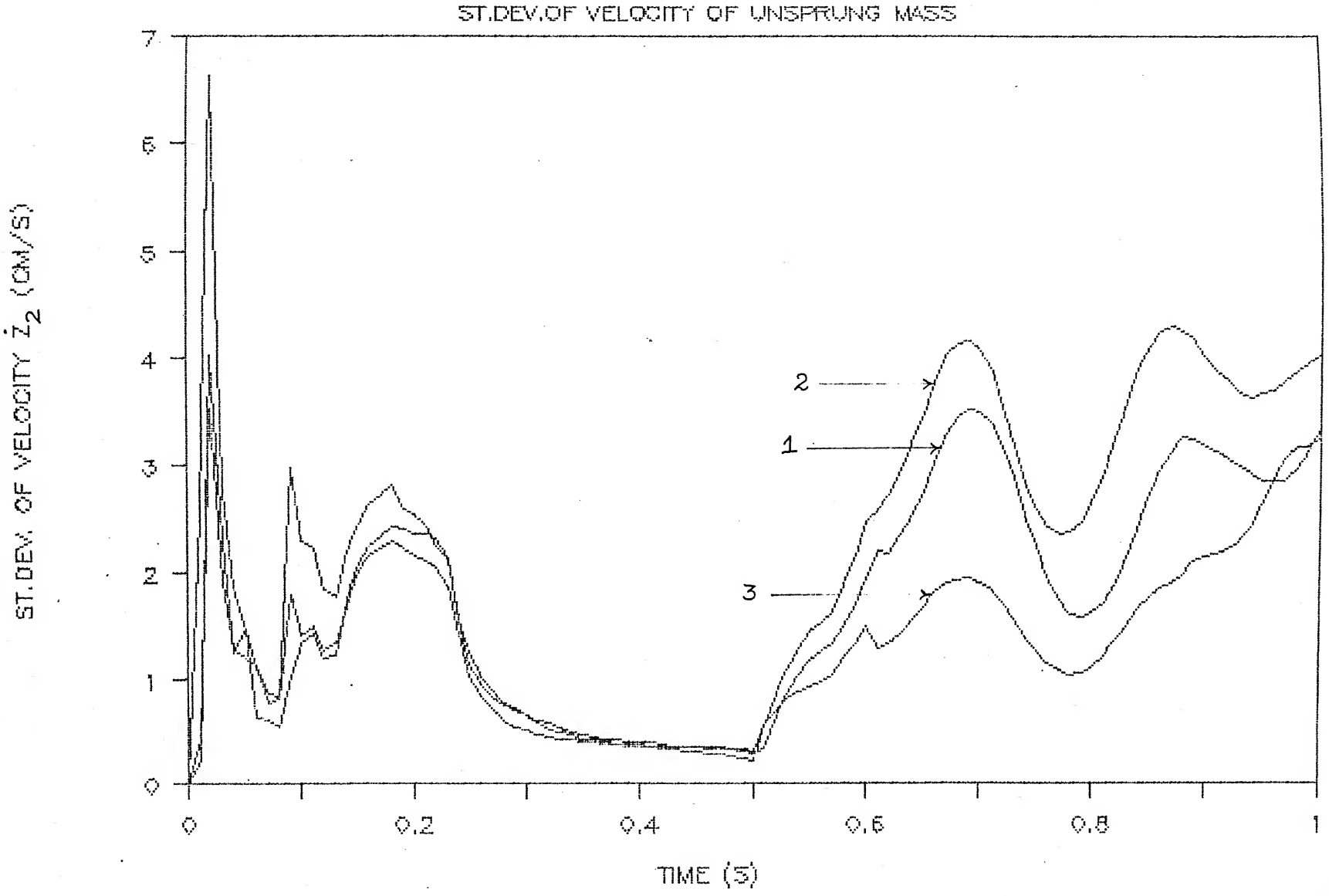

Fig. 4.4a Landing run,Roughness variation;Standard Deviation of Velocity Response.

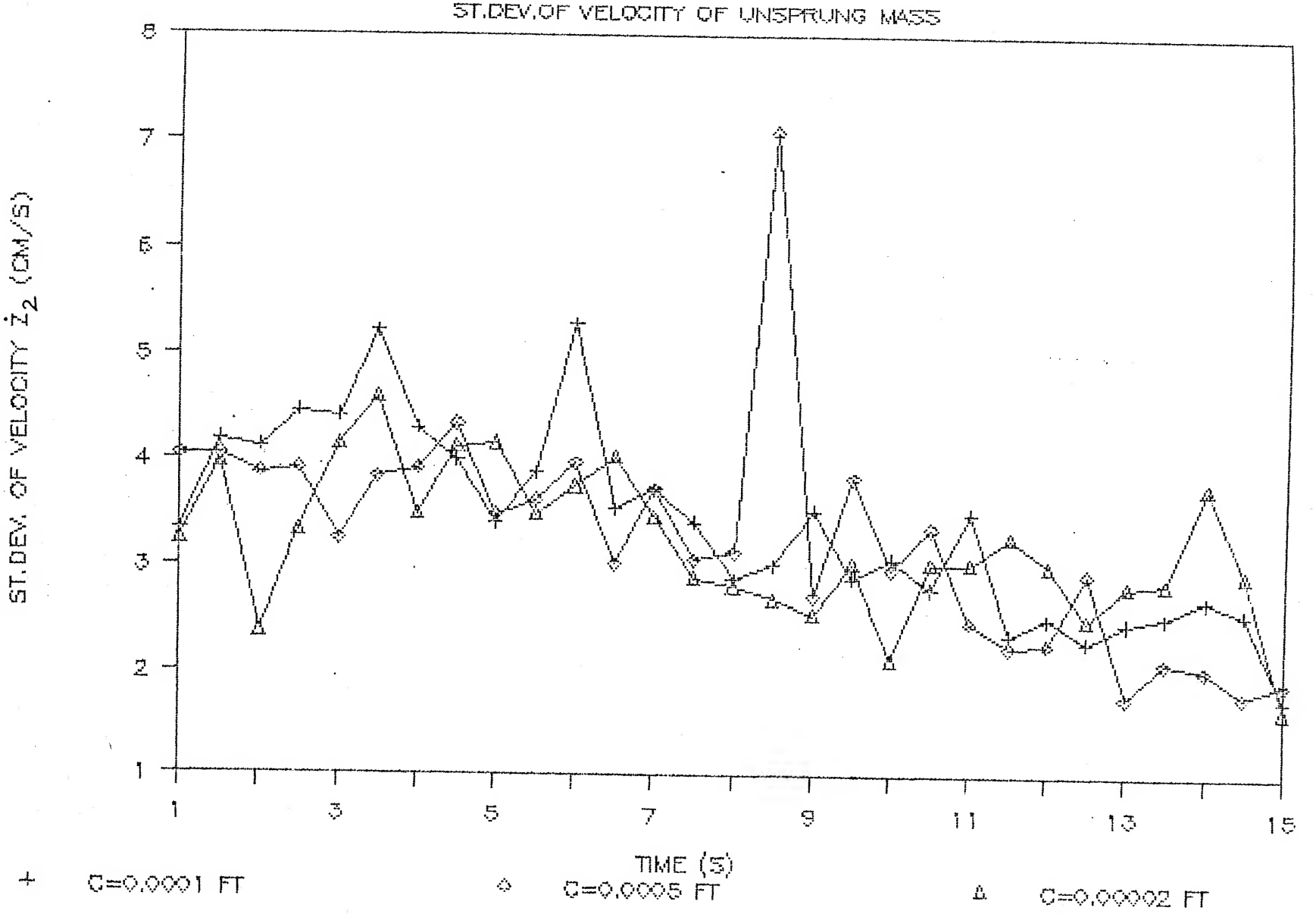

Fig. 4.4b Landing run, Roughness variation; Standard Deviation of Velocity Response.

ii) The broken up graph for one second duration shows the presence of five resonances at 0.025, 0.1, 0.2, 0.7 and 0.85 seconds.

iii) For a particular value of roughness constant, C = 0.0005 ft., there is a resonance at around 8.5 seconds, otherwise there is no significantly large variation due to the roughness. The value of the standard deviation of velocity drops as time progresses.

4.2.8. Standard Deviation of the Velocity of Sprung mass

The standard deviation of the velocity response of sprung mass is presented in Figures 4.4c and 4.4d. The salient points are :

i) Effect of roughness is more dominant for the first one second of the run.

ii) For the first one second resonances are observed at 0.2, 0.7 and 0.9 seconds.

iii) For the C value of 0.0005 ft. a peak is observed at 8.5 seconds.

iv) The value also decreases continuously with time and at 15 seconds is very close to 1 cm/s.

4.2.9. Mean Acceleration of the Unsprung mass

Figures 4.5a, 4.5b and 4.5c show the response of the mean acceleration of the unsprung mass. The main features of these

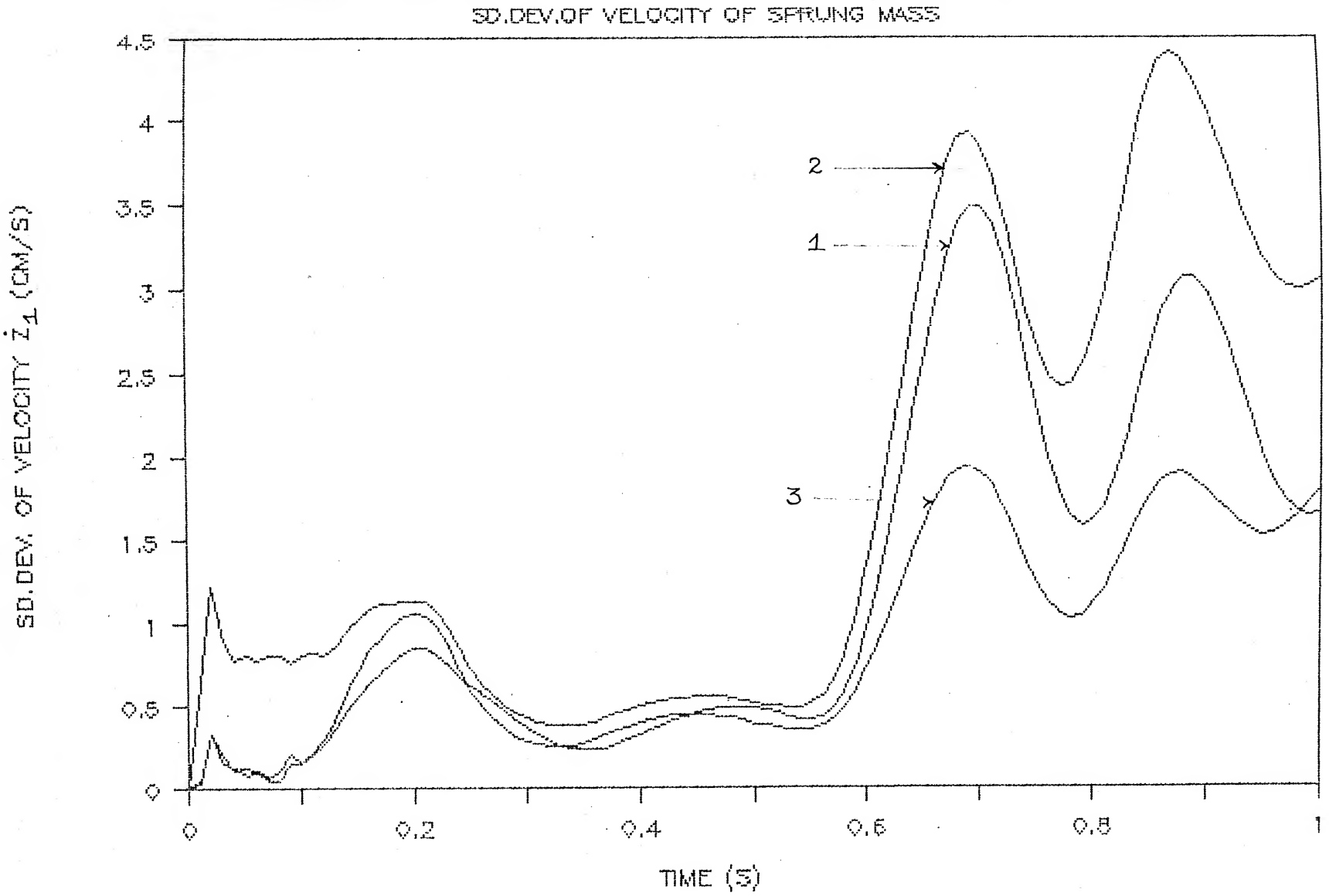

Fig. 4.4c Landing run,Roughness variation;Standard Deviation of Velocity Response.

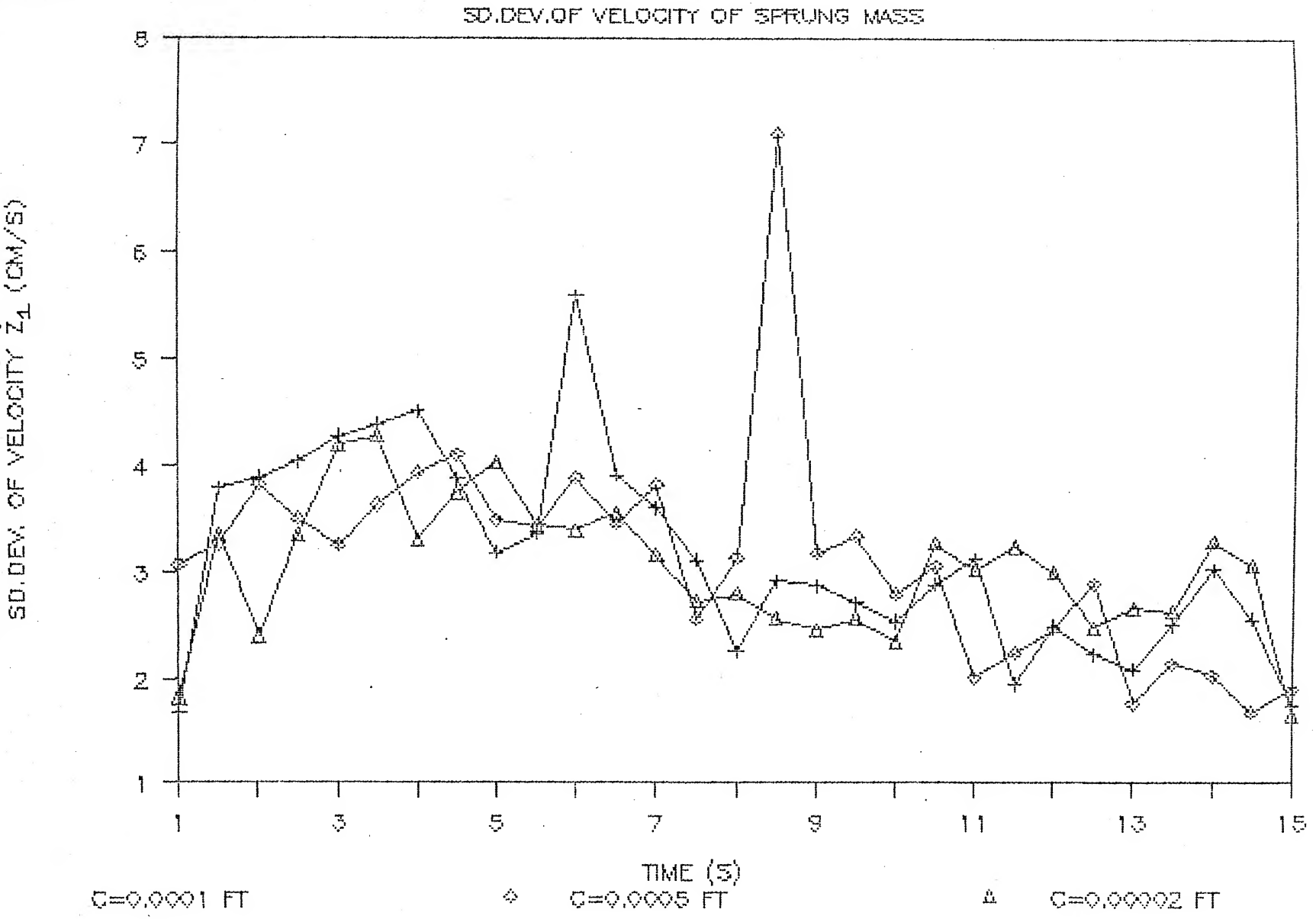

Fig. 4.4d Landing run,Roughness variation;Standard Deviation of Velocity Response.

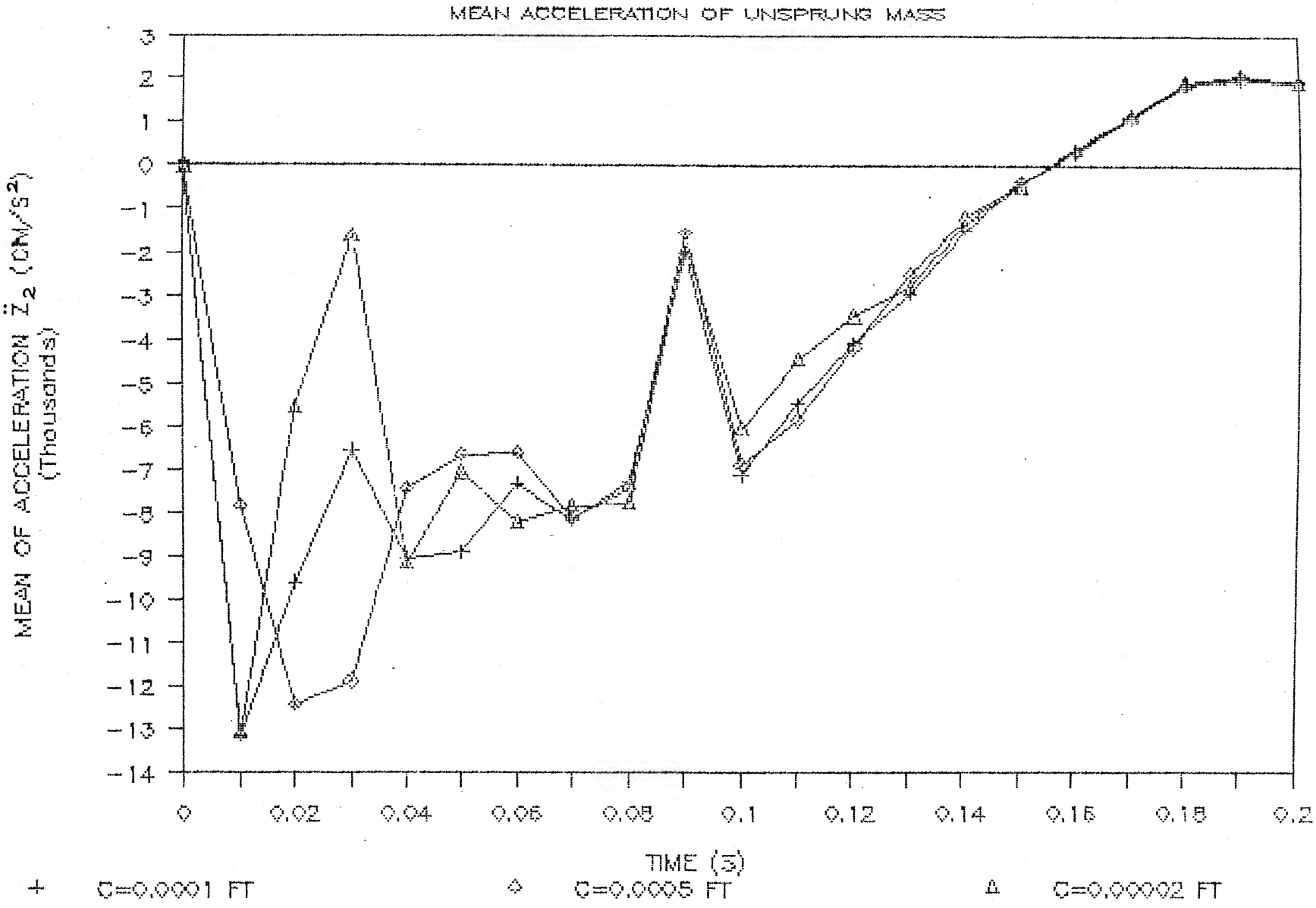

Fig. 4.5a Landing run,Roughness variation;Mean Acceleration Response.

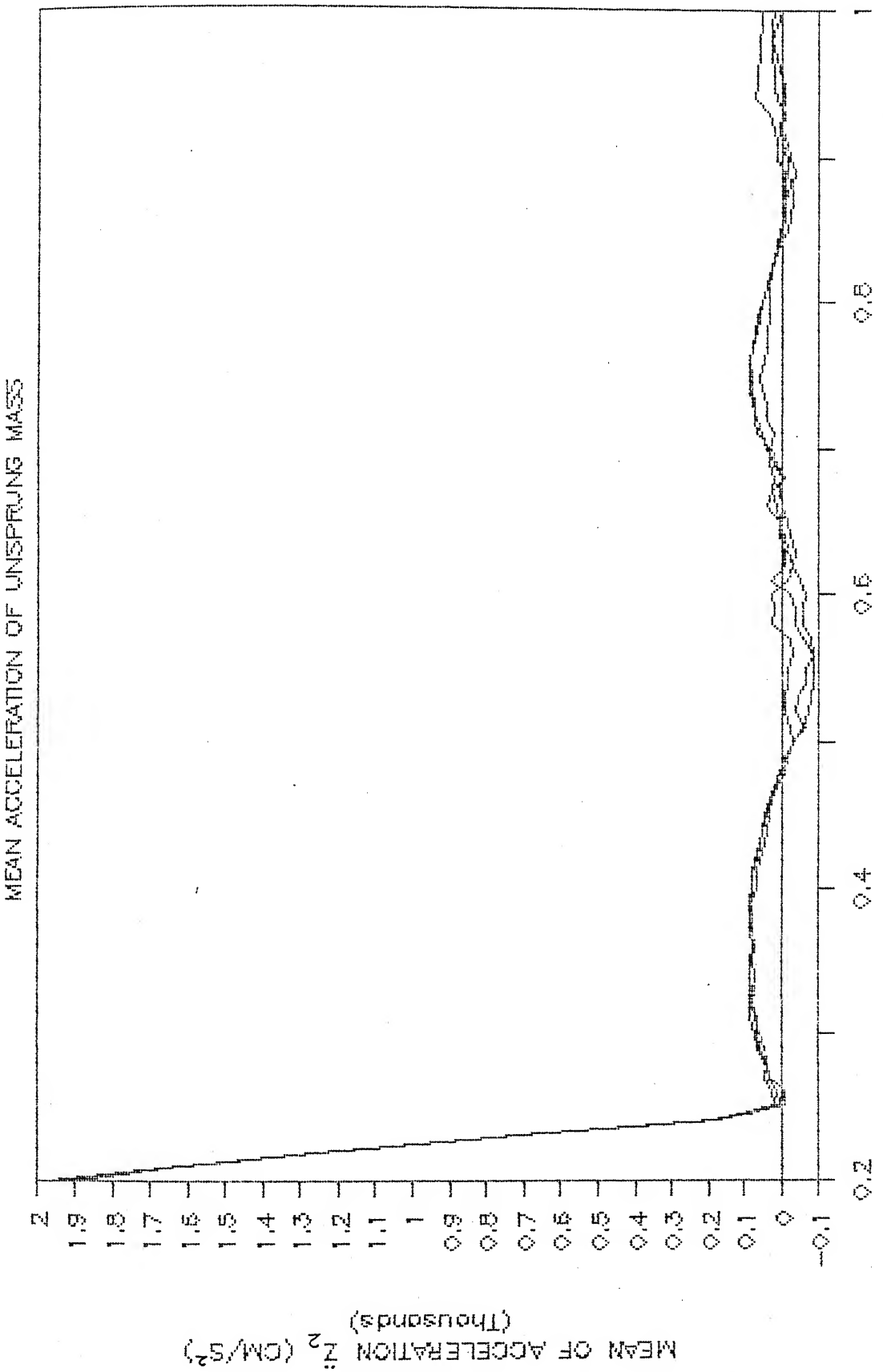

Fig. 4.5b Landing run,Roughness variation;Mean Acceleration Response.

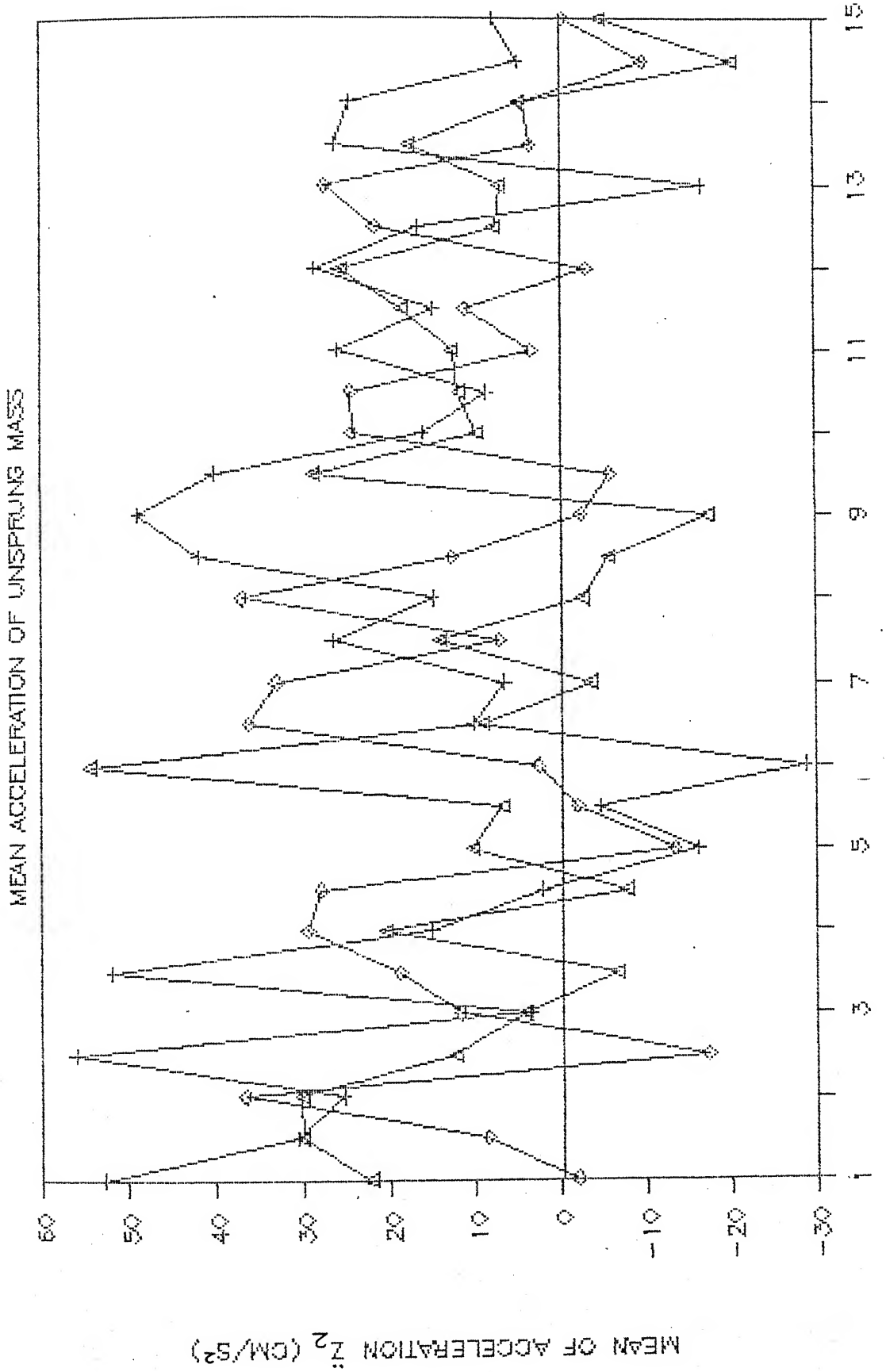

Fig. 4.5c Landing run, Roughness variation; Mean Acceleration Response.

figures are :

i) At the time of impact, the value of the mean acceleration is very high, roughly to the tune of 13 to 14 g values upwards. The negative sign indicates that instantaneously the force due to this acceleration tries to lift the wheel off the track.

ii) For the higher values of C, at C = 0.0005 ft and C = 0.0001 ft, a strong decrease in acceleration takes place at around 0.03 second and then once again there is a more steady drop after 0.04 second.

iii) Effect of the variation in roughness constant is not very dominantly observed.

iv) The value of the mean acceleration keeps on reducing and at 15 seconds it is close to 0.01 g.

4.2.10. Mean Acceleration of the Sprung mass

Figures 4.5d to 4.5f show the response of mean acceleration of sprung mass. The interesting points observed are :

i) Maximum value after impact is about 5.5 g, but it slowly keeps on reducing and subsequently steadies at 0.01 g.

ii) There is some effect of the variation in the roughness level of the track.

4.2.11. Standard Deviation of Acceleration of Unsprung mass

The response of standard deviation of acceleration of the

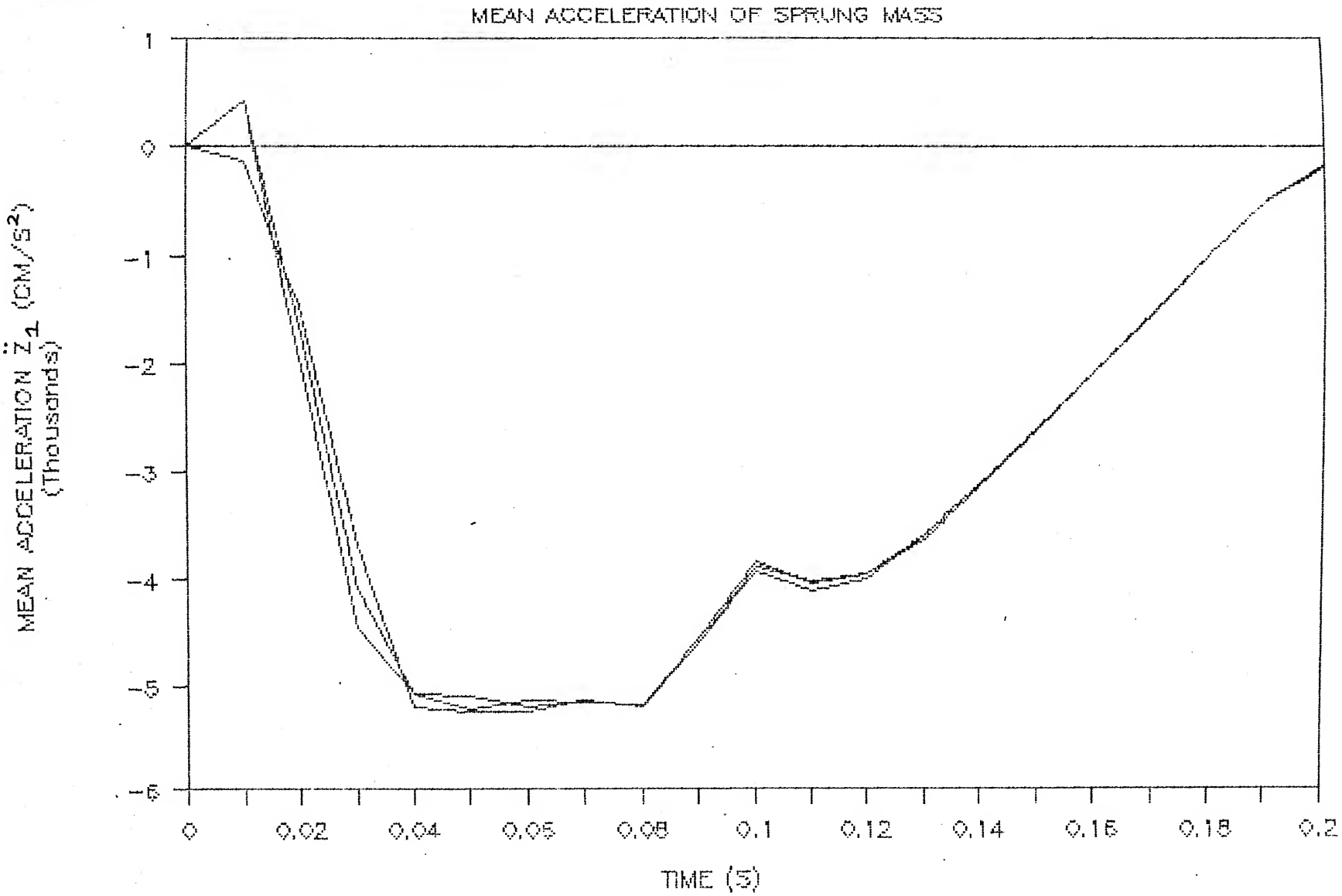

Fig. 4.5d Landing run,Roughness variation;Mean Acceleration Response.

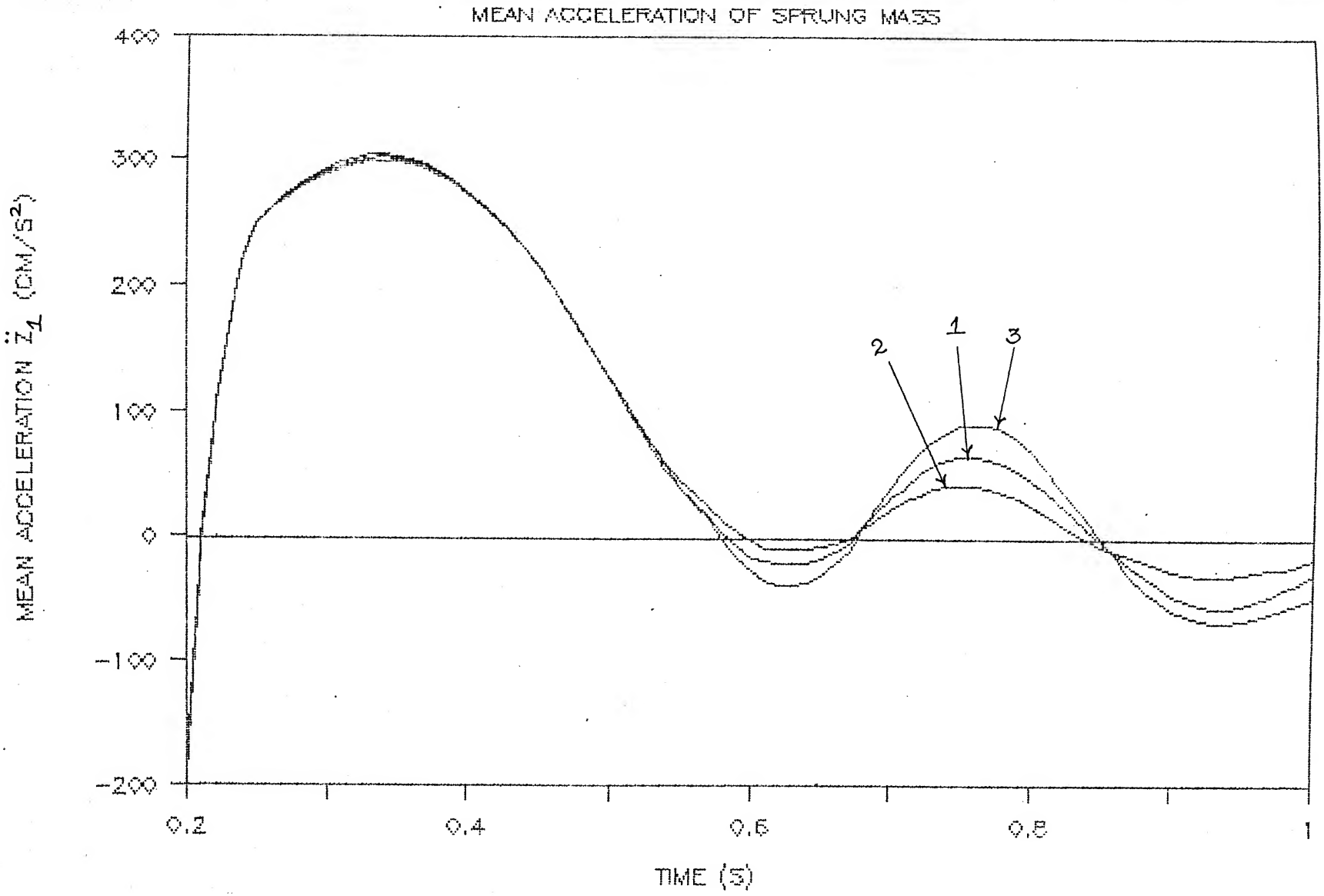

1 C=0.0001 FT 2 C=0.0005 FT 3 C=0.00002 FT

Fig. 4.5e Landing run,Roughness variation;Mean Acceleration Response.

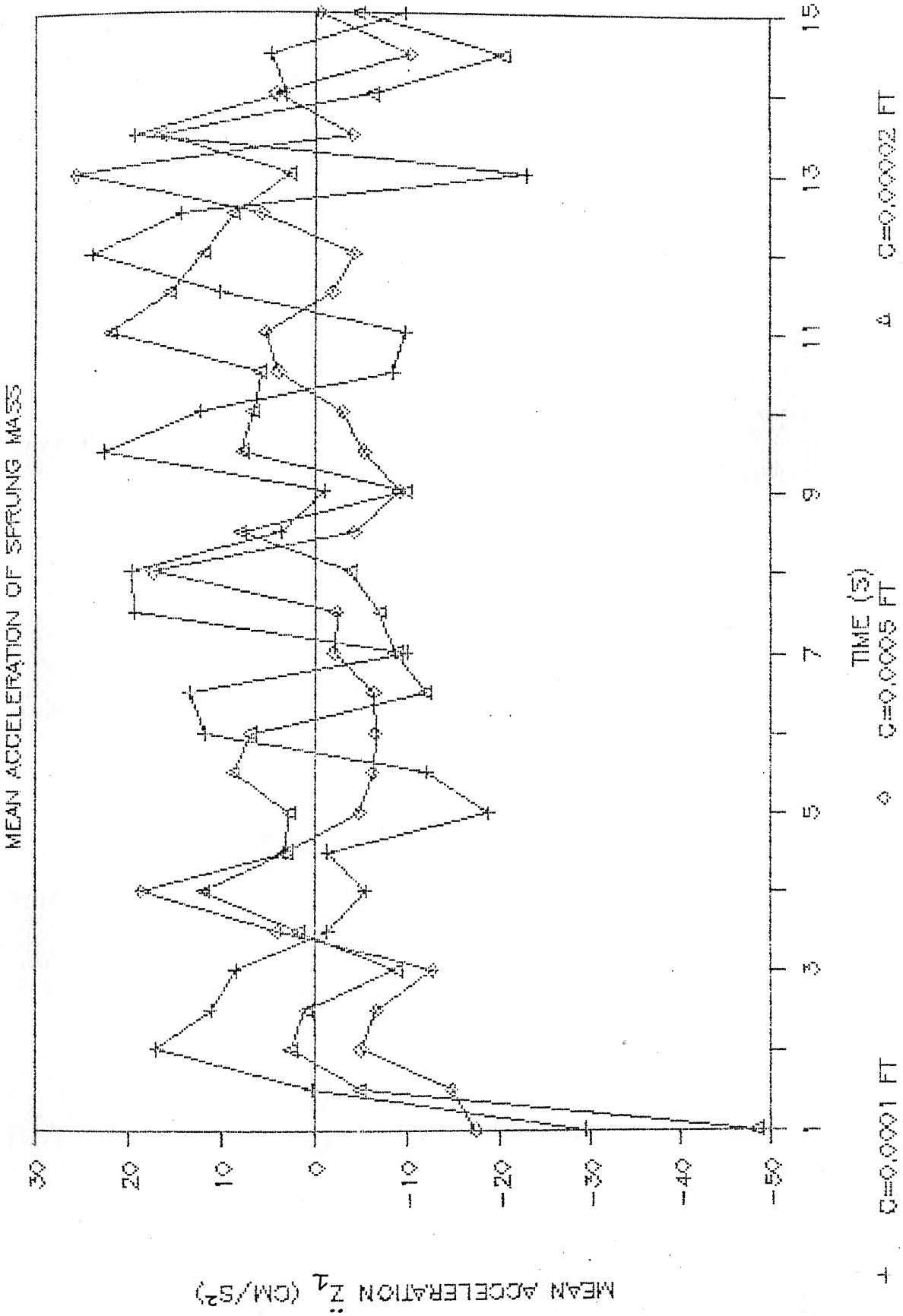

Fig. 4.5f Landing run,Roughness variation;Mean Acceleration Response.

unsprung mass is shown in Figures 4.6a to 4.6c. The observations are :

i) Upto a time of 0.04 seconds after touchdown the value is very high, around 13 to 14 g.

ii) The effect of roughness is also visibly observed upto 0.04 second and from 0.6 to 1 second.

iii) Resonance is observed at 0.6 and 0.95 seconds.

iv) The value keeps on decreasing as time passes and from 1 to 15 seconds there does not seem to be a strong influence of roughness level.

4.2.12. Standard Deviation of Acceleration of Sprung mass

Figures 4.6d to 4.6f show the standard deviation of acceleration response of the sprung mass. The points of interest are :

i) Similar observations are made as for the unsprung mass with the only difference being the numerical values. The maximum value is about 1.2 g.

ii) Resonance levels are also less than that for the unsprung mass.

4.3 *Landing Run with Variation in Sink Velocity*

For studying the effect of the variation of the sink velocity at touchdown, the value of the roughness constant was kept unchanged at 0.0001 ft. The mean slope is maintained unchanged at

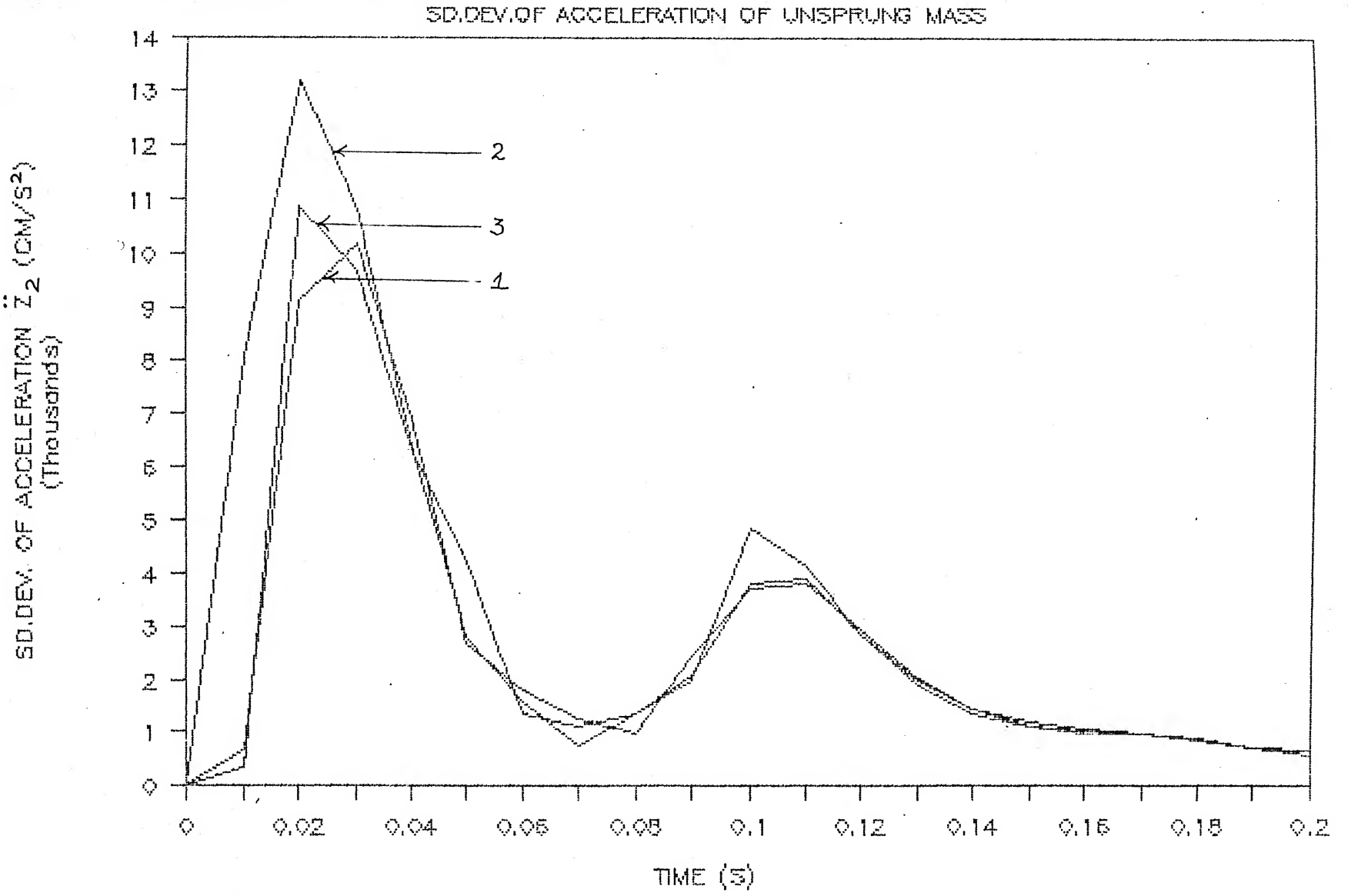

Fig. 4.6a Landing run,Roughness variation;Standard Deviation of Acceleration Response.

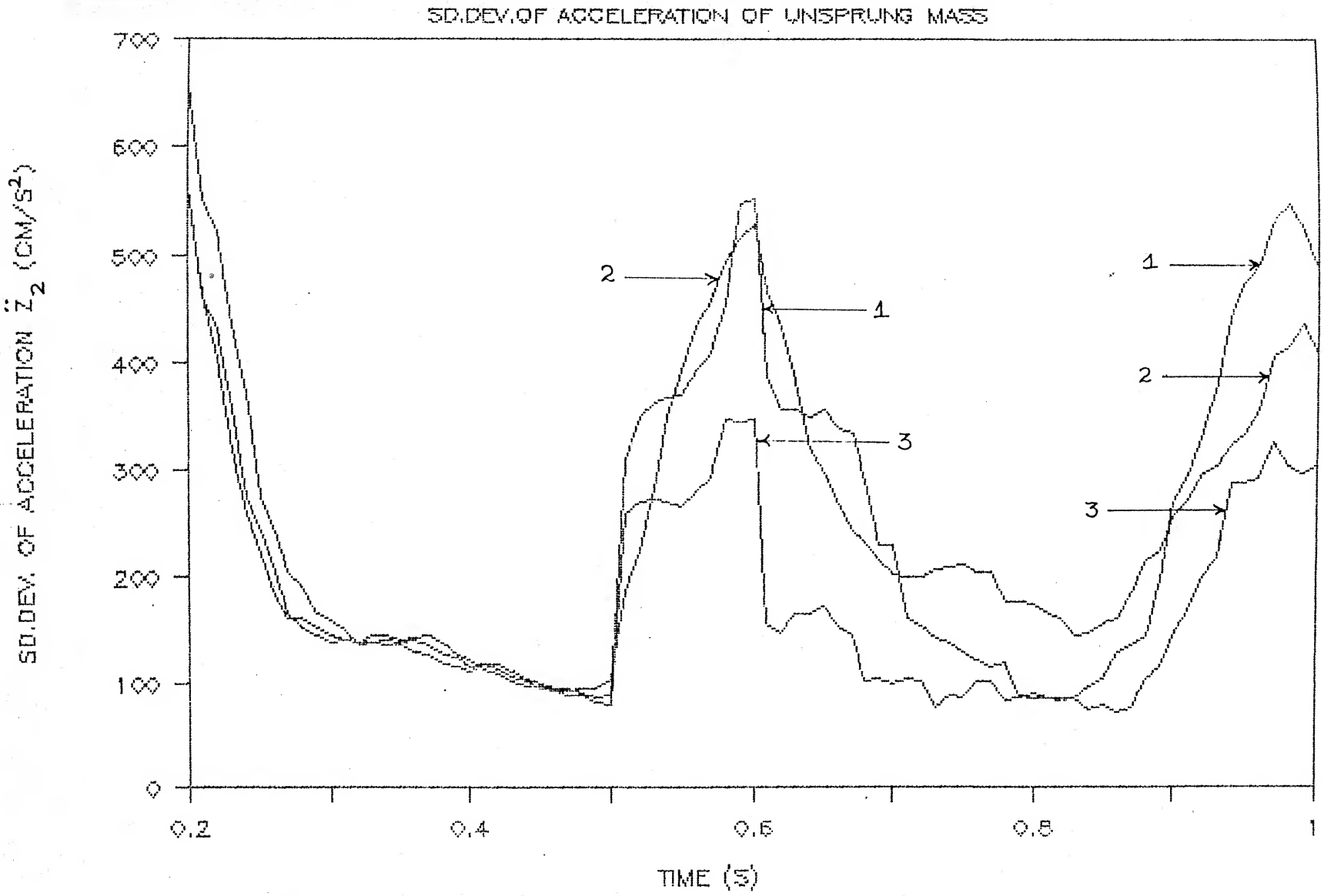

Fig. 4.6b Landing run,Roughness variation;Standard Deviation of Acceleration Response.

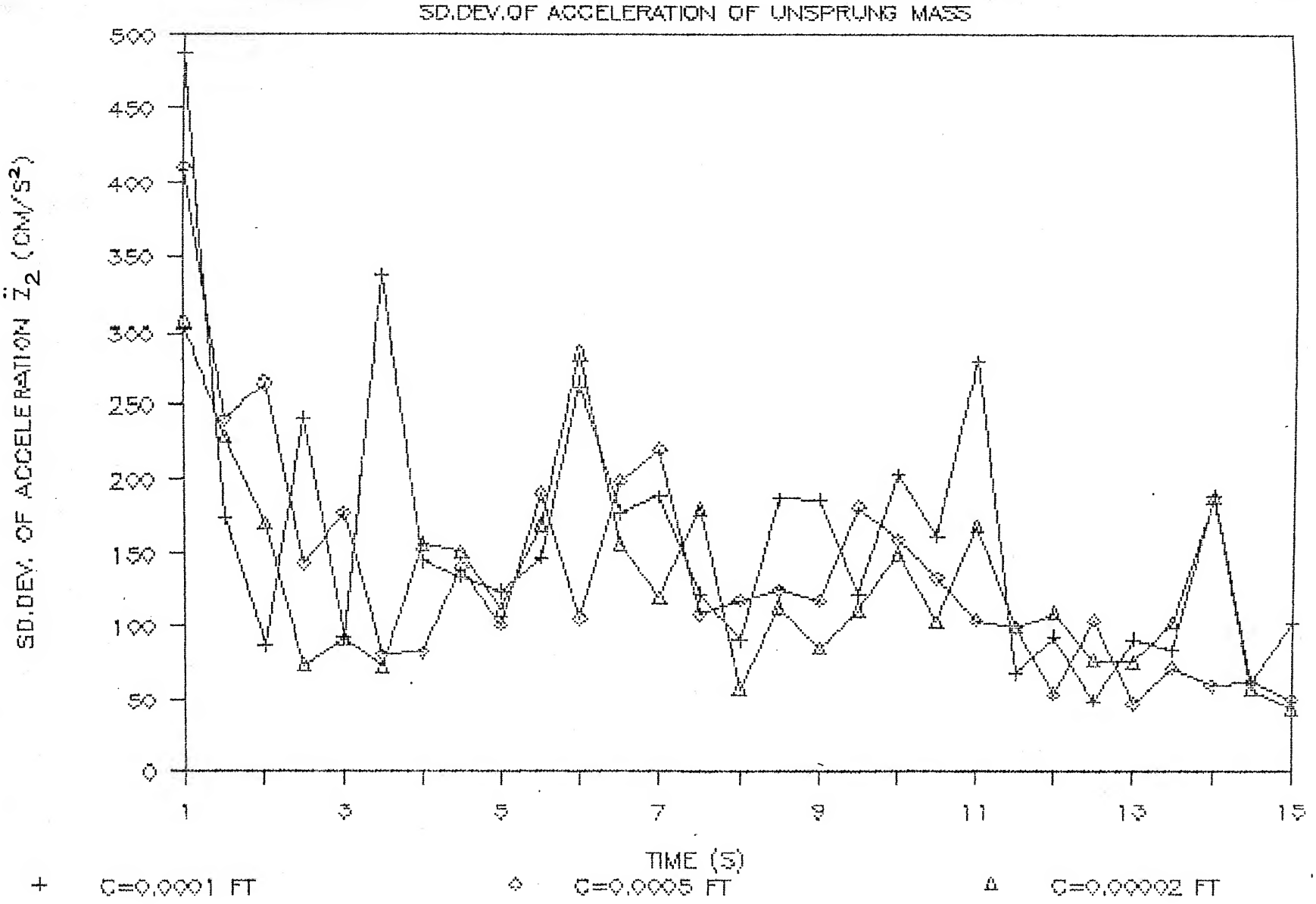

Fig. 4.6c Landing run,Roughness variation;Standard Deviation of Acceleration Response.

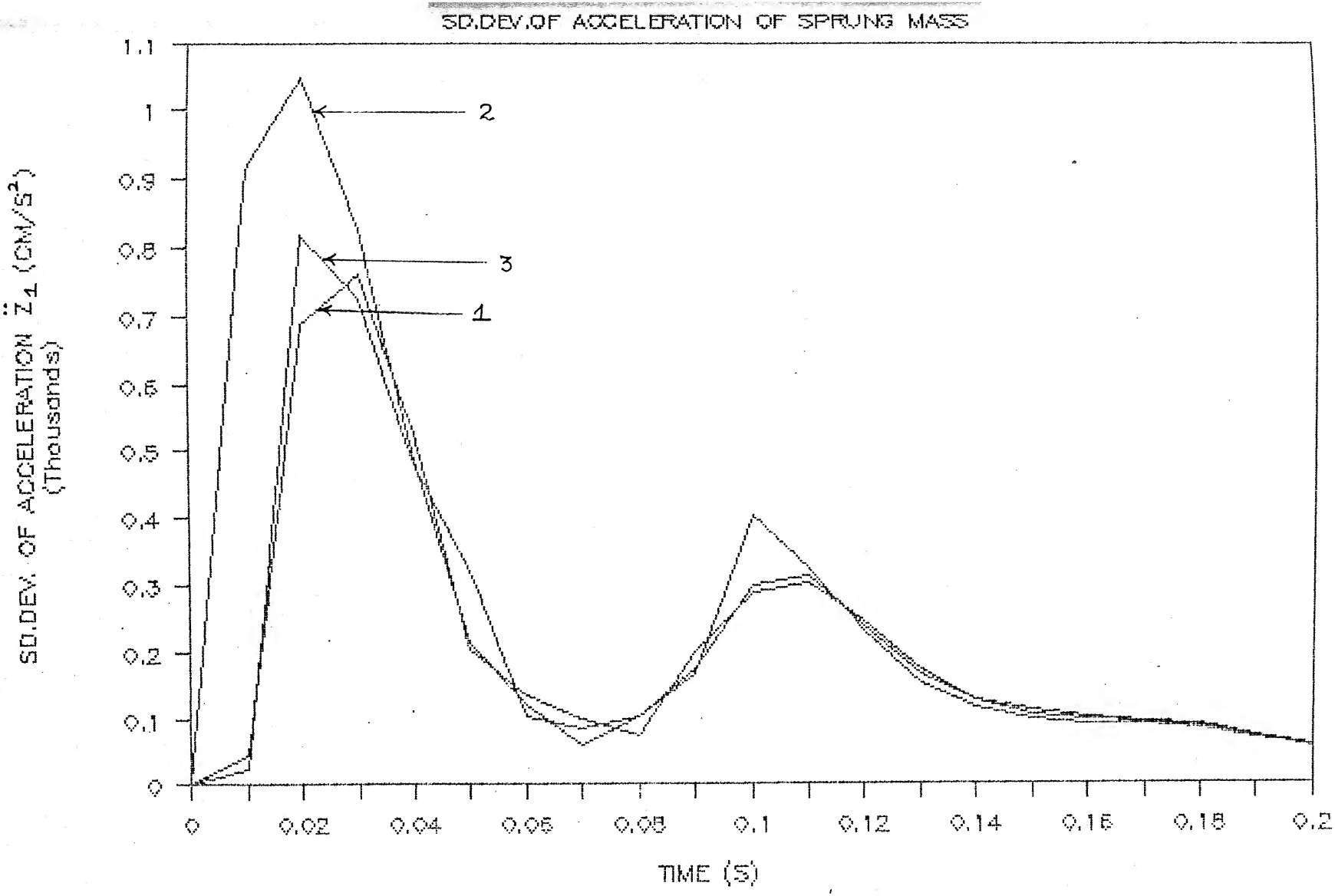

1 C=0.0001 FT 2 C=0.0005 FT 3 C=0.00002 FT

Fig. 4.6d Landing run,Roughness variation;Standard Deviation of Acceleration Response.

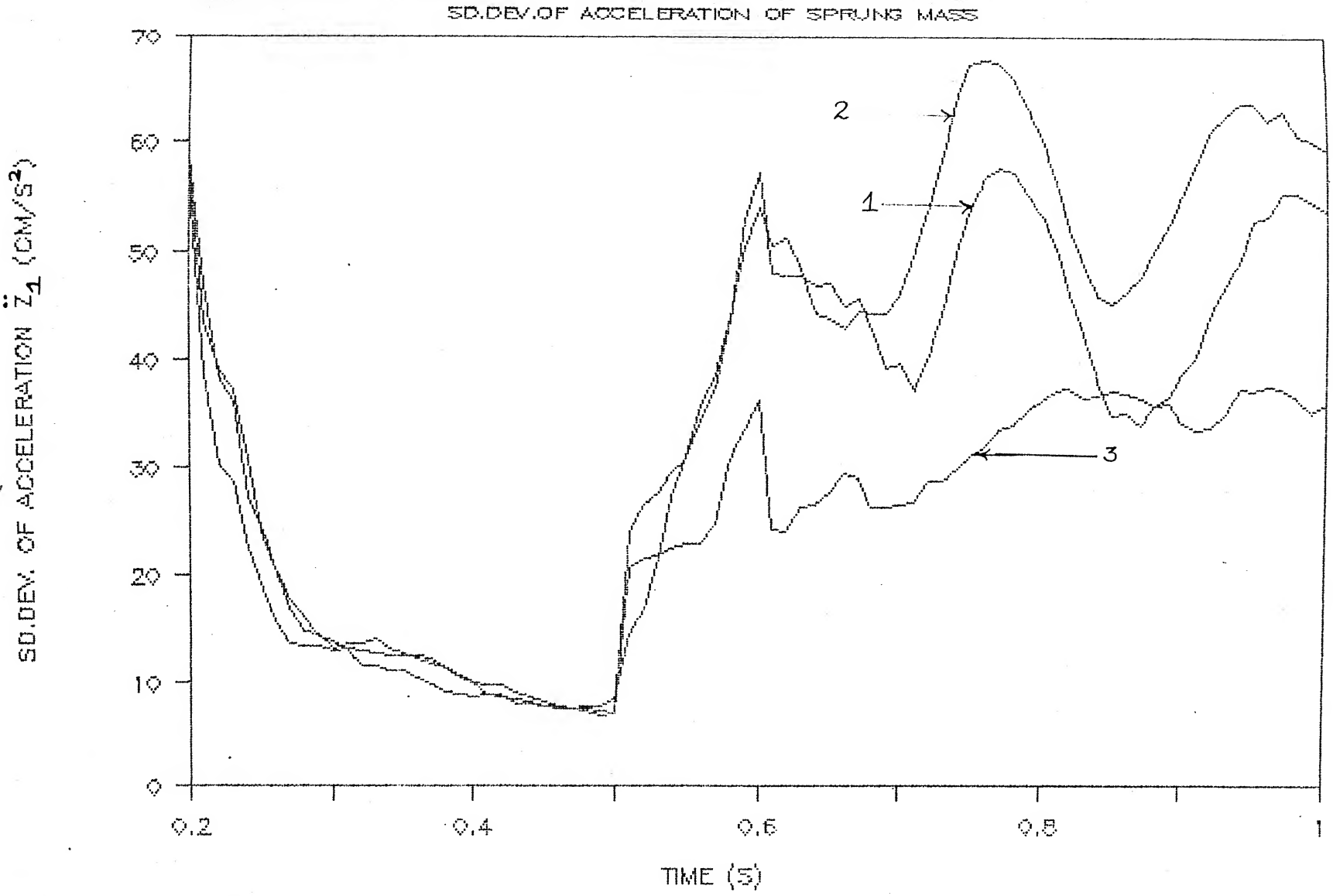

Fig. 4.6e Landing run,Roughness variation;Standard Deviation of Acceleration Response.

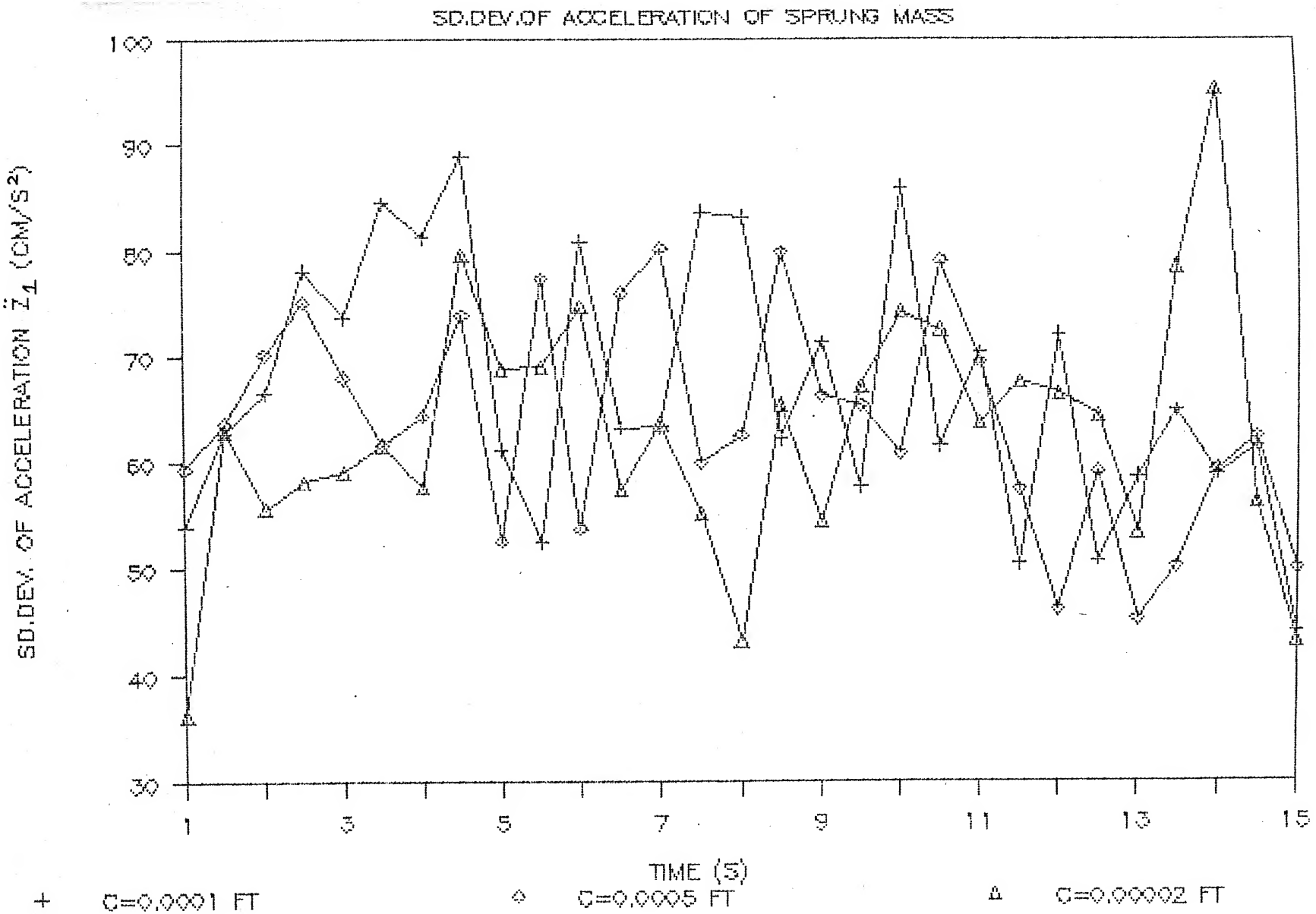

Fig. 4.6f Landing run,Roughness variation;Standard Deviation of Acceleration Response.

1 in 1000. The values of the sink velocity are taken as 350, 250 and 100 cm/s.

4.3.1 Mean Displacement of the Unsprung mass

The response of the mean displacement of the unsprung mass is portrayed in Figures 4.7a and 4.7b. The salient points worth noting are :

i) The variation in the sink velocity has a marked effect on the maximum mean displacement of the unsprung mass. The effect is very clearly observed upto a time of 0.6 second after touchdown.

ii) As time progresses the heaving reduces considerably and after about 1 second the motion of the unsprung mass settles down and follows the mean slope.

iii) Once touchdown is affected the aircraft does not get airborne and there is no balooning.

4.3.2 Mean Displacement of the Sprung mass

Figures 4.7c and 4.7d show the response of the mean displacement of the sprung mass. The points worth mentioning are :

i) The effect of the variation in the sink velocity of the aircraft at touchdown is very clearly noticeable for a time duration of 0.7 second after touchdown. But later on this effect is not predominant.

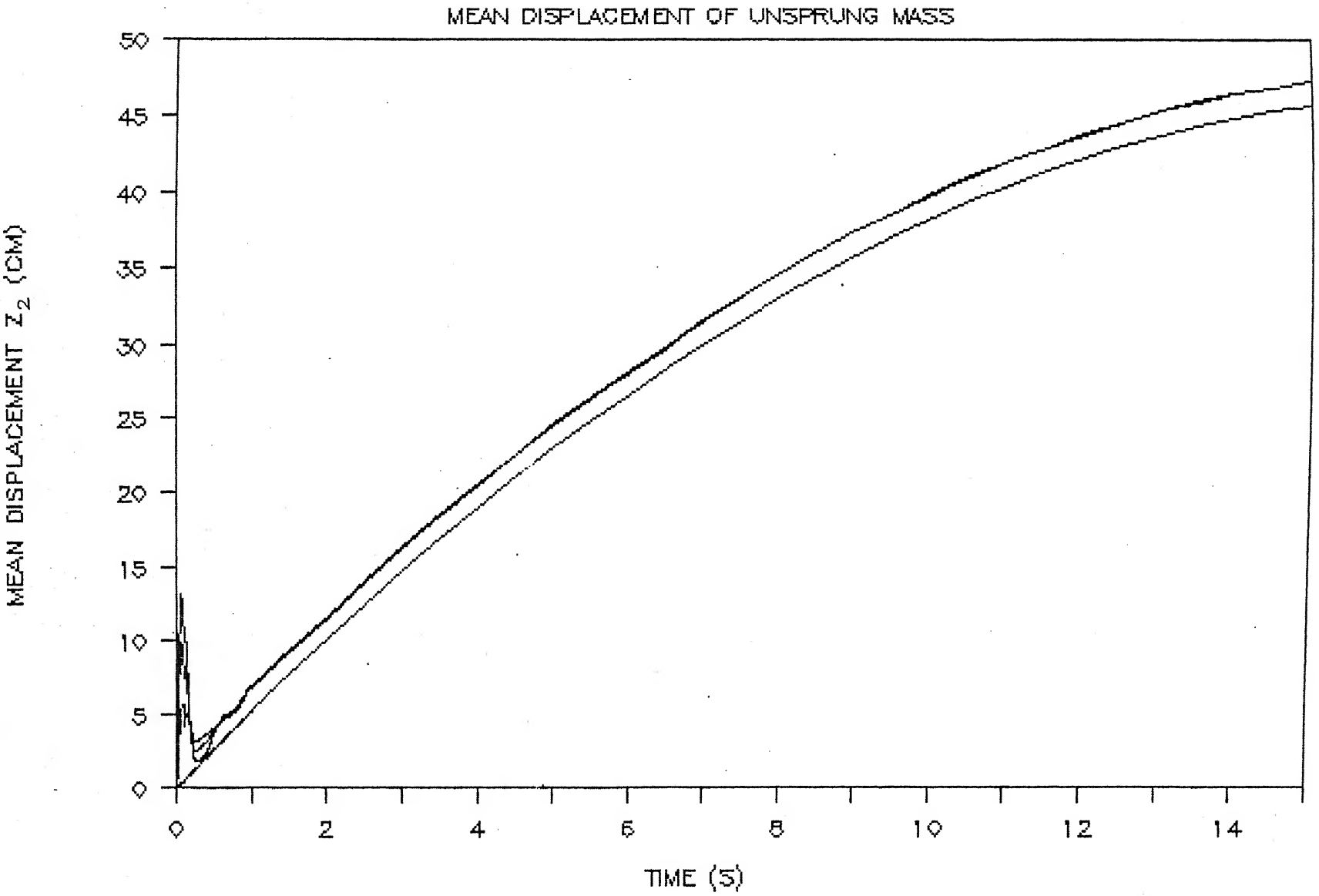

Fig. 4.7a Landing run, Sink Velocity variation; Mean Displacement Response.

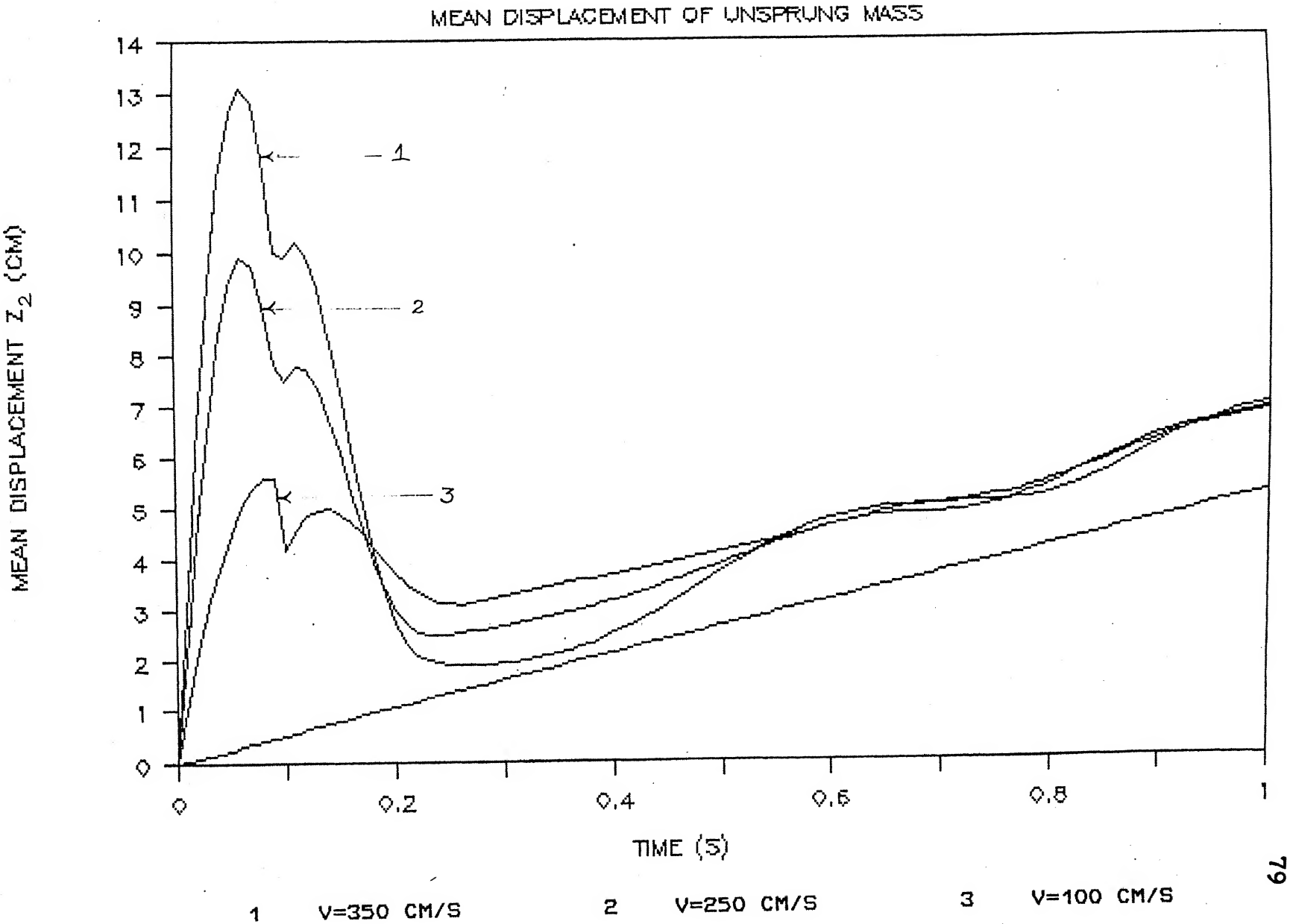

Fig. 4.7b Landing run, Sink Velocity variation; Mean Displacement Response.

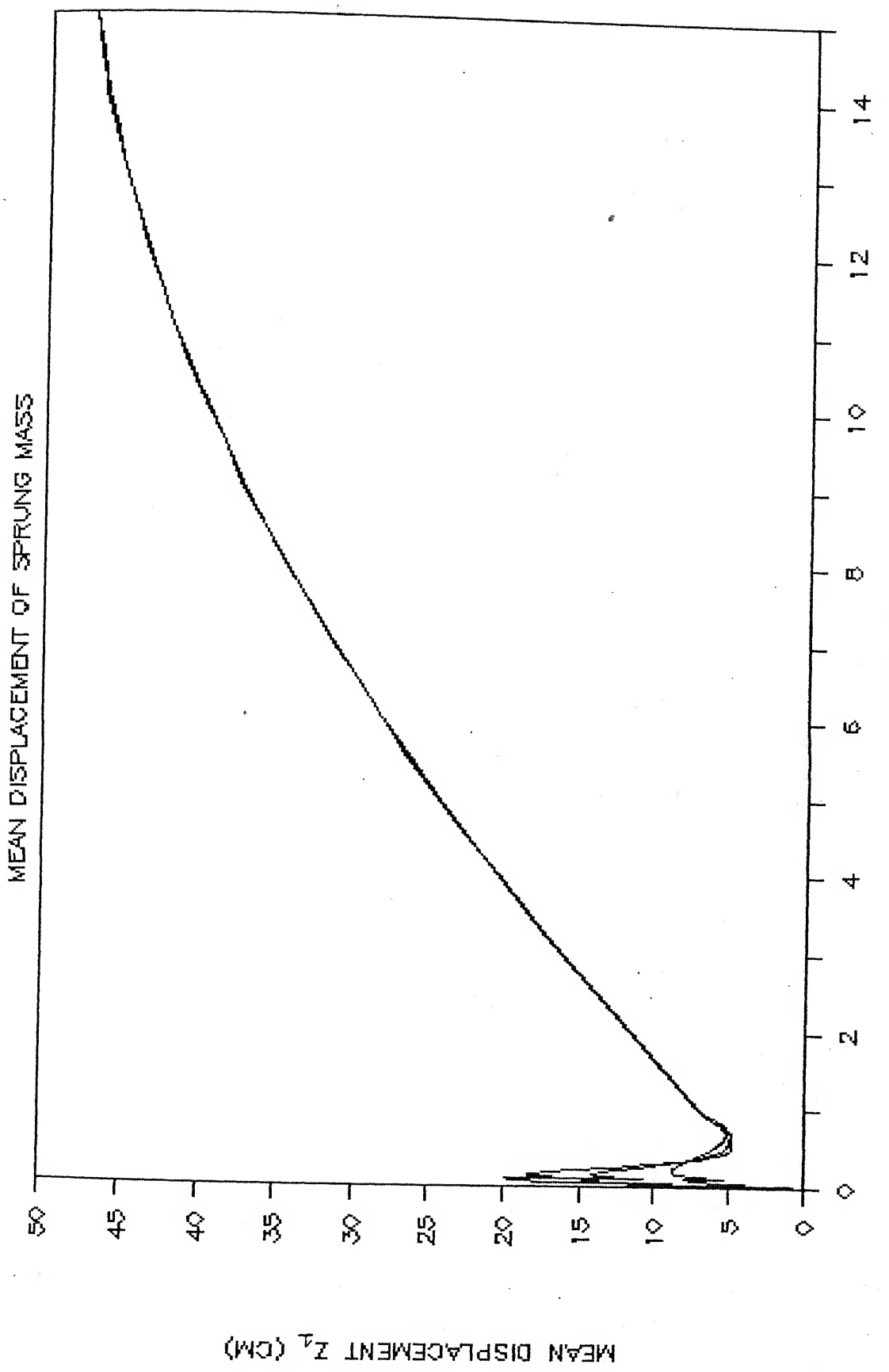

Fig. 4.7c Landing run, Sink Velocity variation; Mean Displacement Response.

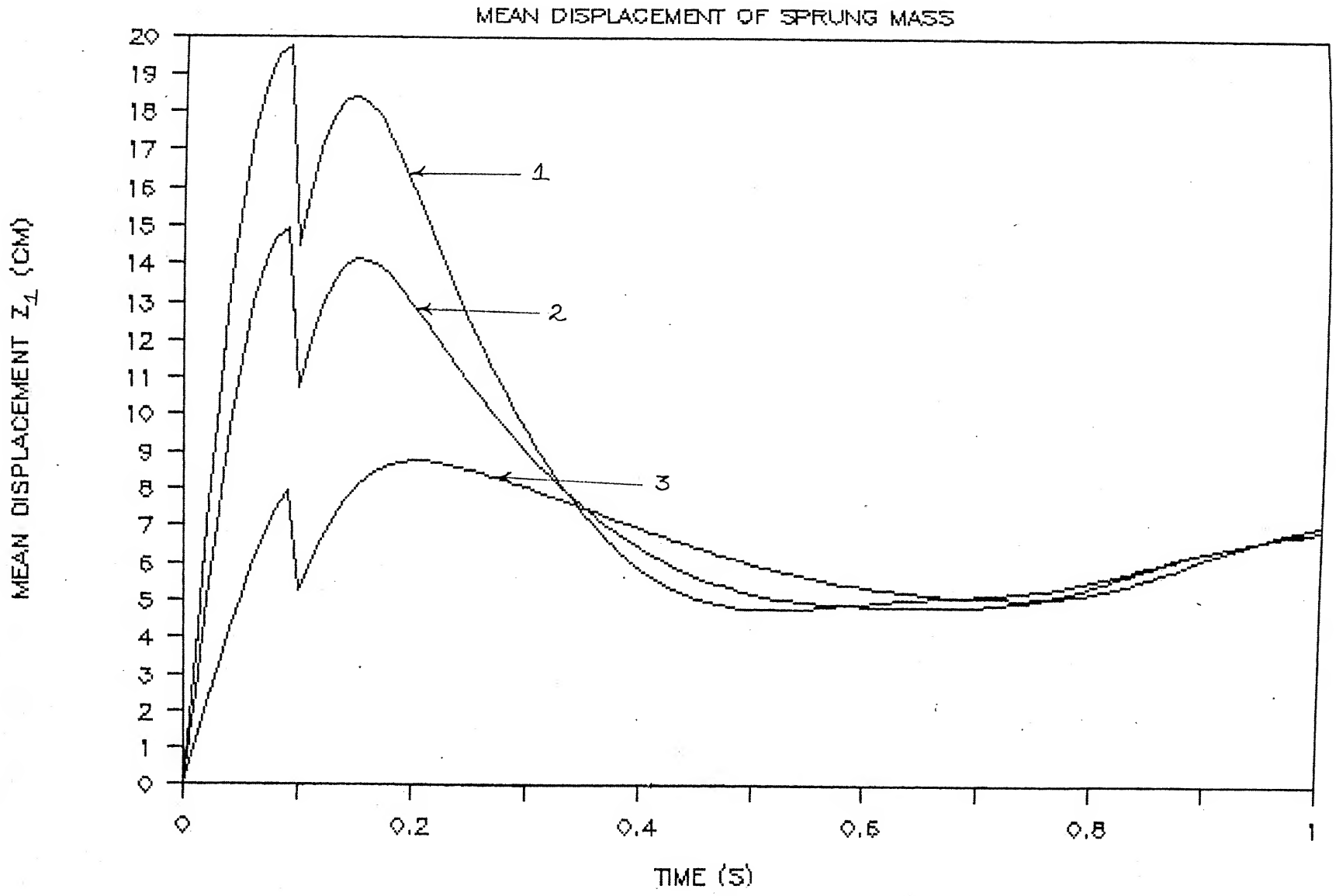

Fig. 4.7d Landing run, Sink Velocity variation; Mean Displacement Response.

ii) The mean displacement response reaches a maximum at 0.1 sec after touchdown. Subsequently, it drops and shows a resonance at 0.2 sec. This behaviour is observed for all the three sink velocities considered.

iii) At higher sink velocities of 350 and 250 cm/s the resonance value is smaller than that at the impact peak. The difference between these two grows smaller with reduction in the sink velocity. At the sink velocity of 100 cm/s the resonance value becomes higher than the impact peak.

4.3.3 Standard Deviation of the Displacement of Unsprung mass

The response of the standard deviation of the unsprung mass is shown in Figures 4.8a and 4.8b. The points observed are :

i) The effect of the variation in the sink velocity of the aircraft is clearly visible.

ii) Resonance of the displacement occurs very sharply at V_s = 350 cm/s at around 0.8 second after touchdown.

iii) The numerical value of the standard deviation of displacement shows a decreasing trend as time passes during the course of the run. This is true for all the sink velocities studied.

4.3.4 Standard Deviation of the Displacement of Sprung Mass

The response of the standard deviation of displacement of the sprung mass is shown in figures 4.8c and 4.8d. Some salient

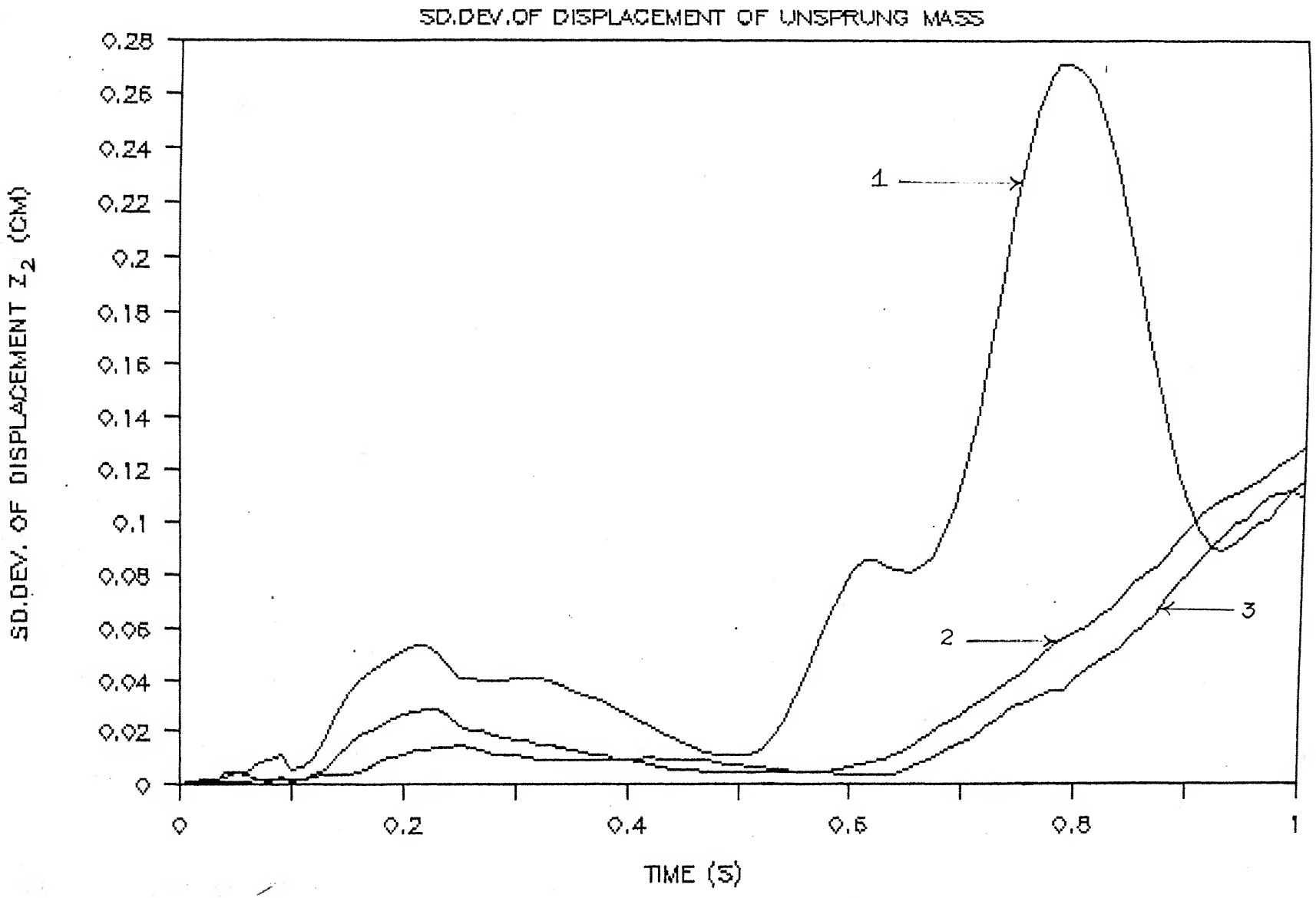

1 V=350 CM/S 2 V=250 CM/S 3 V=100 CM/S

Fig. 4.8a Landing run,Sink Velocity variation; Standard Deviation of Displacement Response.

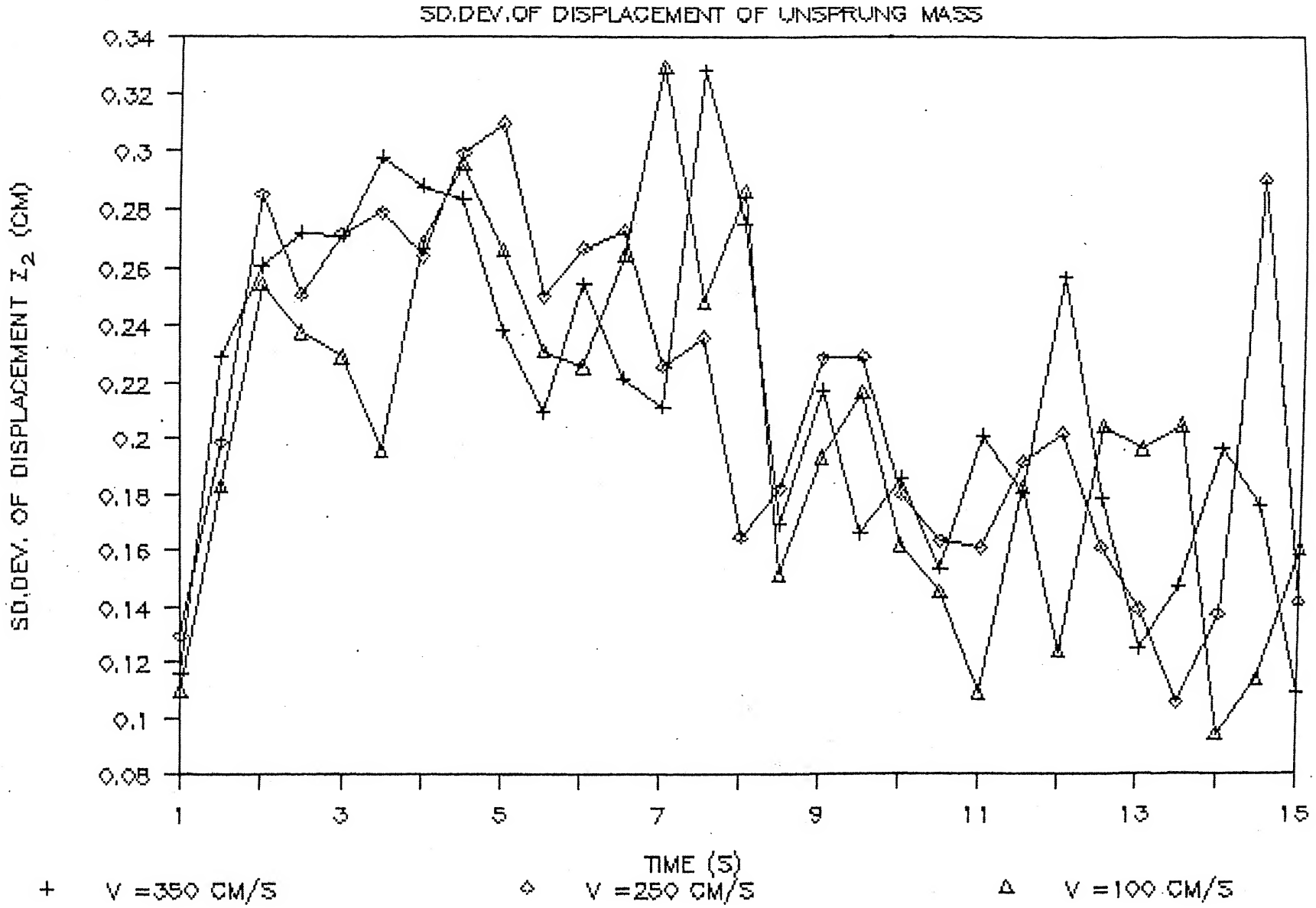

Fig. 4.8b Landing run,Sink Velocity variation; Standard Deviation of Displacement Response.

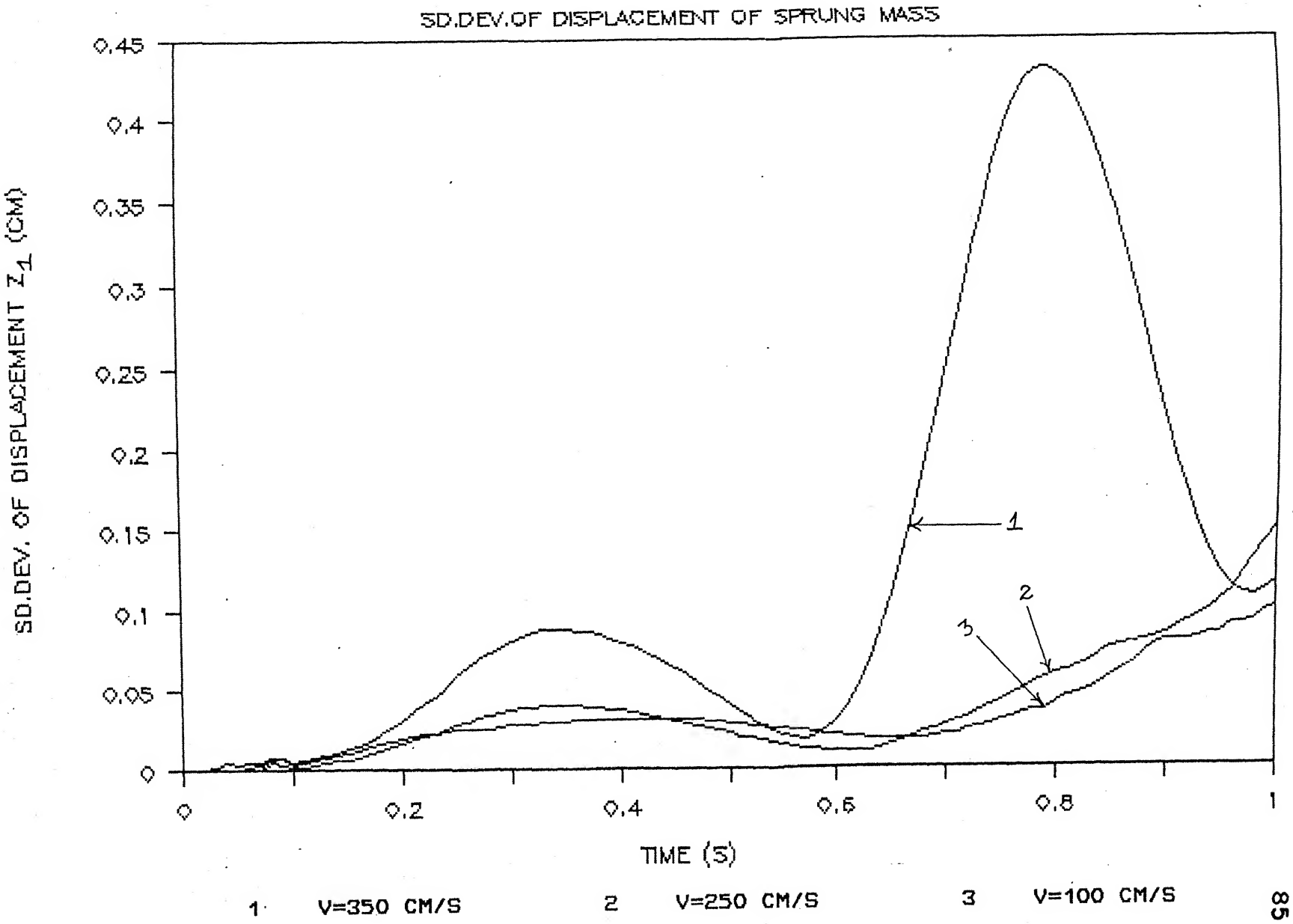

Fig. 4.8c Landing run,Sink Velocity variation; Standard Deviation of Displacement Response.

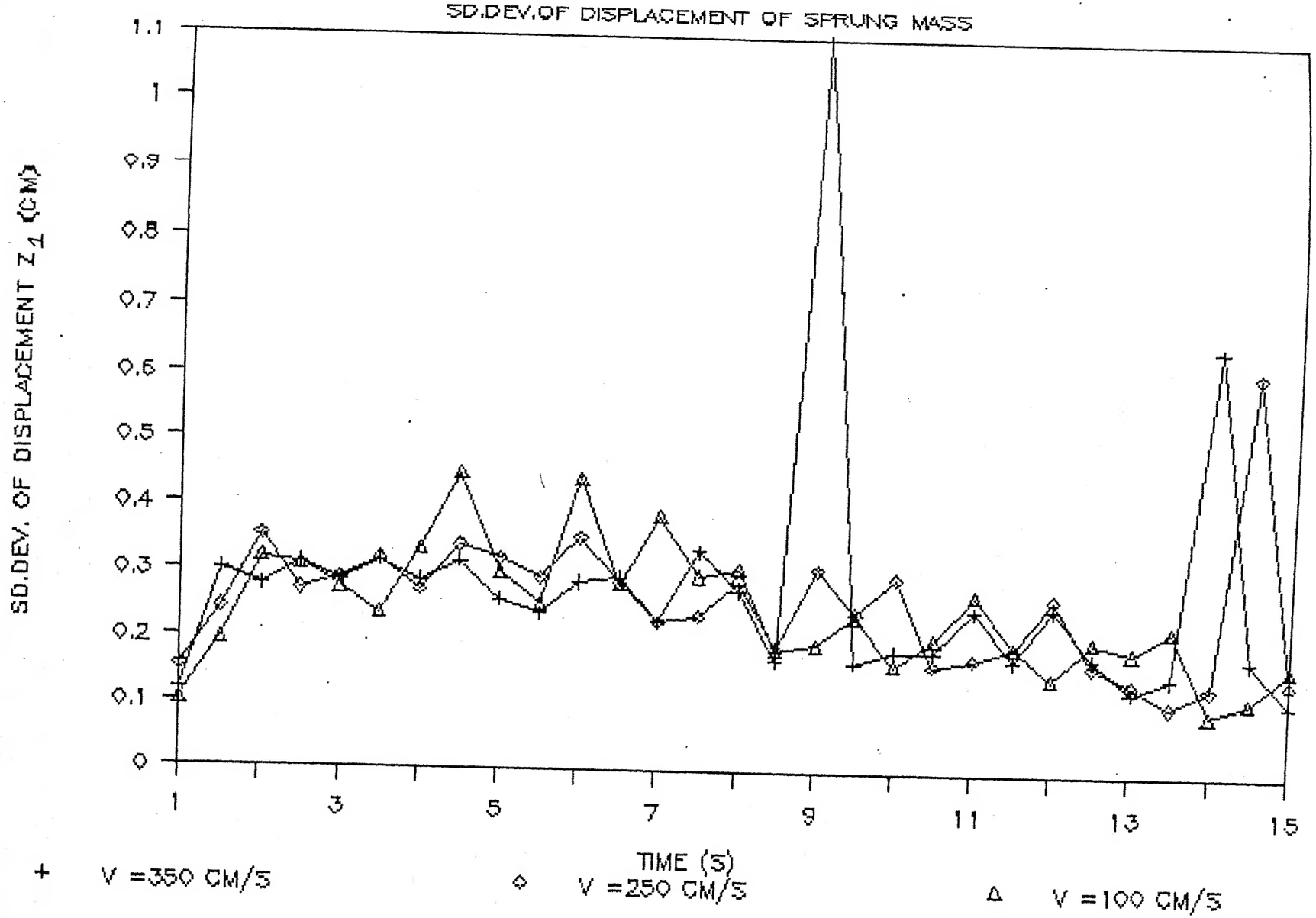

Fig. 4.8d Landing run,Sink Velocity variation; Standard Deviation of Displacement Response.

points are :

i) The effect of the variation in the sink velocity is clearly brought out. As for the time duration of upto 1 second after touchdown it is clearly seen that higher values of sink velocities give higher values of displacement, the same cannot be said confidently for the time duration of 1 to 15 seconds.

ii) A sudden sharp peak value occurs for the sink velocity of 350 cm/s at 0.8 second after touchdown. Two more resonance peaks are observed at 9 seconds and at 12 seconds.

iii) The trend for the standard deviation is a decreasing one for all the sink velocities considered.

4.3.5 Mean Velocity of Unsprung mass

The response for the mean velocity of the unsprung mass is presented in Figures 4.9a to 4.9c. The points observed are :

i) The variation in the sink velocity affects the mean velocity of the unsprung mass.

ii) After a time duration of 0.3 second the mean velocity keeps on fluctuating about the zero level.

4.3.6 Mean Velocity of the Sprung mass

Figures 4.9d to 4.9f depict the response of the mean velocity of the sprung mass. The observations made are :

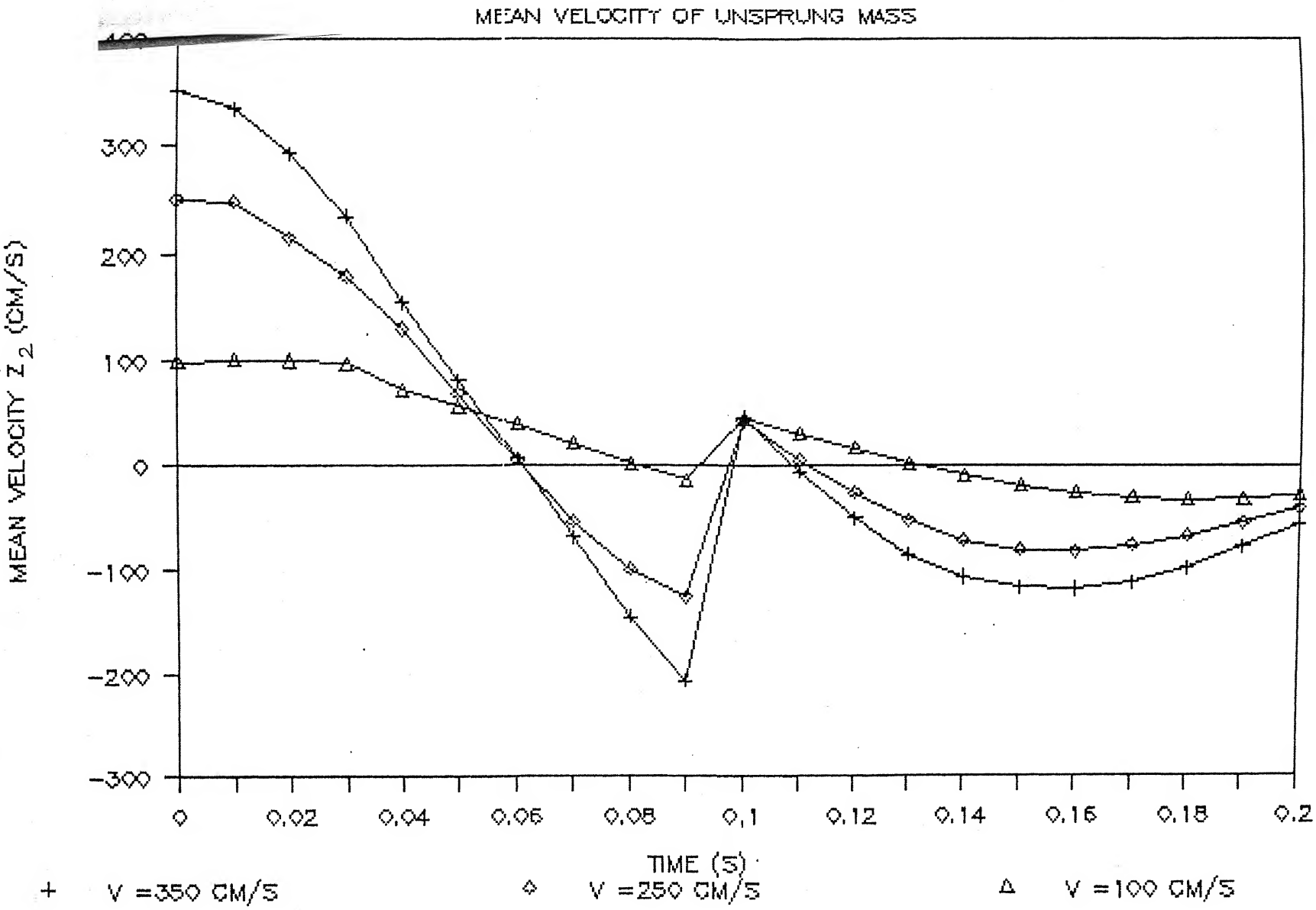

Fig. 4.9a Landing run,Sink Velocity variation;Mean Velocity Response.

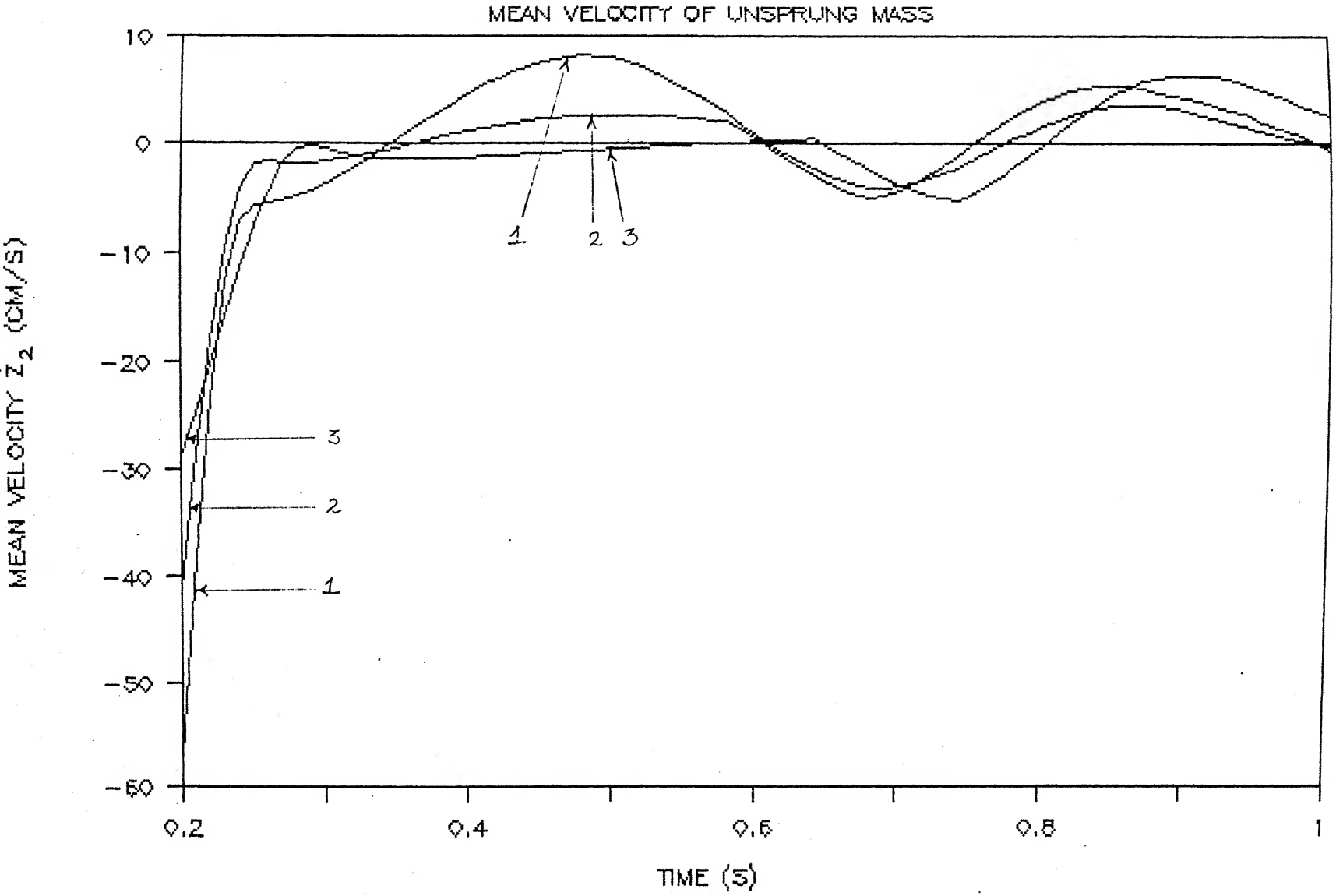

Fig. 4.9b Landing run,Sink Velocity variation;Mean Velocity Response.

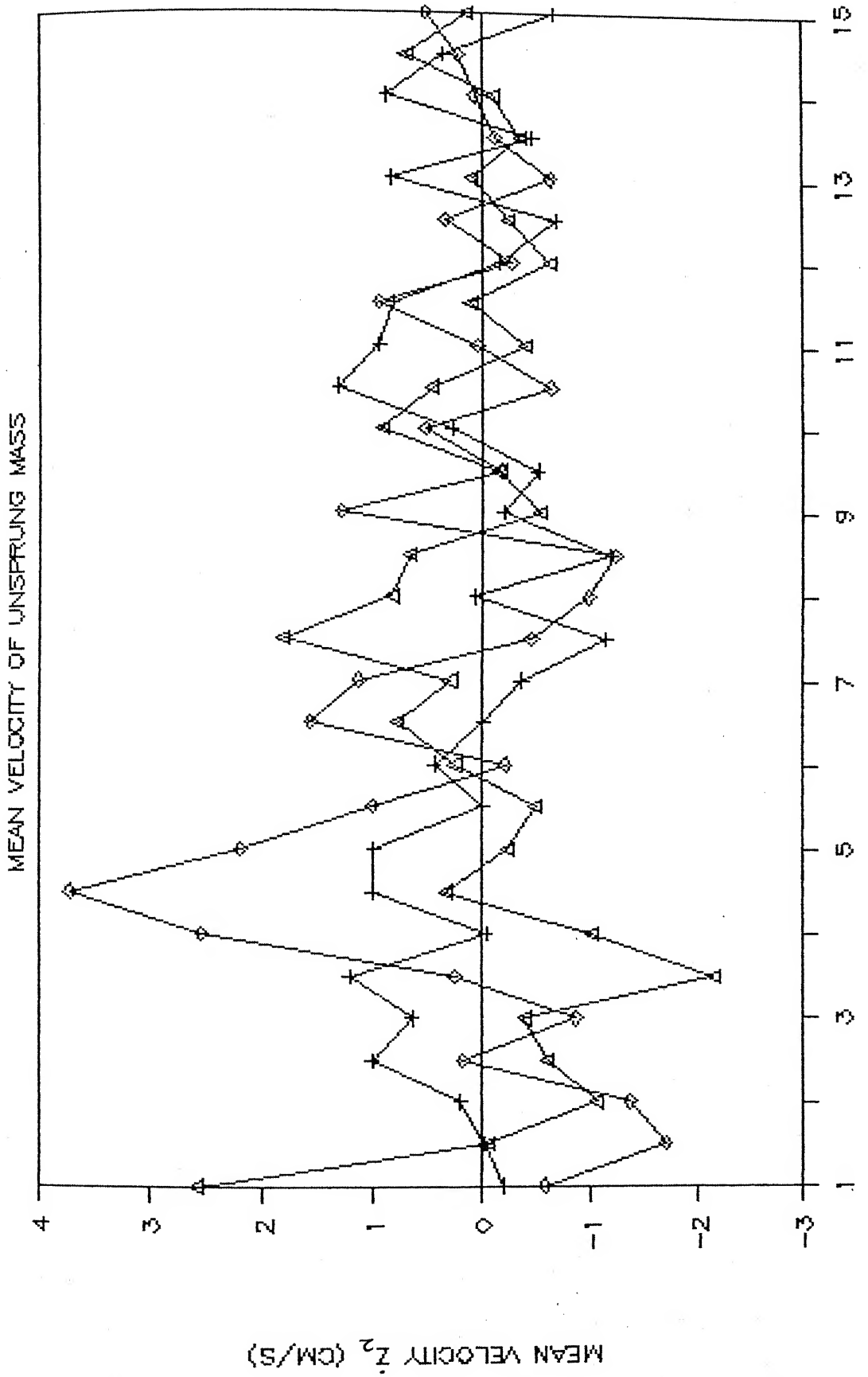

Fig. 4.9c Landing run,Sink Velocity variation;Mean Velocity Response.

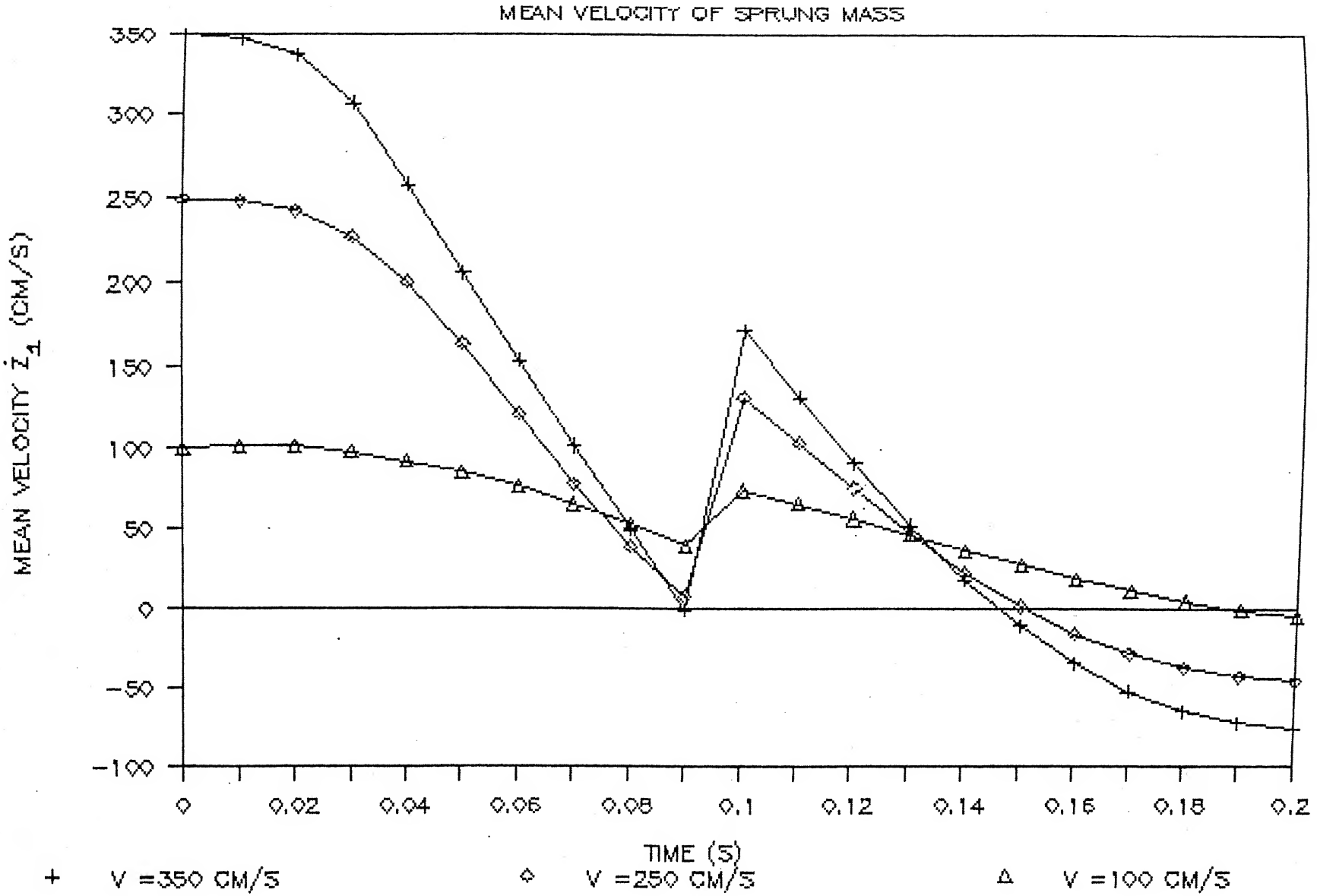

Fig. 4.9d Landing run,Sink Velocity variation;Mean Velocity Response.

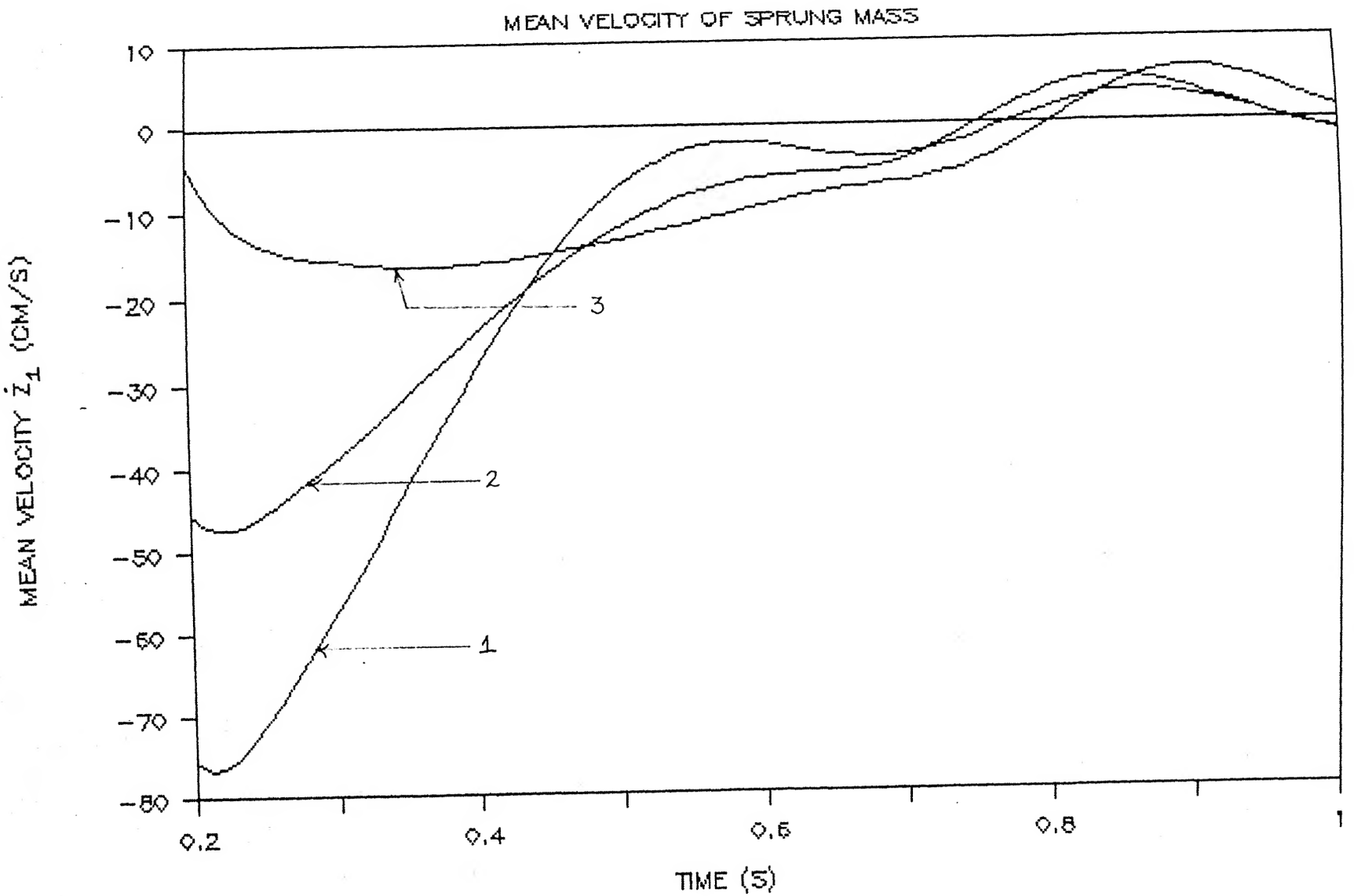

Fig. 4.9e Landing run,Sink Velocity variation;Mean Velocity Response.

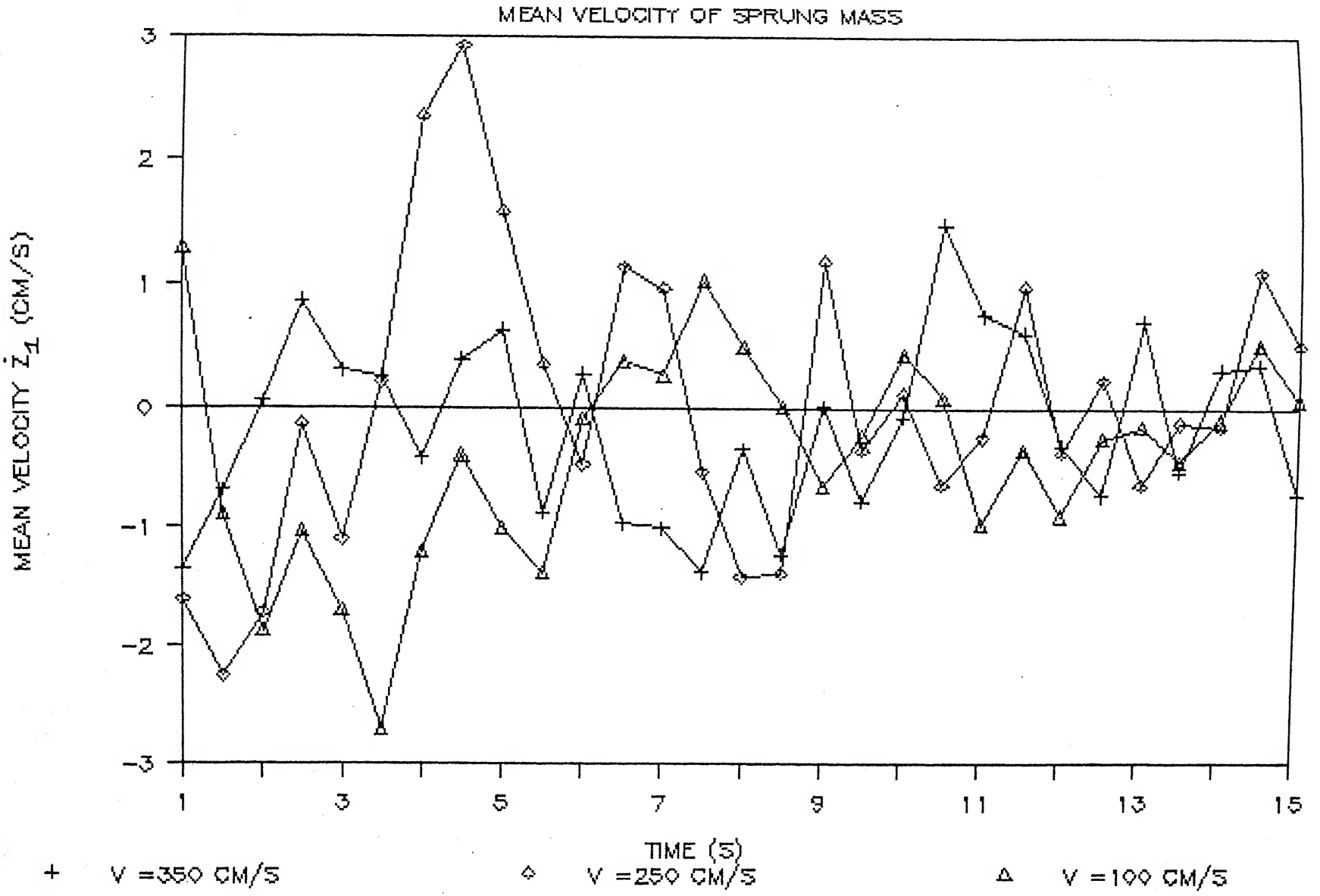

Fig. 4.9f Landing run,Sink Velocity variation;Mean Velocity Response.

i) The effect of variation in sink velocity is felt, but as in the case of the unsprung mass, a definite pattern in the response behaviour is not obvious.

ii) After a time duration of 0.8 second after touchdown the mean velocity starts fluctuating at the zero level. This can be very well seen in Figure 3.9f.

4.3.7 Standard Deviation of Velocity of Unsprung mass

The response of the standard deviation of velocity of the unsprung mass is portrayed in Figures 4.10a to 4.10c. The essential points observed are :

i) For the first 0.2 seconds of time duration the numerical values of the velocity of unsprung mass are higher for higher sink velocities and vice versa.

ii) For the time duration of 0.2 to 1 second after touchdown for the sink velocity of 350 cm/s there are two reasonances at 0.7 and 0.9 seconds. For the sink velocity of 250 cm/s there is a single resonance at 0.95 sec, whereas the sink velocity of 100 cm/s does not have a resonance. Thus the higher the sink velocities, the earlier is the possibility of the occurrence of resonance.

iii) The trend of the numerical values is found to be a decreasing one.

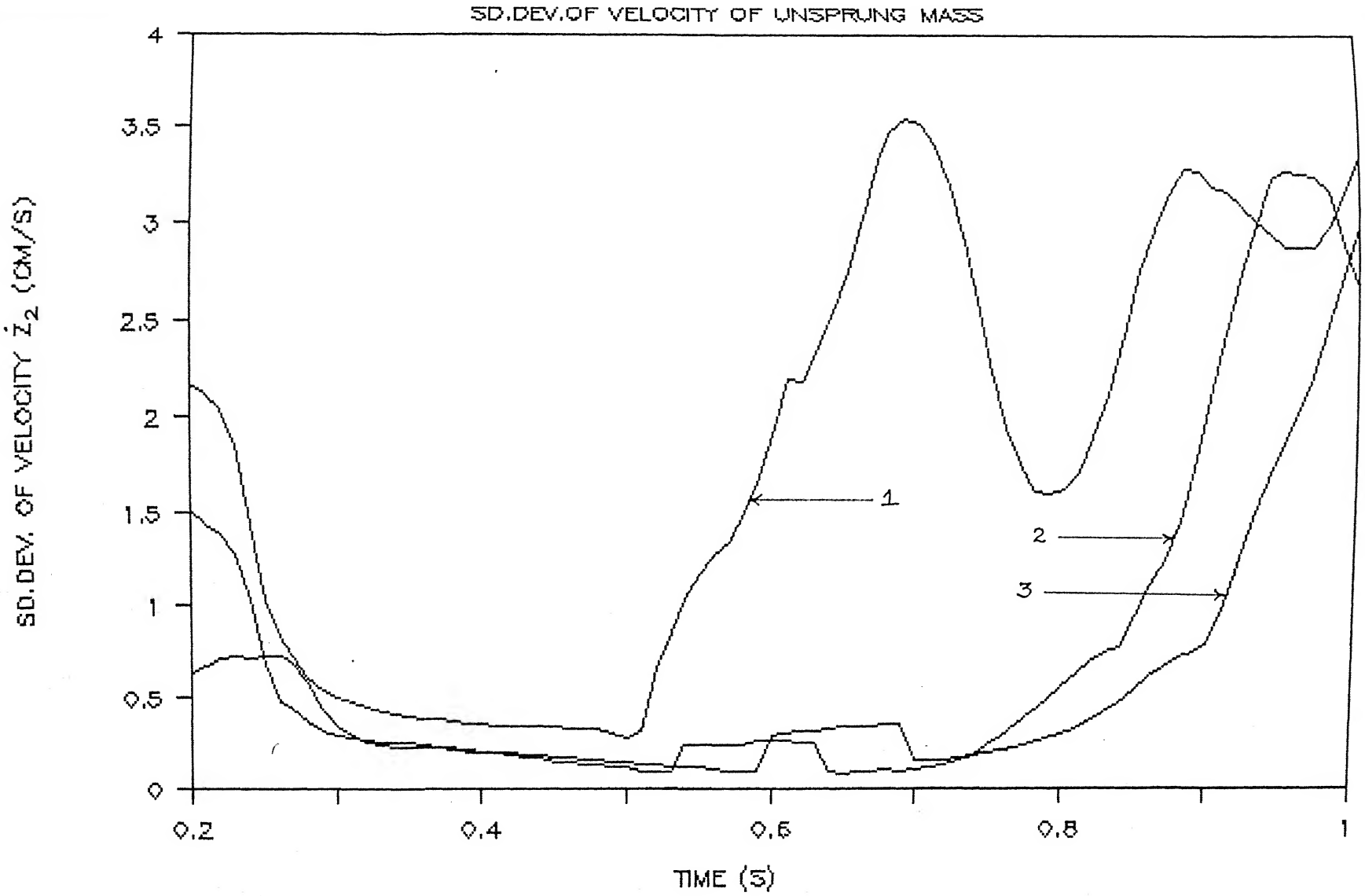

Fig. 4.10b Landing run,Sink Velocity variation;Standard Deviation of Velocity Response.

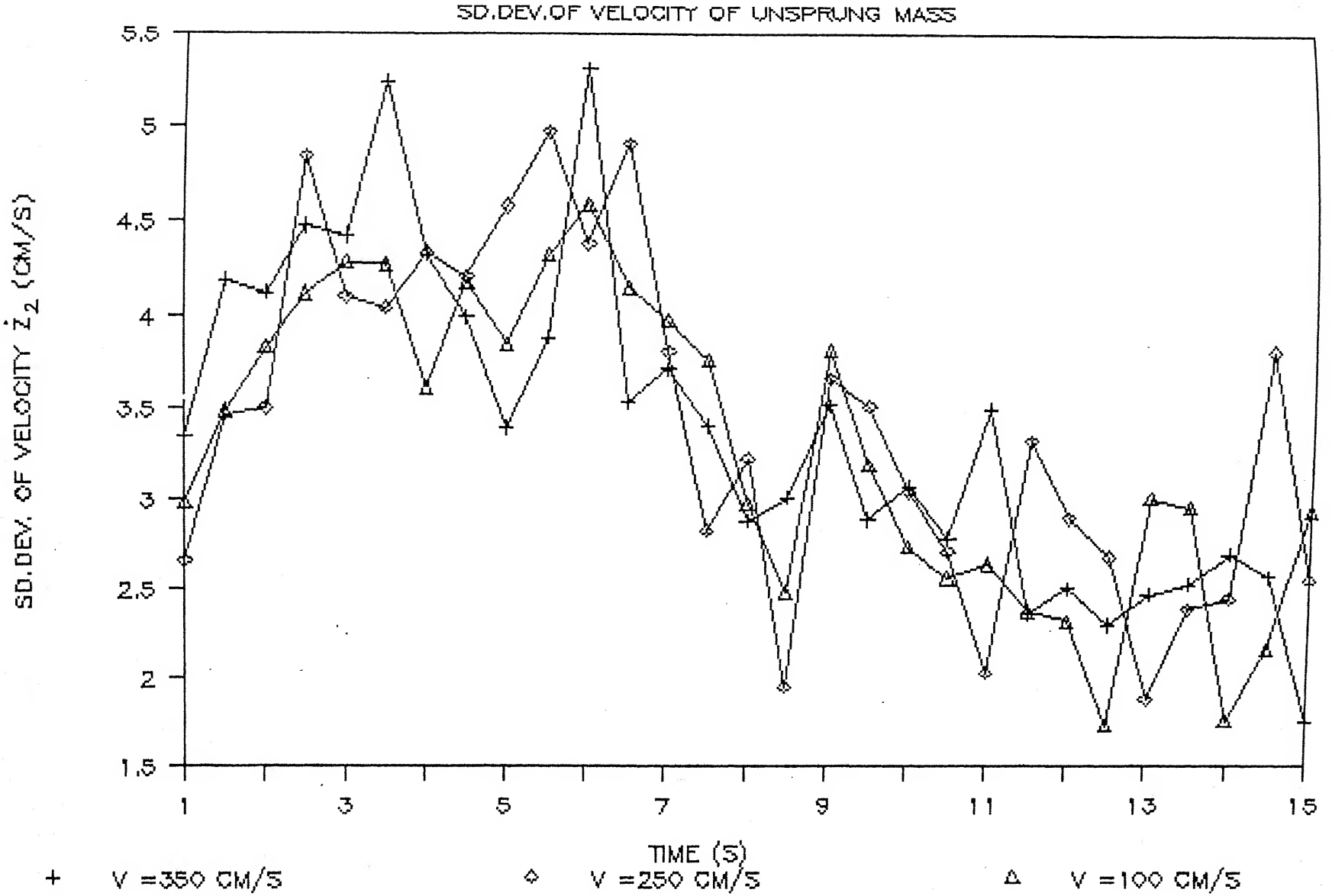

Fig. 4.10e Landing run,Sink Velocity variation;Standard Deviation of Velocity Response.

4.3.8 Standard Deviation of Velocity of Sprung mass

Figures 4.10d and 4.10e present the standard deviation of the velocity response of the sprung mass. The observations made are :

i) There is a clear effect of the variation of the sink velocity on the standard deviation of the velocity of the sprung mass.

ii) For the time duration of 0 to 1 second resonance is observed at 0.2, 0.7 and 0.9 seconds for the sink velocity of 350 cm/s. For sink velocity V_s = 250 cm/s, resonance is observed at 0.2 and 0.95 seconds, whereas there is no resonance for V_s = 100 cm/s. The observation is identical to that for the unsprung mass.

4.3.9 Mean Acceleration of the Unsprung mass

The response of the mean acceleration of the unsprung mass is shown in Figures 4.11a to 4.11c. The noteworthy points are :

i) There is an effect of the variation in the sink velocity. Higher sink velocities give higher acceleration values at the time of impact.

ii) The trend of the mean acceleration response is a sharply declining one. This is true for all the sink velocities considered.

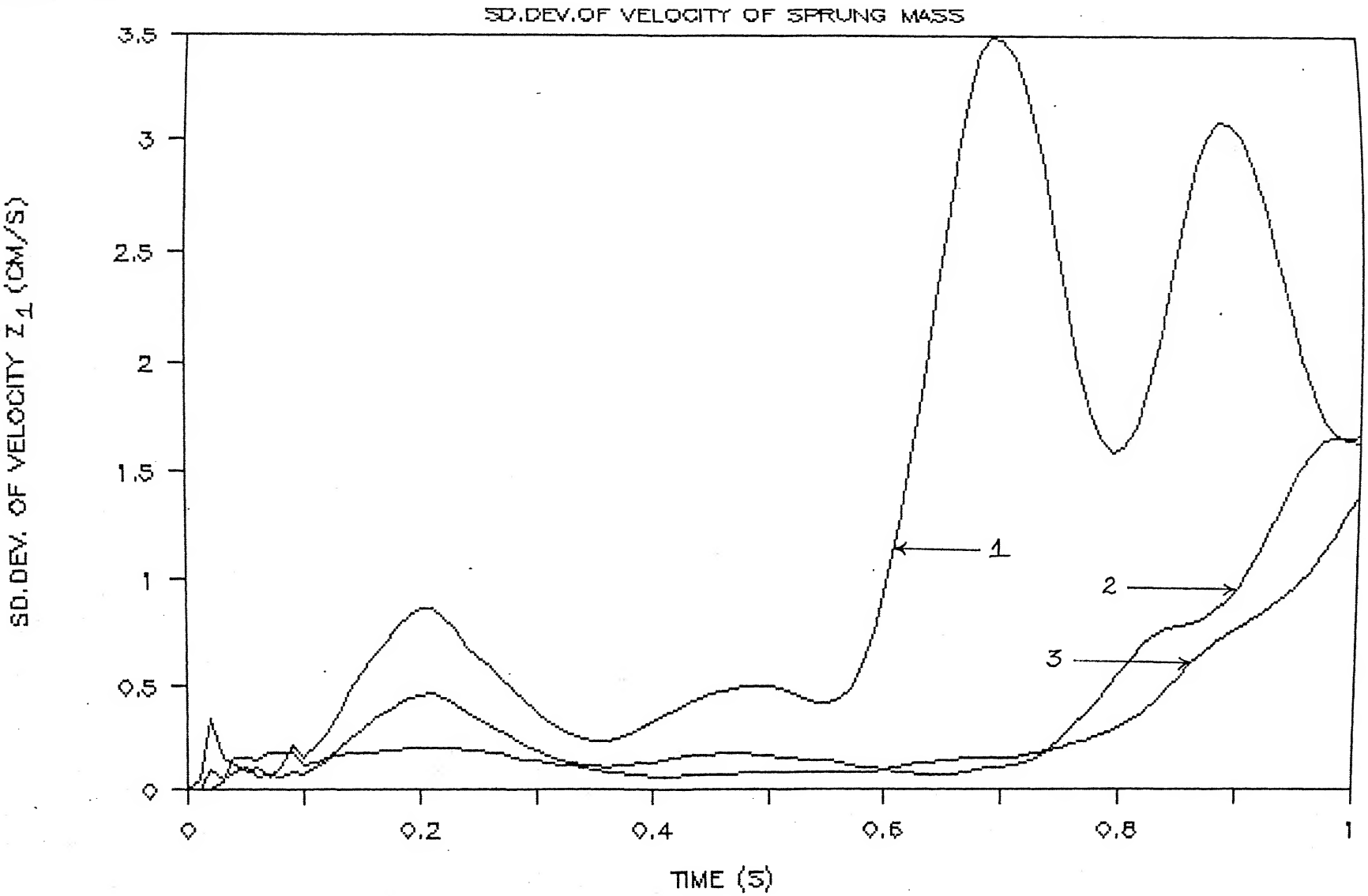

Fig. 4.10d Landing run,Sink Velocity variation;Standard Deviation of Velocity Response.

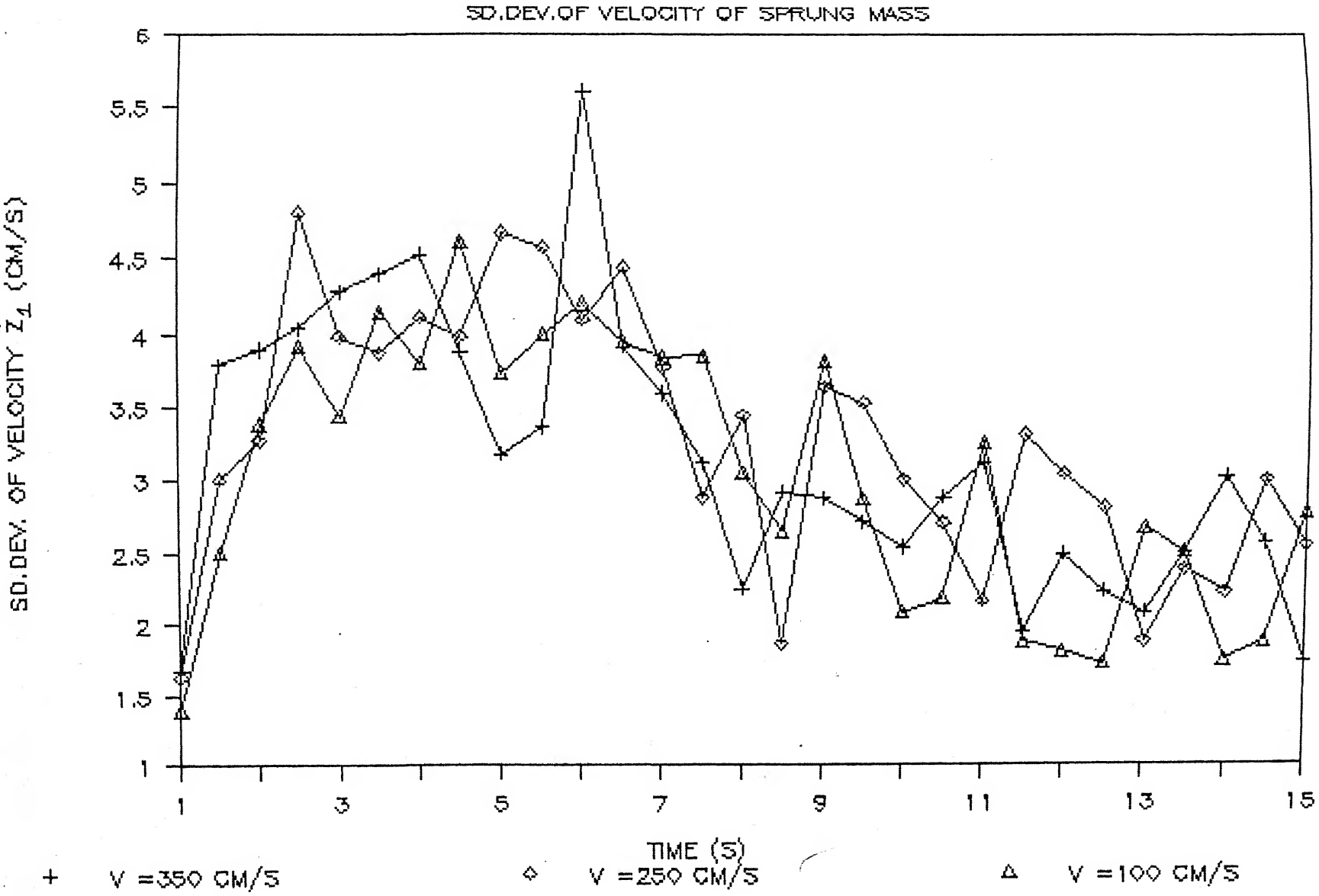

Fig. 4.10e Landing run,Sink Velocity variation;Standard Deviation of Velocity Response.

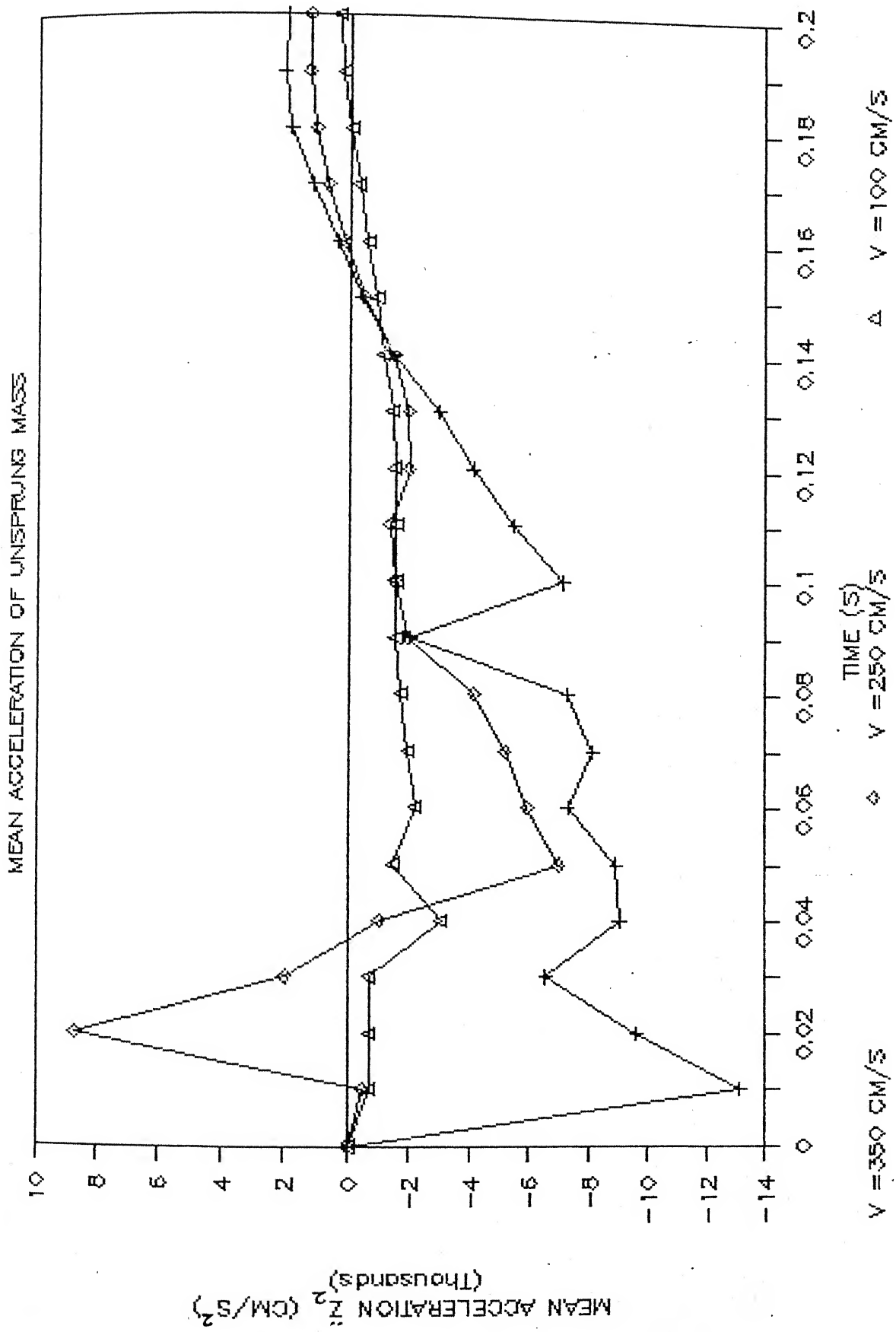

Fig. 4.11a Landing run,Sink Velocity variation;Mean Acceleration Response.

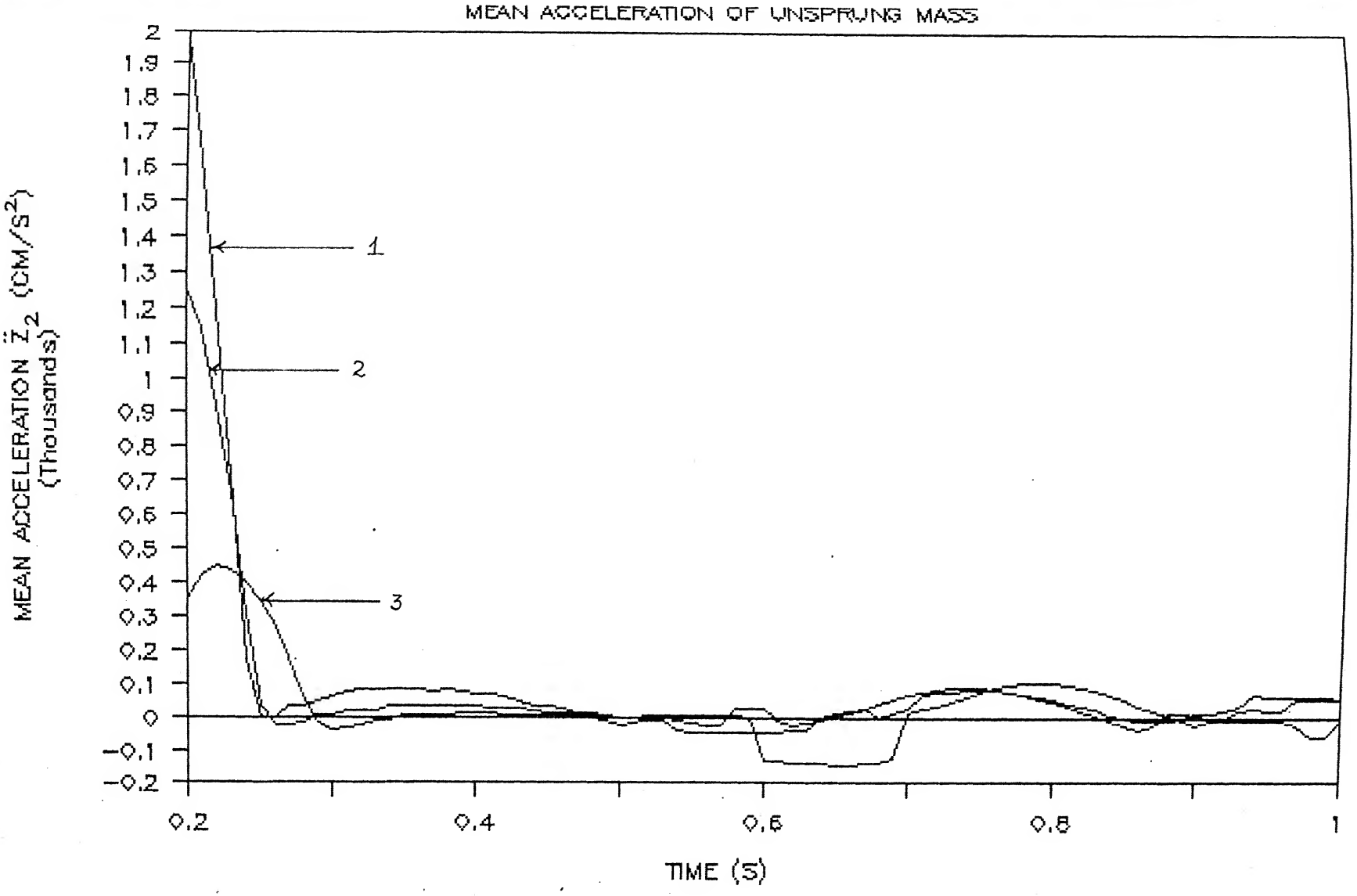

Fig. 4.11b Landing run,Sink Velocity variation;Mean Acceleration Response.

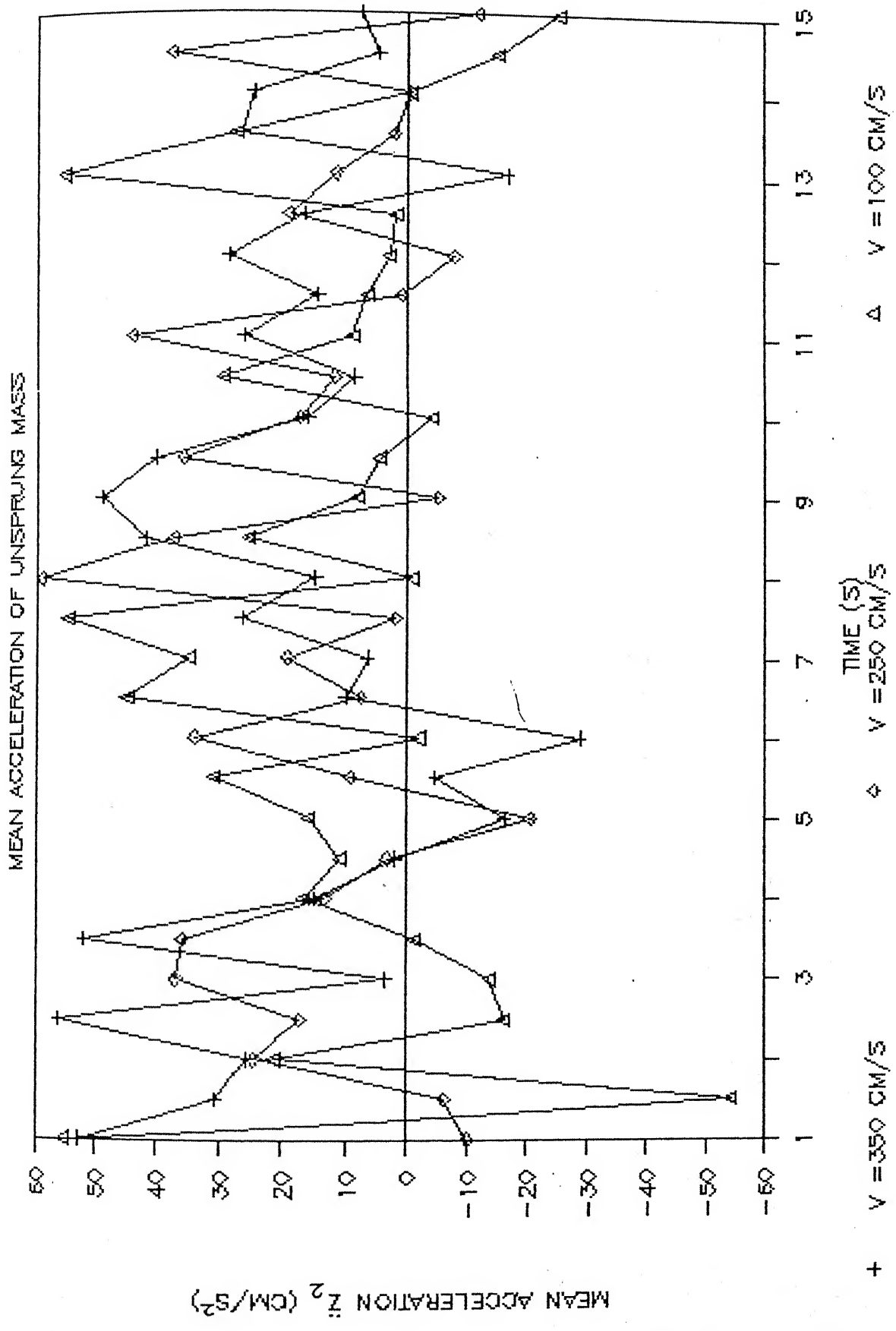

Fig. 4.11c Landing run,Sink Velocity variation;Mean Acceleration Response.

4.3.10 Mean Acceleration of the Sprung mass

The response of the mean acceleration of the sprung mass is presented in figures 4.11d to 4.11f. The observations made are :

i) The effect of higher sink velocities, at a time just after touchdown is to increase the values of the accelerations of the sprung mass.

ii) After 0.6 second the value of acceleration starts fluctuating around the zero level.

4.3.11 Standard Deviation of Acceleration of Unsprung mass

Figures 4.12a to 4.12c present the response of the standard deviation of acceleration of the unsprung mass. The observations made are :

i) The higher the value of the sink velocity, the higher the value of standard deviation of acceleration.

ii) Resonance occurs for all the sink velocities at around 0.6 and 0.95 seconds after touchdown.

iii) The trend is a decreasing one.

4.3.12 Standard Deviation of Acceleration of the Sprung mass

Figures 4.12d to 4.12f present the response of the standard deviation of acceleration of the sprung mass. The observations made are :

i) The values of standard deviation of acceleration at

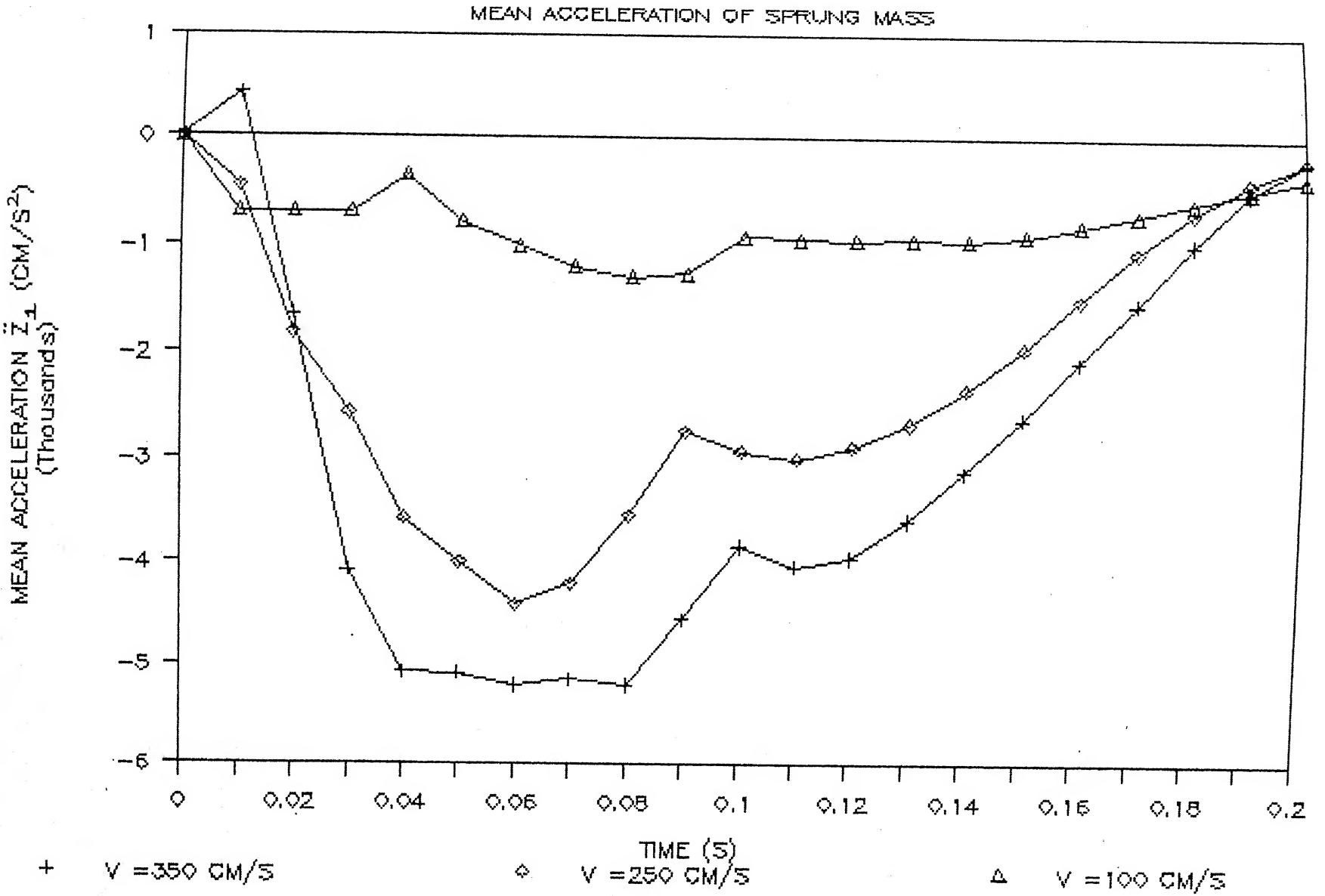

Fig. 4.11d Landing run, Sink Velocity variation; Mean Acceleration Response.

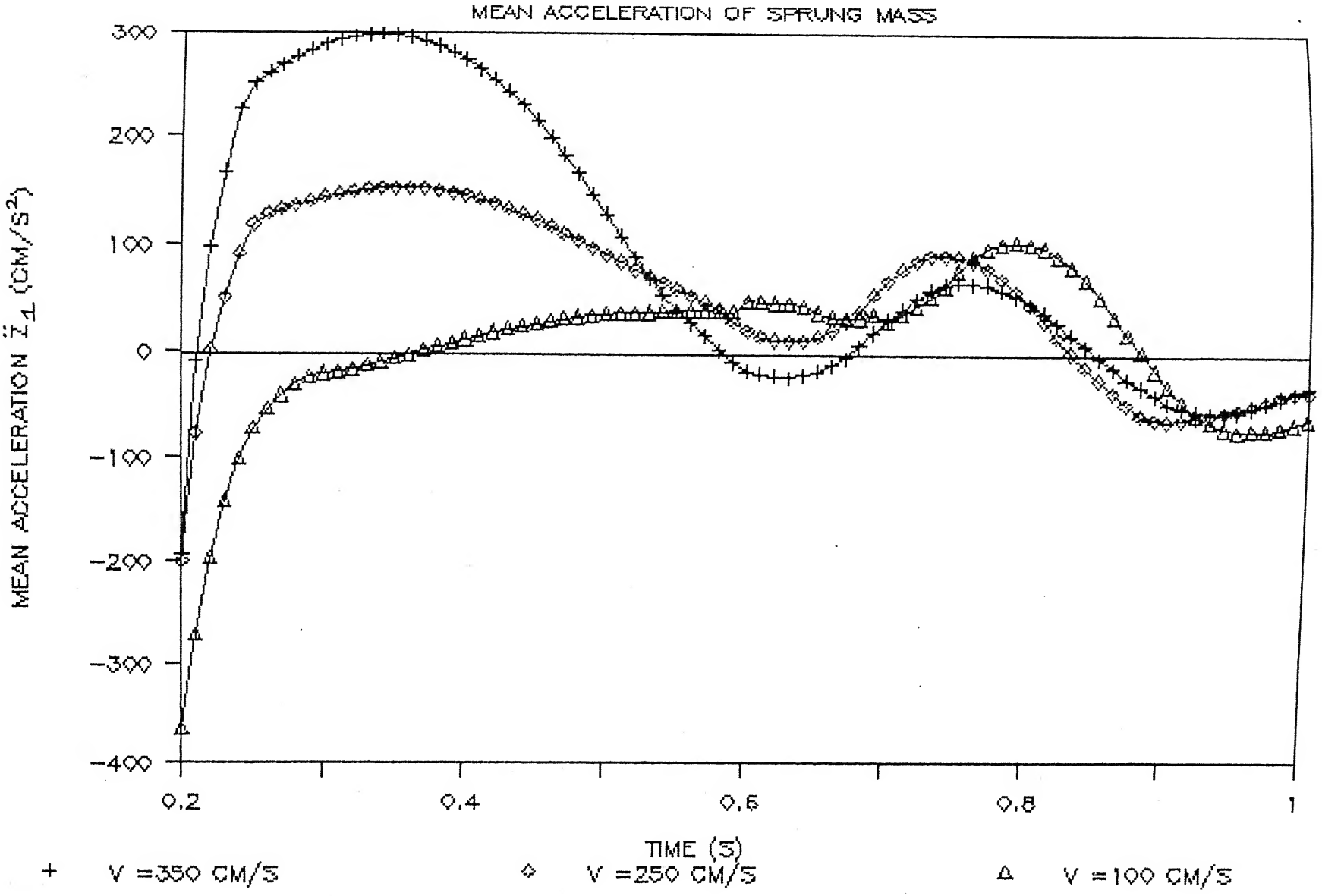

Fig. 4.11e Landing run,Sink Velocity variation;Mean Acceleration Response.

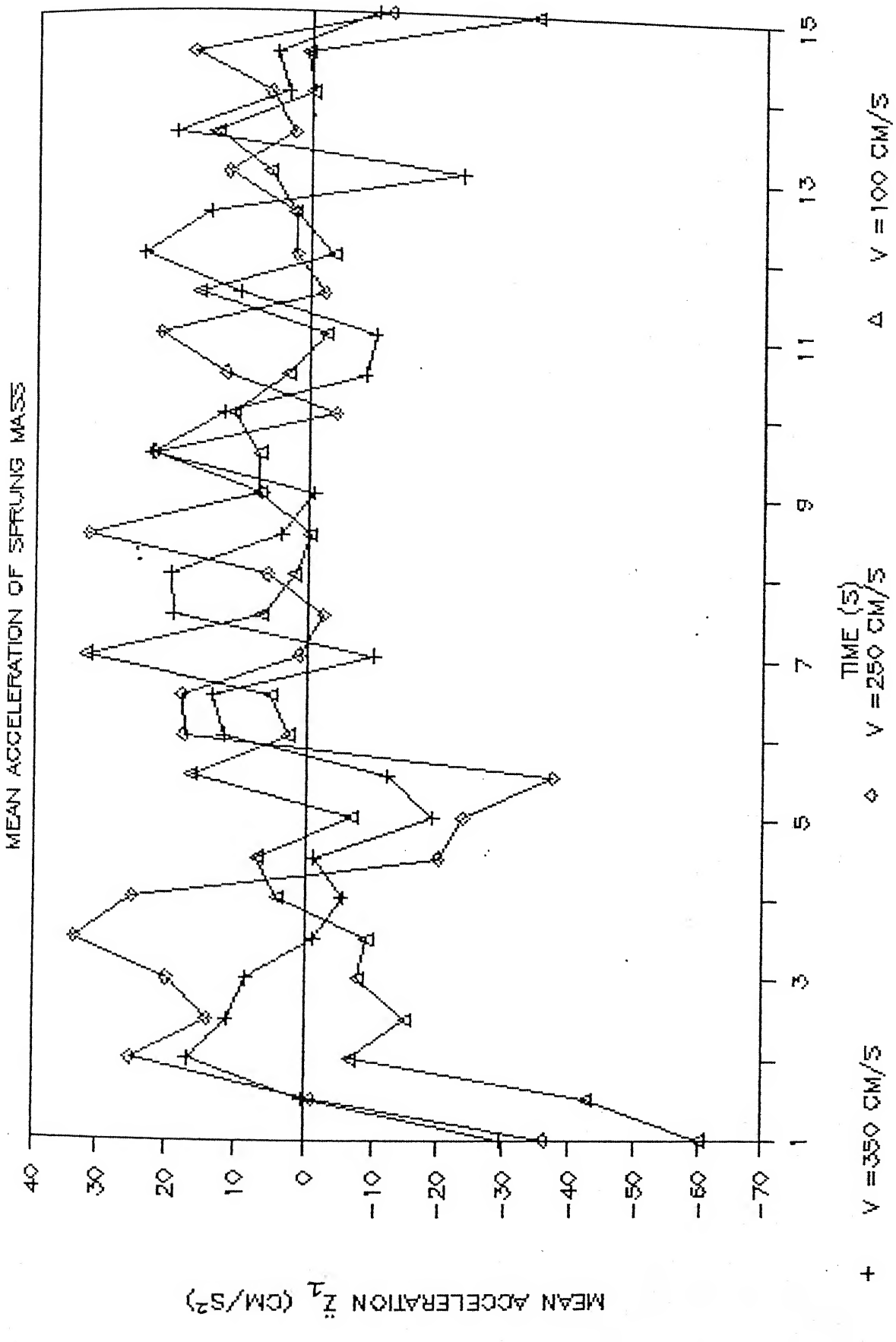

Fig. 4.11f Landing run,Sink Velocity variation;Mean Acceleration Response.

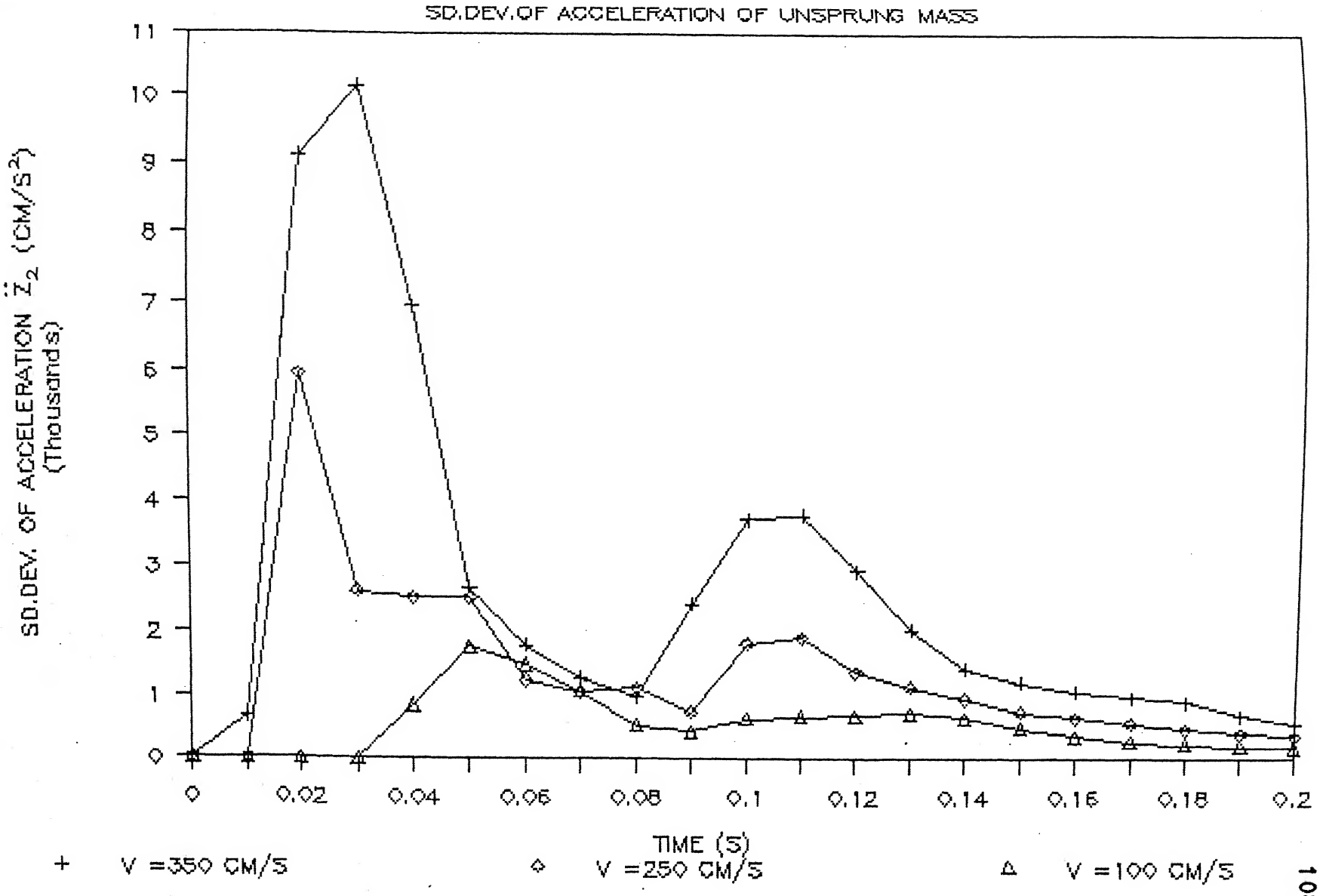

Fig. 4.12a Landing run,Sink Velocity variation;Standard Deviation of Acceleration Response.

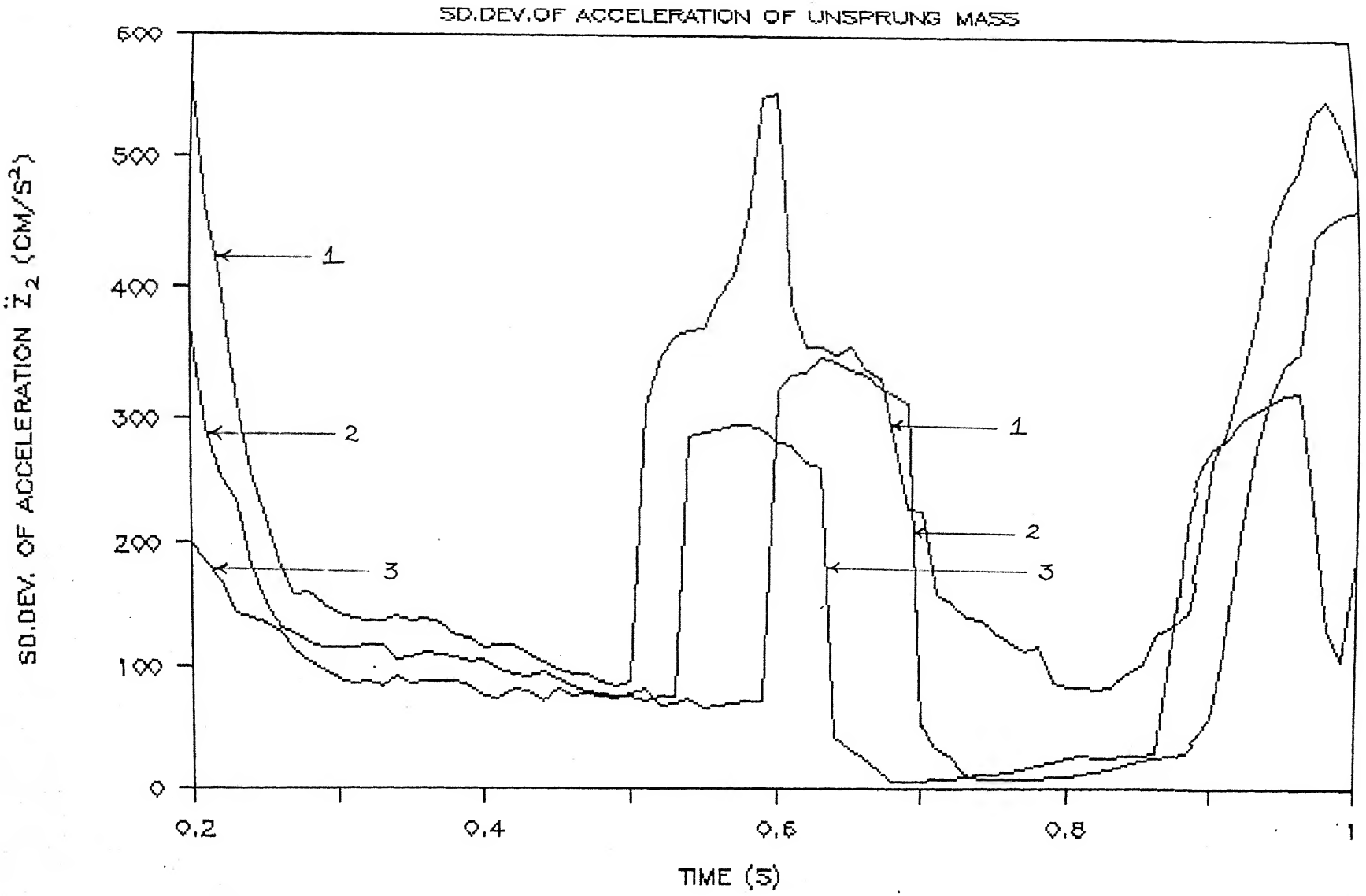

Fig. 4.12b Landing run,Sink Velocity variation;Standard Deviation of Acceleration Response.

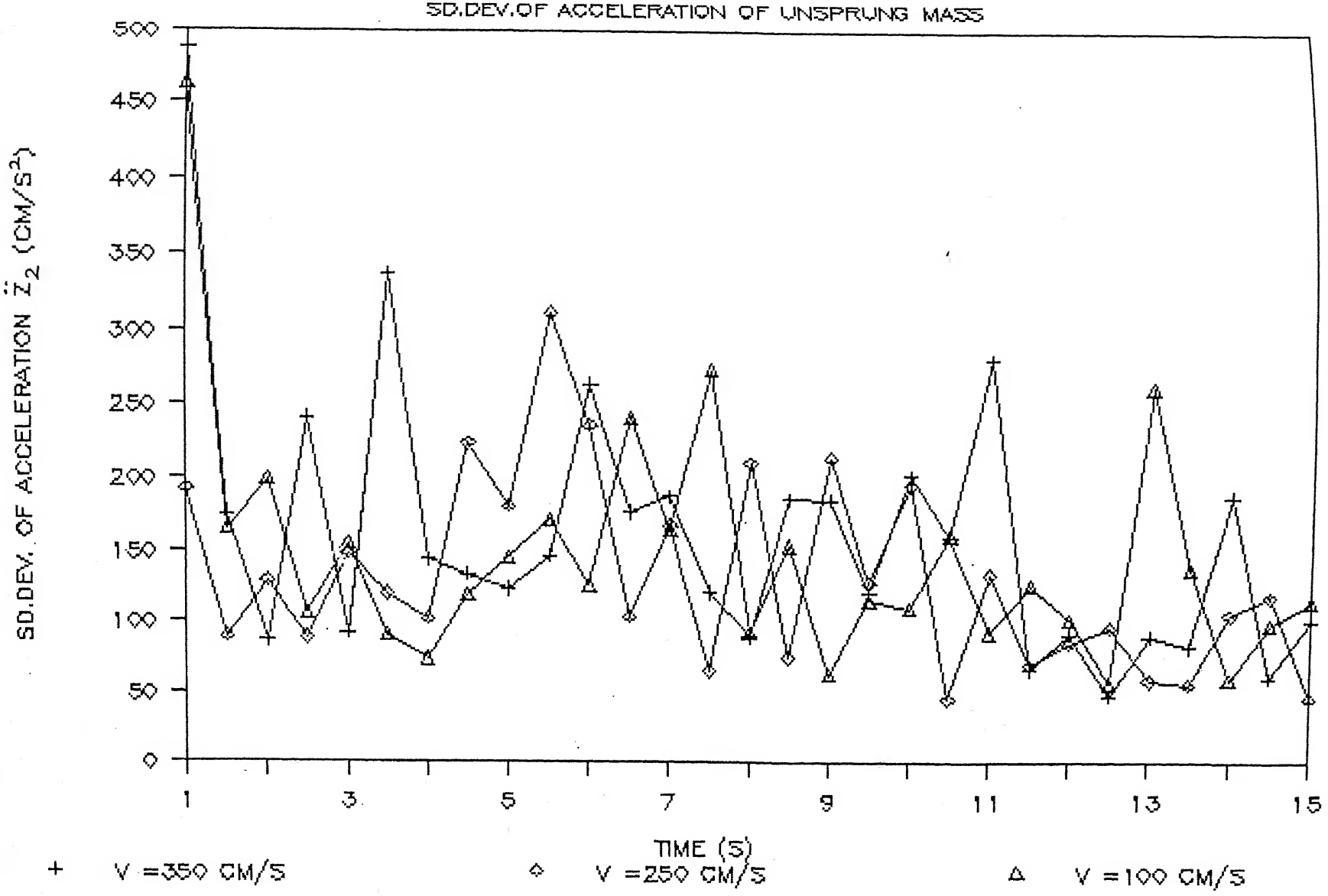

Fig. 4.12c Landing run,Sink Velocity variation;Standard Deviation of Acceleration Response.

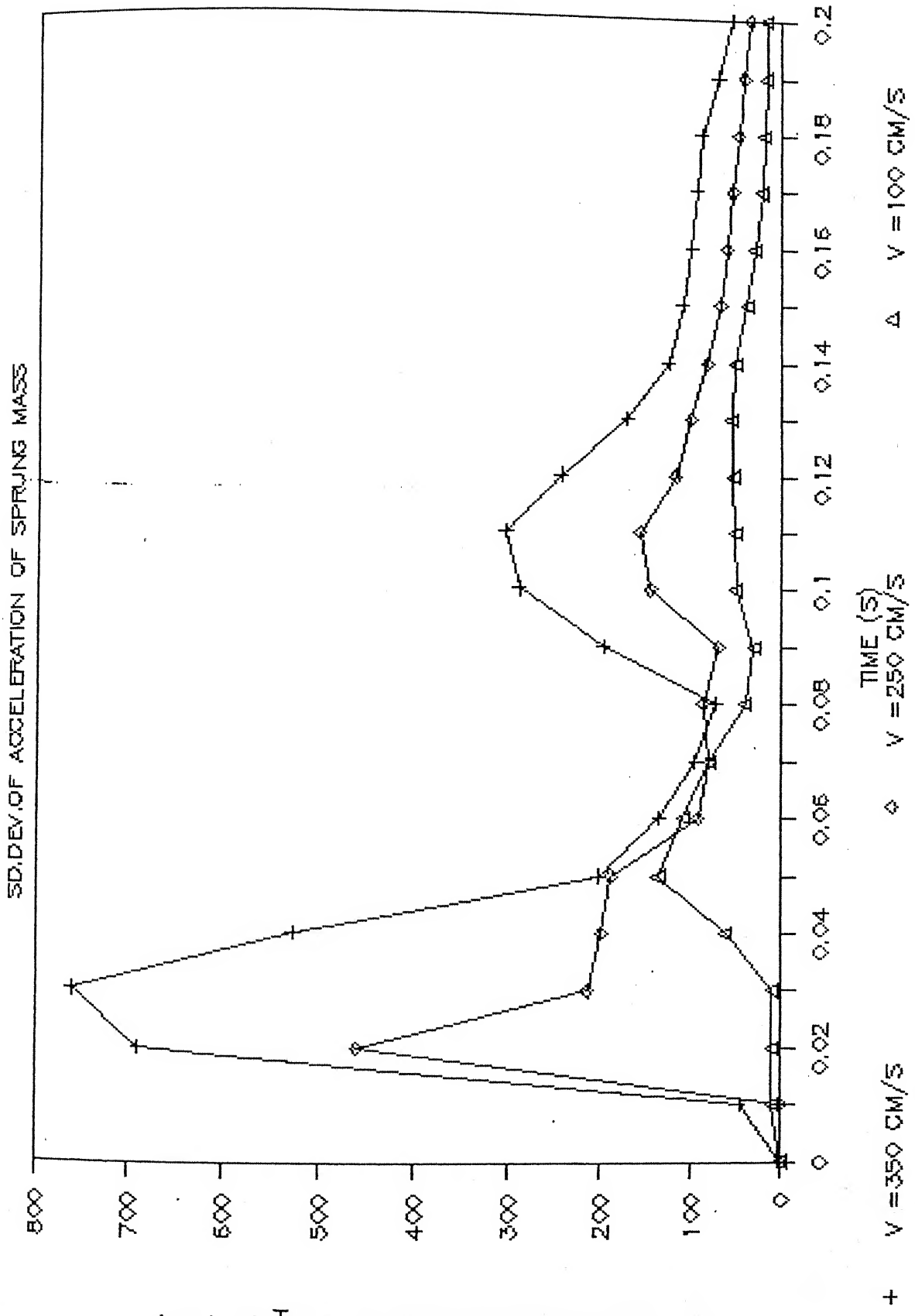

Fig. 4.12d Landing run,Sink Velocity variation;Standard Deviation of Acceleration Response.

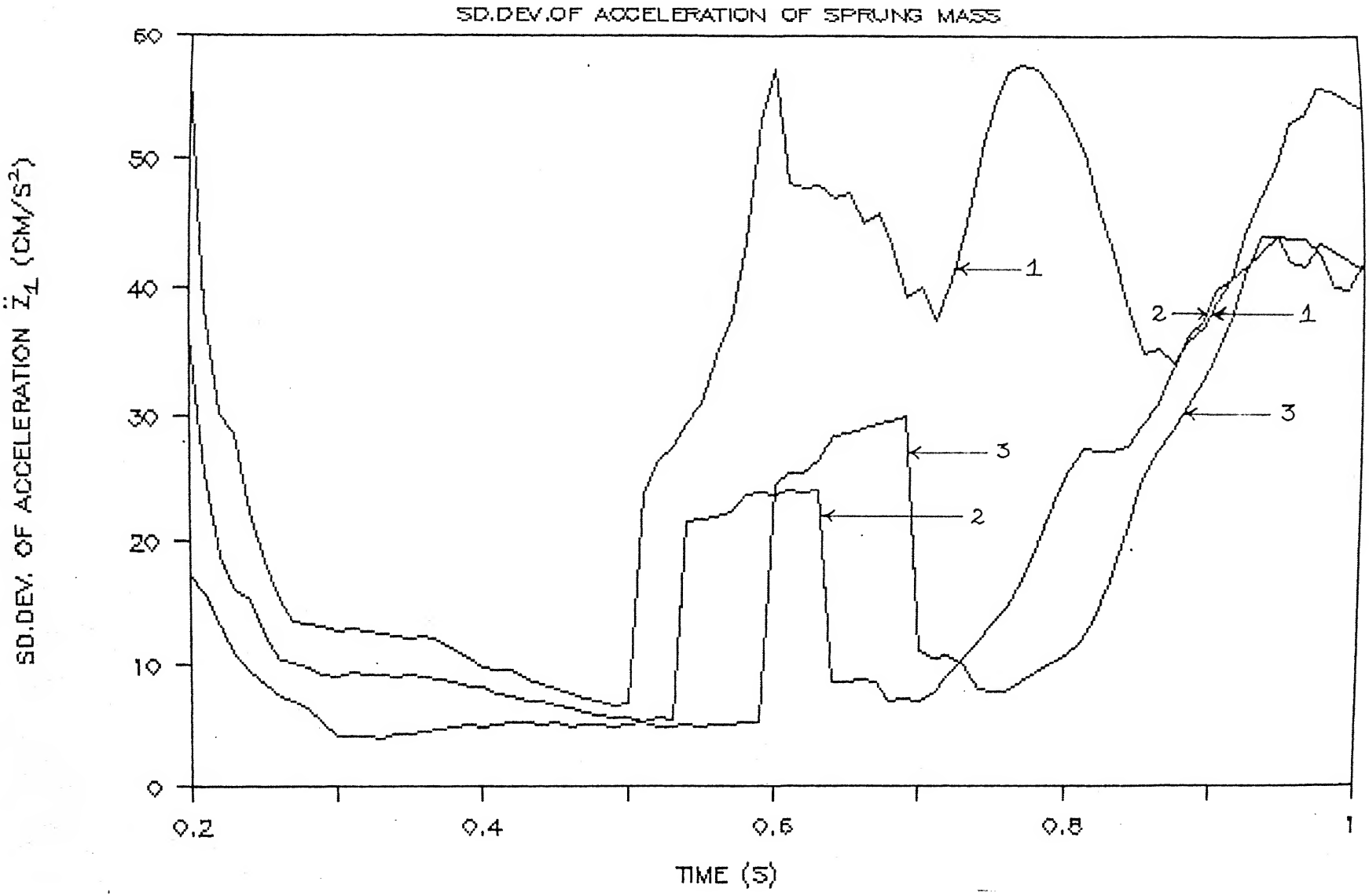

Fig. 4.12e Landing run,Sink Velocity variation;Standard Deviation of Acceleration Response.

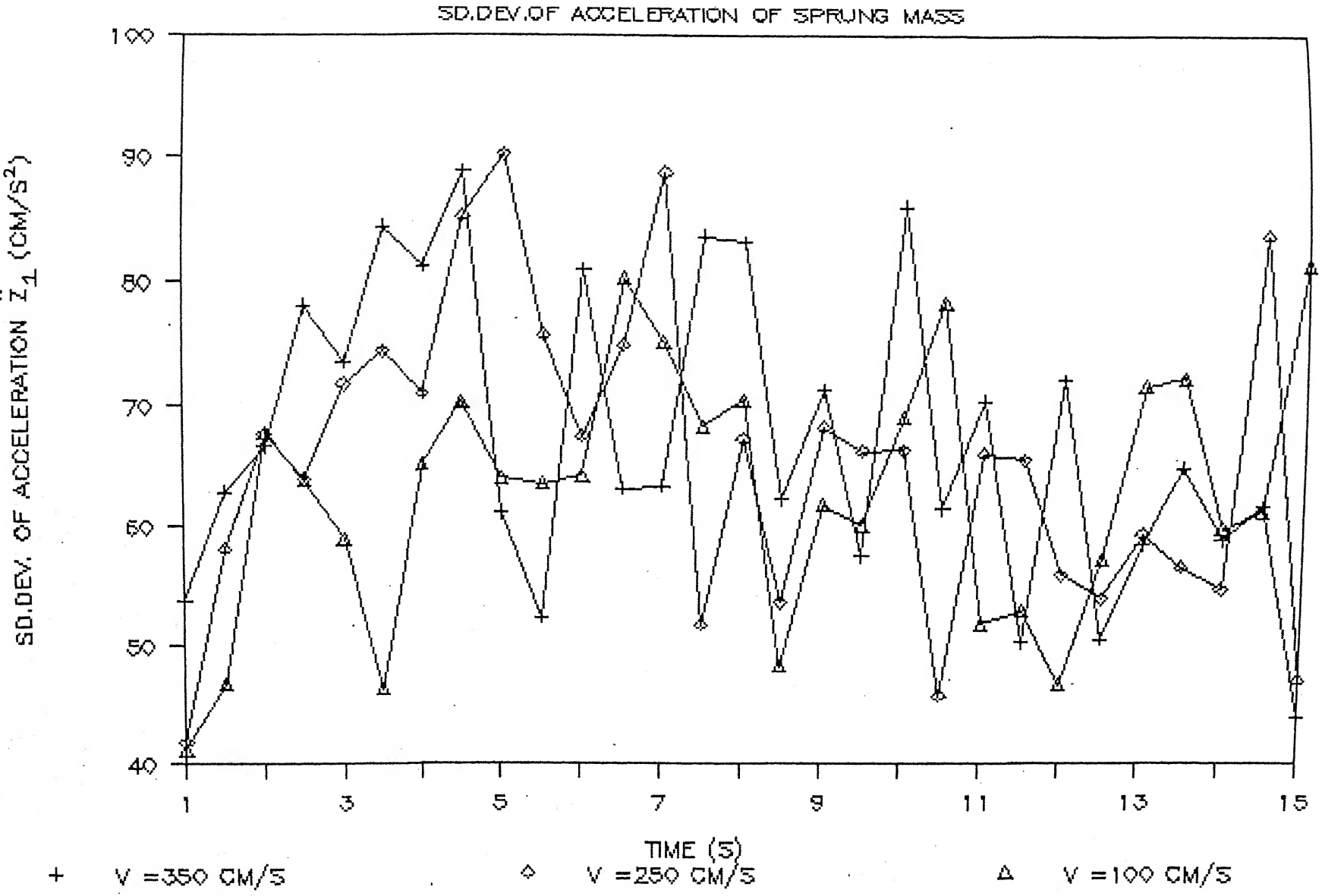

Fig. 4.12f Landing run,Sink Velocity variation;Standard Deviation of Acceleration Response.

higher sink velocities are higher than those at lower sink velocities.

ii) The resonance characteristics are similar to those of the unsprung mass.

iii) The overall numerical values are lower than those of the unsprung mass.

4.4 *Take-off run with variation in Track Roughness*

For the take-off run the variation in the roughness of the runway track is studied. The aircraft takes off from a track having a constant mean slope. The values of the roughness constant C are taken as 0.0001, 0.0005 and 0.00002 in ft. units.

4.4.1 Mean Displacement of the Unsprung mass

The response of the mean displacement of the unsprung mass is presented in Figure 4.13a. The observations made are :

i) There is very little or negligible effect of the variation in the roughness level of the track.

ii) Initially at the start of the take-off run the unsprung mass keeps heaving but after about 2 seconds the heaving gives way to the gradual decrease in the tyre deflection.

iii) The aircraft take-off takes place at around 15.5 seconds after the start of the run.

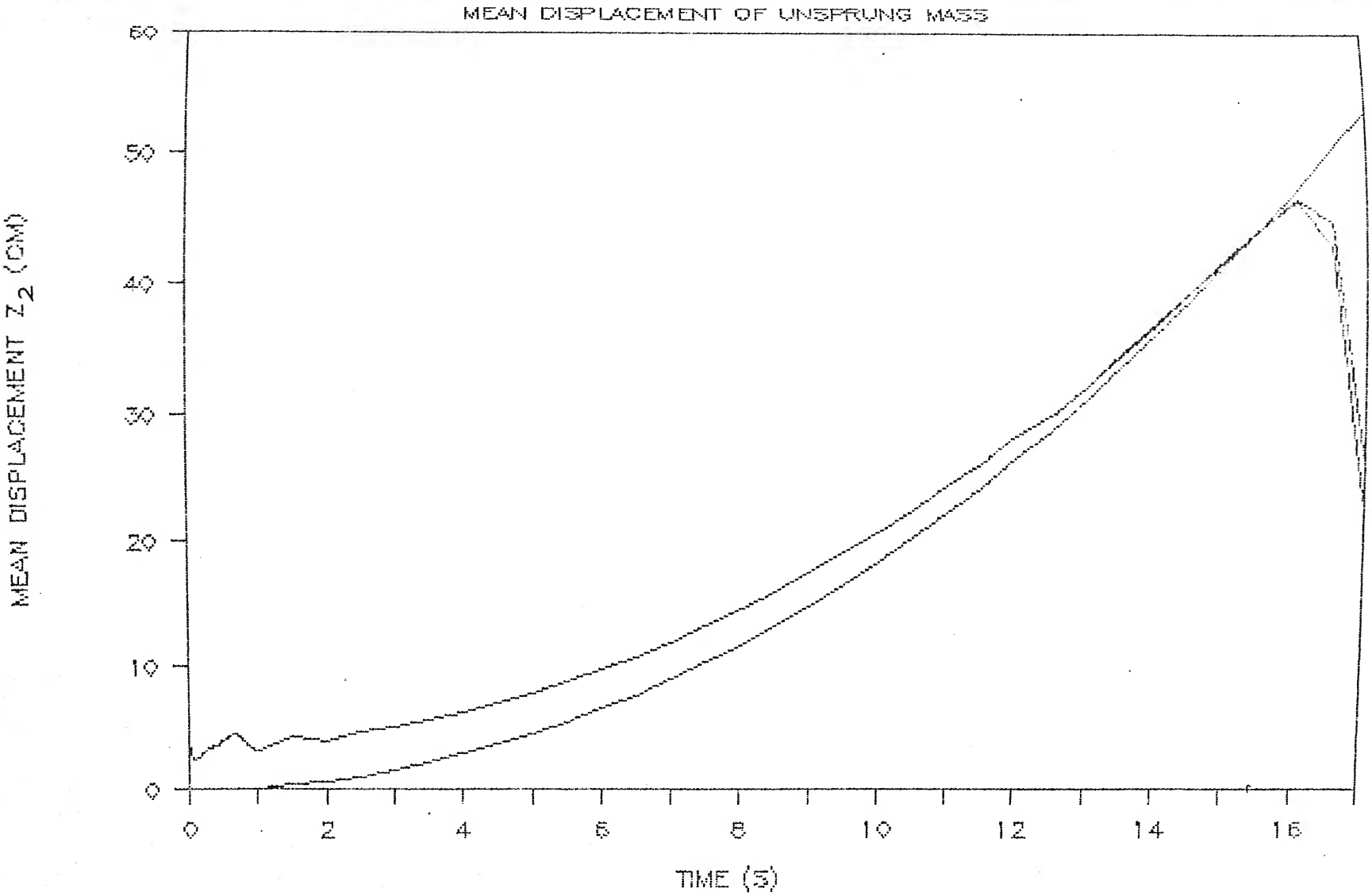

Fig. 4.13a Take-off run,Roughness variation;Mean Displacement Response.

4.4.2 Mean Displacement of the Sprung mass

Figure 4.13b shows the response of the mean displacement of the sprung mass. The observations are :

i) Initially upto around 4 seconds there is heavy heaving of the sprung mass which dies down subsequently. Then there is a gradual increase in the response due to the motion of the aircraft on the mean slope.

ii) There is a drop in the value of the response at around 13 seconds indicating a valley after resonance. Then there is a sharp increase until the take-off point is reached.

iii) The effect of the variation in the track roughness is negligibly small.

4.4.3 Standard Deviation of Displacement of Unsprung mass

The response of the standard deviation of displacement of the unsprung mass is represented by Figures 4.14a to 4.14c. The observations made from them are :

i) Effect of variation of the track roughness is visible, but it is not possible to define a set pattern as a result of this variation.

ii) The trend of the standard deviation response is an increasing one, but once the take-off is attained the standard deviation suddenly shoots up.

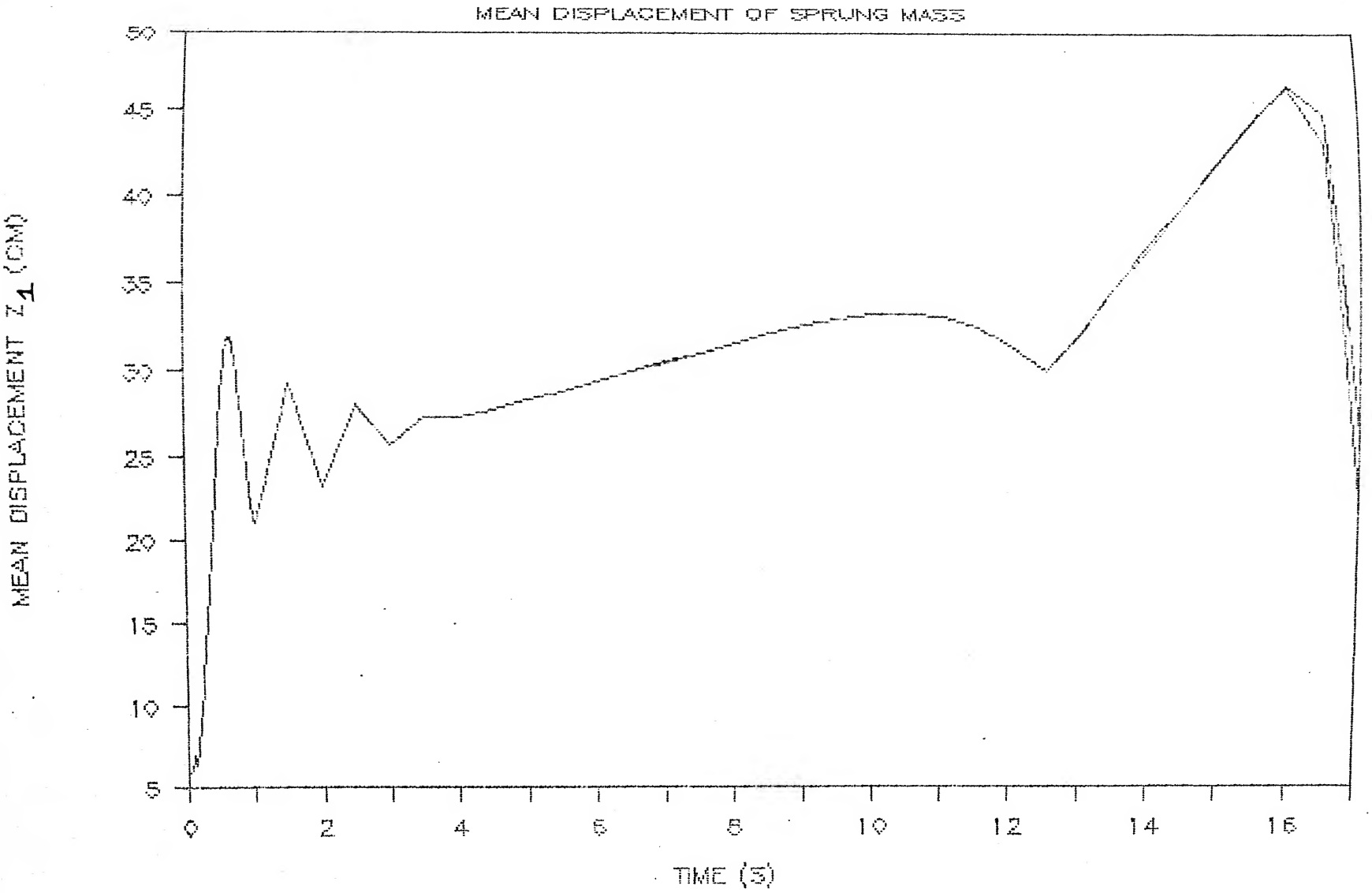

Fig. 4.13b Take-off run,Roughness variation;Mean Displacement Response.

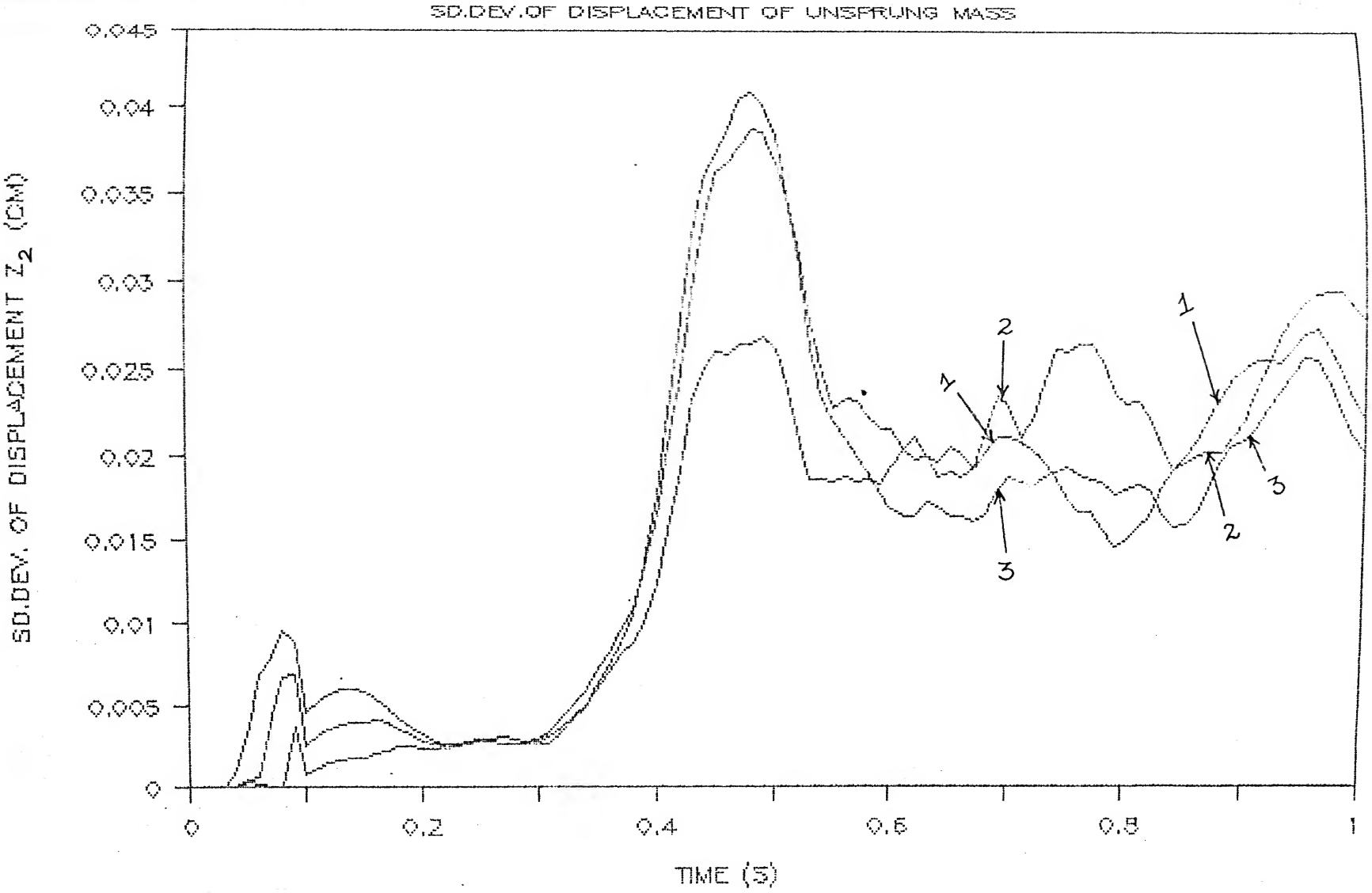

1 C=0.0001 FT 2 C=0.0005 FT 3 C=0.00002 FT

Fig. 4.14a Take-off run, Roughness variation; Standard Deviation of Displacement Response.

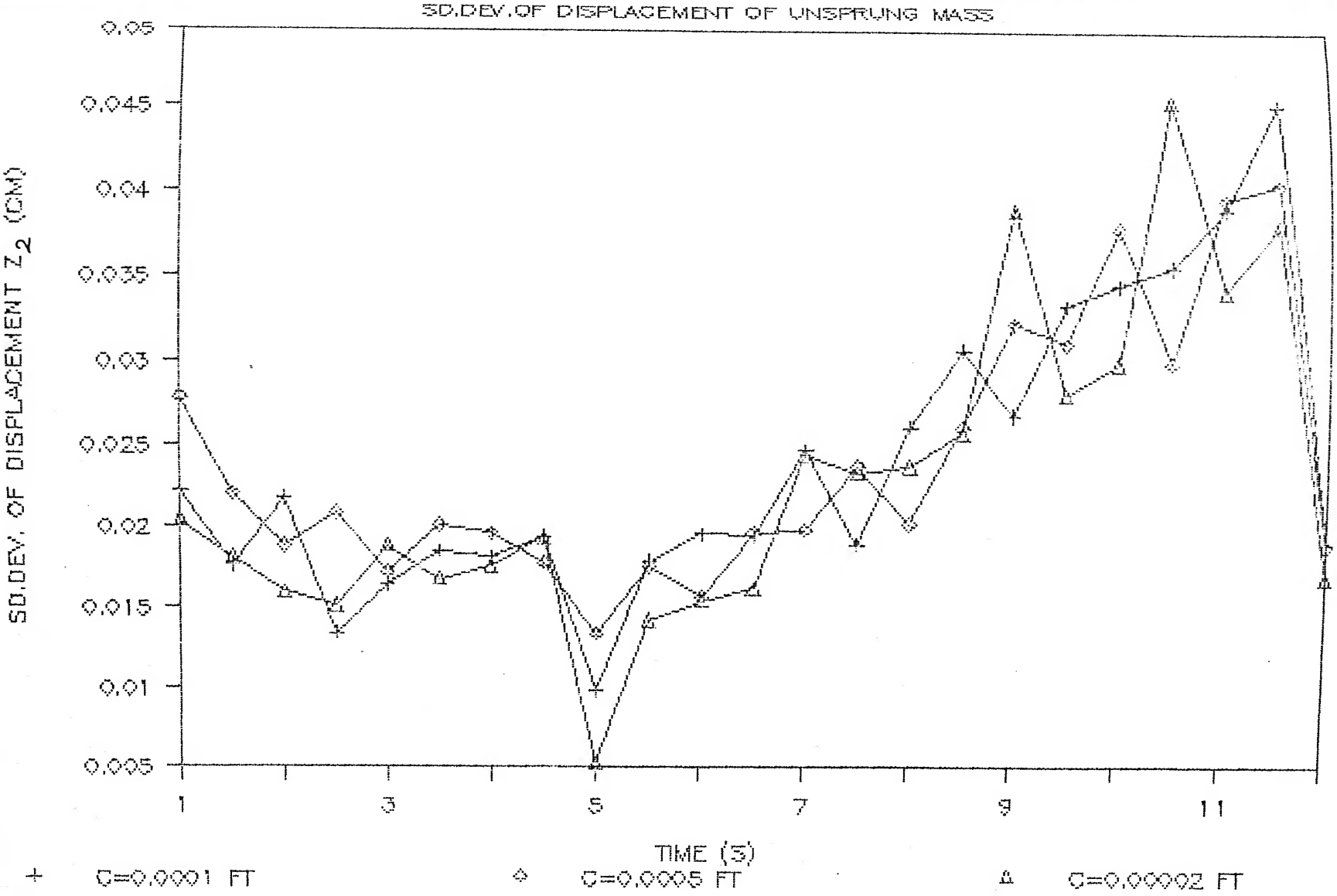

Fig. 4.14b Take-off run,Roughness variation;Standard Deviation of Displacement Response.

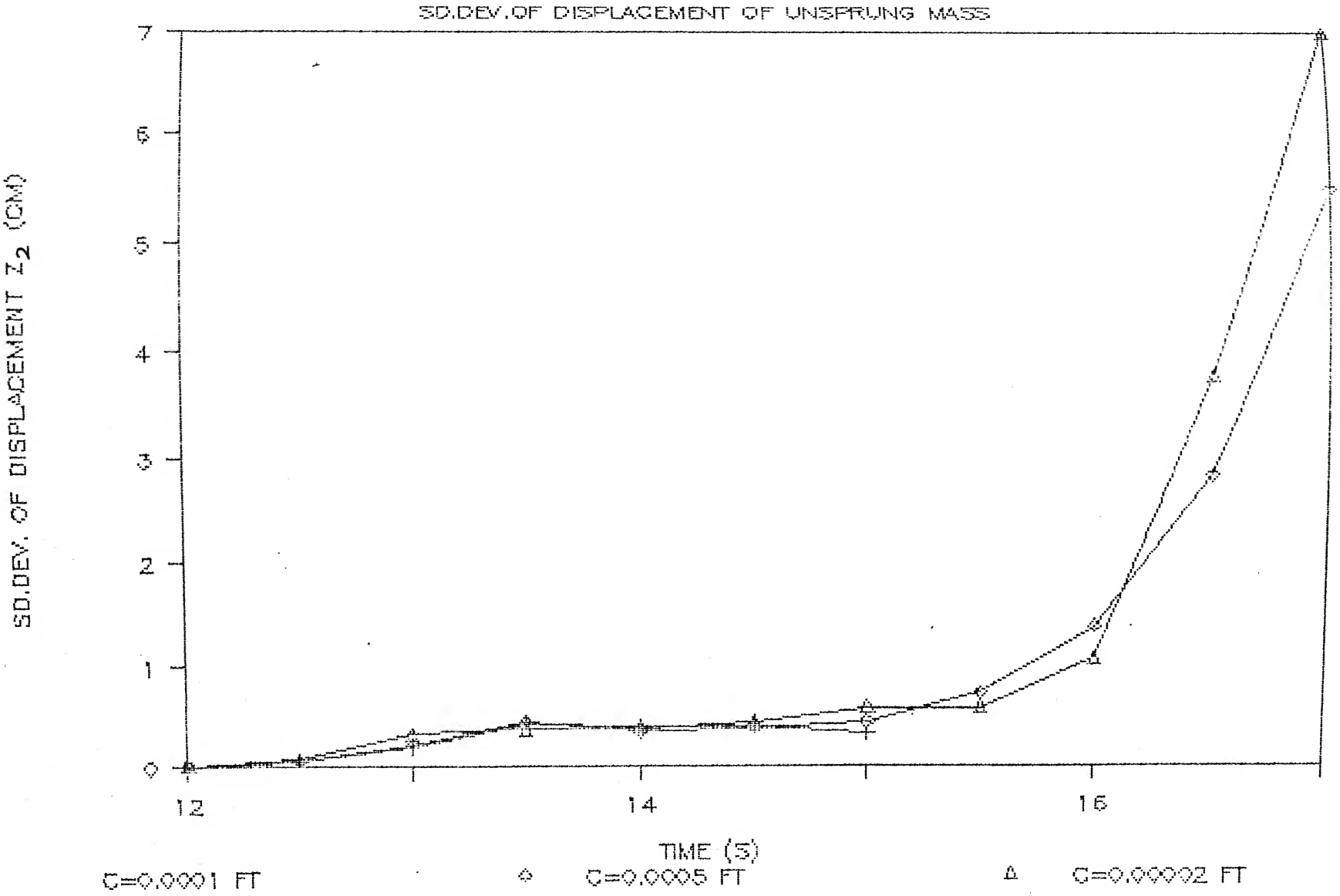

Fig. 4.14c Take-off run,Roughness variation;Standard Deviation of Displacement Response.

iii) A clear resonance is realised at around 0.5 seconds from the start of the run.

4.4.4 Standard Deviation of the Displacement of Sprung mass

Figures 4.14d to 4.14f show the standard deviation of displacement response of sprung mass. The following points can be highlighted :

i) The effect of the variation of the track roughness is easily visible. Upto a time of 1 second, the increase in the track roughness leads to an increase in the numerical values of standard deviation.

ii) A couple of resonances are observed, one at 0.6 second and the other at 1 second.

iii) The trend of standard deviation after the resonance is a decreasing one upto 12 seconds. After 12 seconds the deviation again starts increasing and once the take-off point is reached it immediately shoots up.

4.4.5 Mean Velocity of the Unsprung mass

The response of the mean velocity of the unsprung mass is represented in Figures 4.15a to 4.15c. The prime observations made are :

i) The effect of the variation in the roughness level of the track is felt, but the roughness variation does not indicate a set pattern.

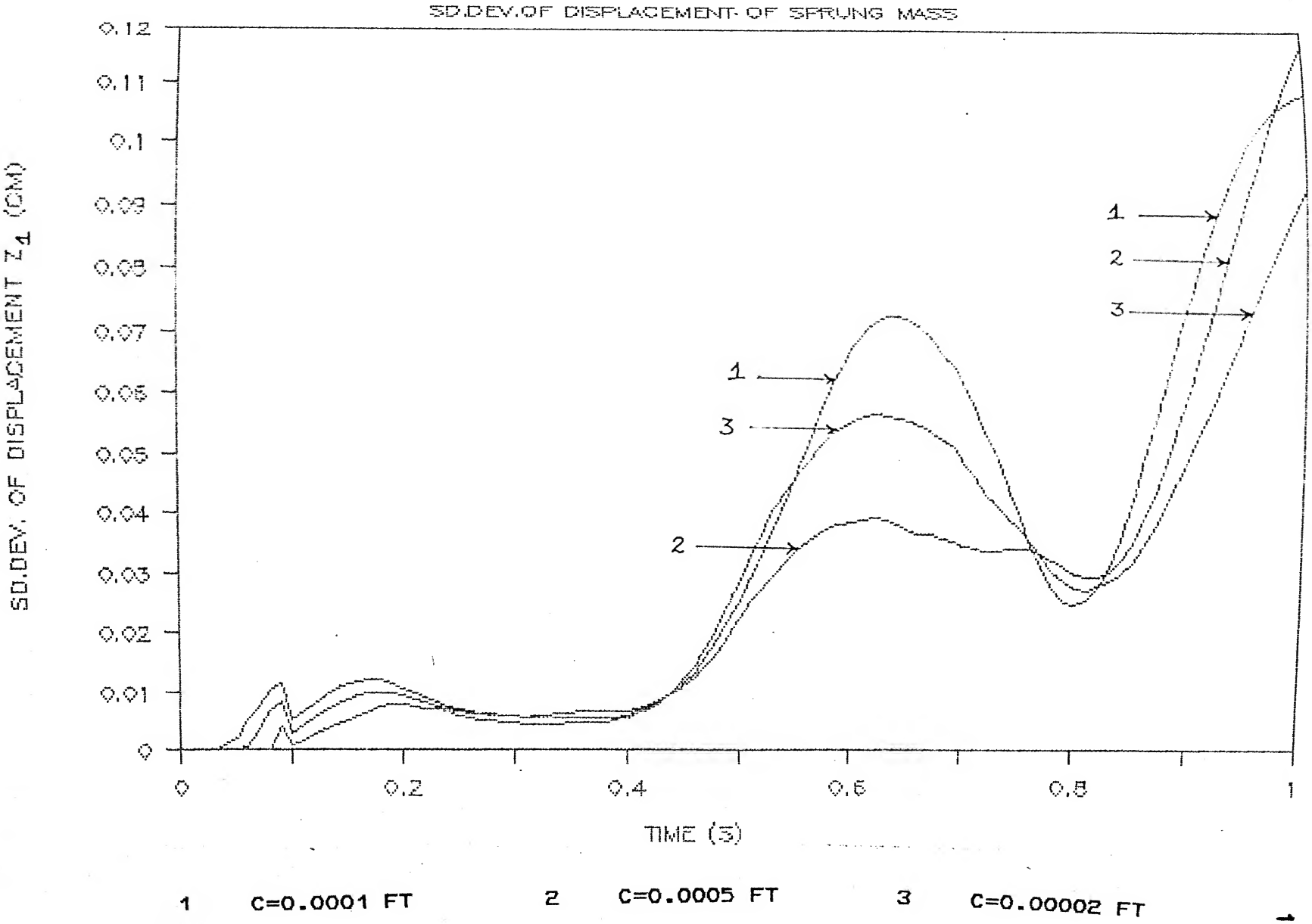

Fig. 4.14d Take-off run,Roughness variation;Standard Deviation of Displacement Response.

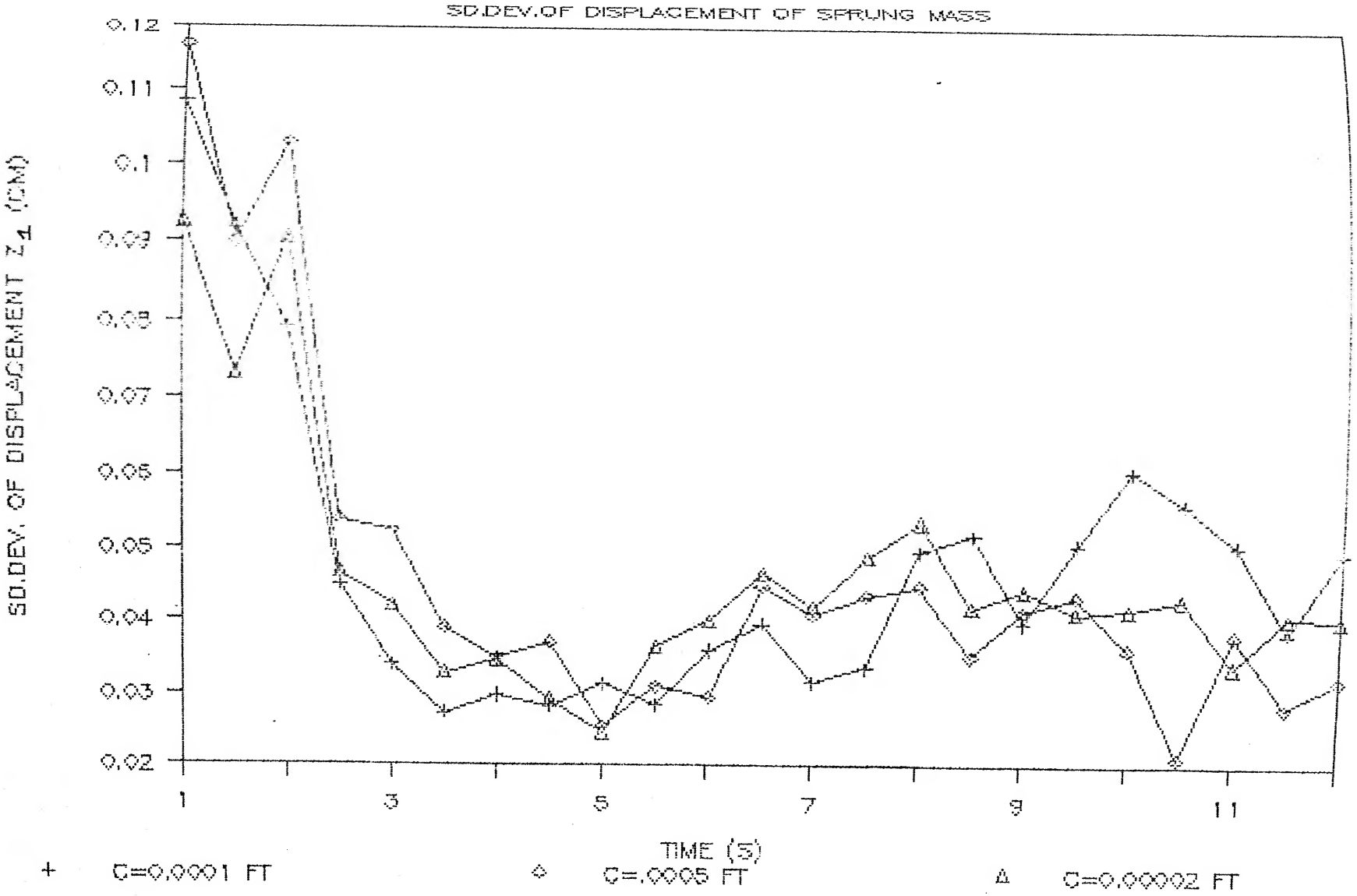

Fig. 4.14e Take-off run,Roughness variation;Standard Deviation of Displacement Response.

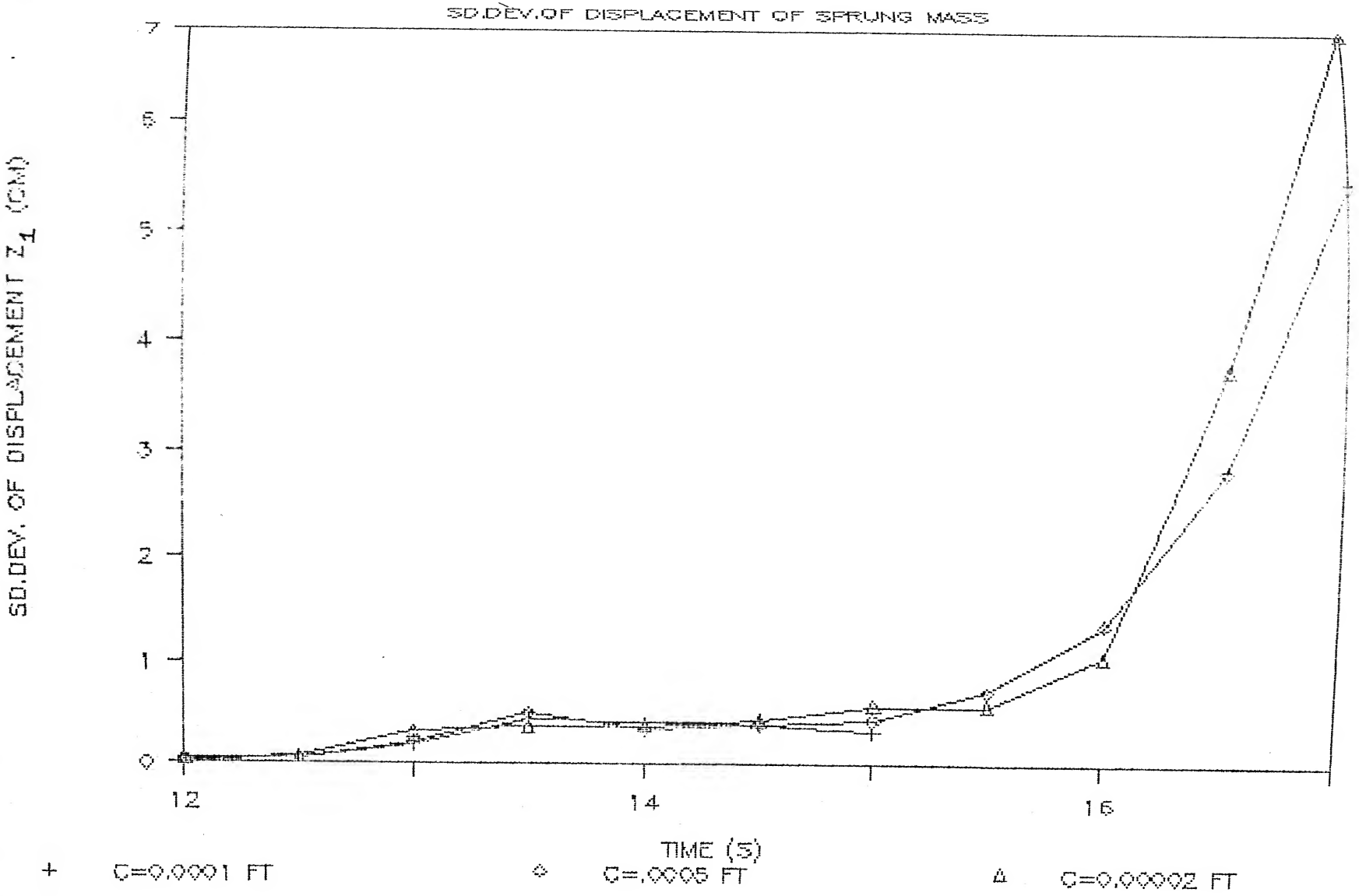

Fig. 4.14f Take-off run,Roughness variation;Standard Deviation of Displacement Response.

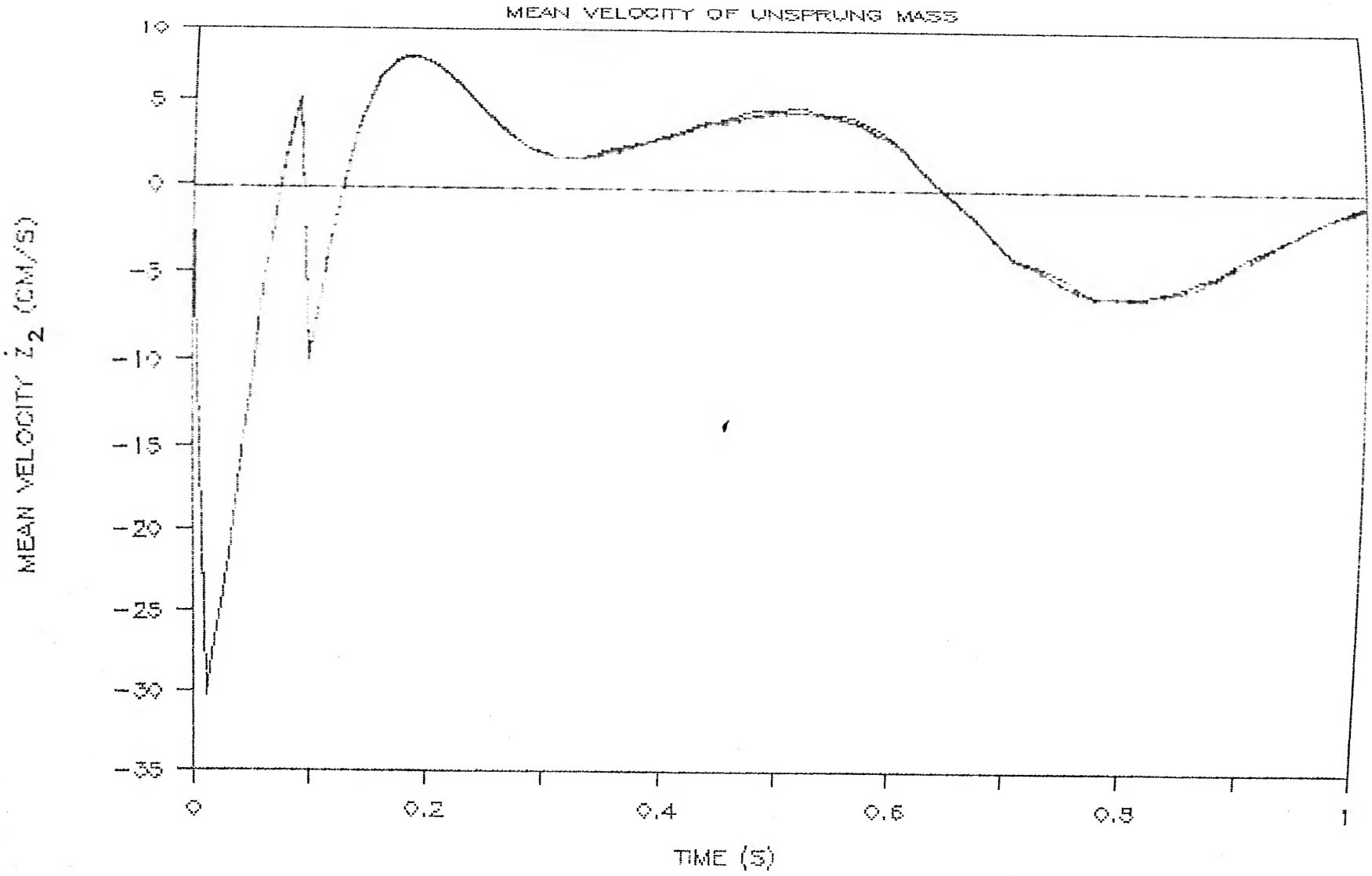

Fig. 4.15a Take-off run,Roughness variation; Mean Velocity Response.

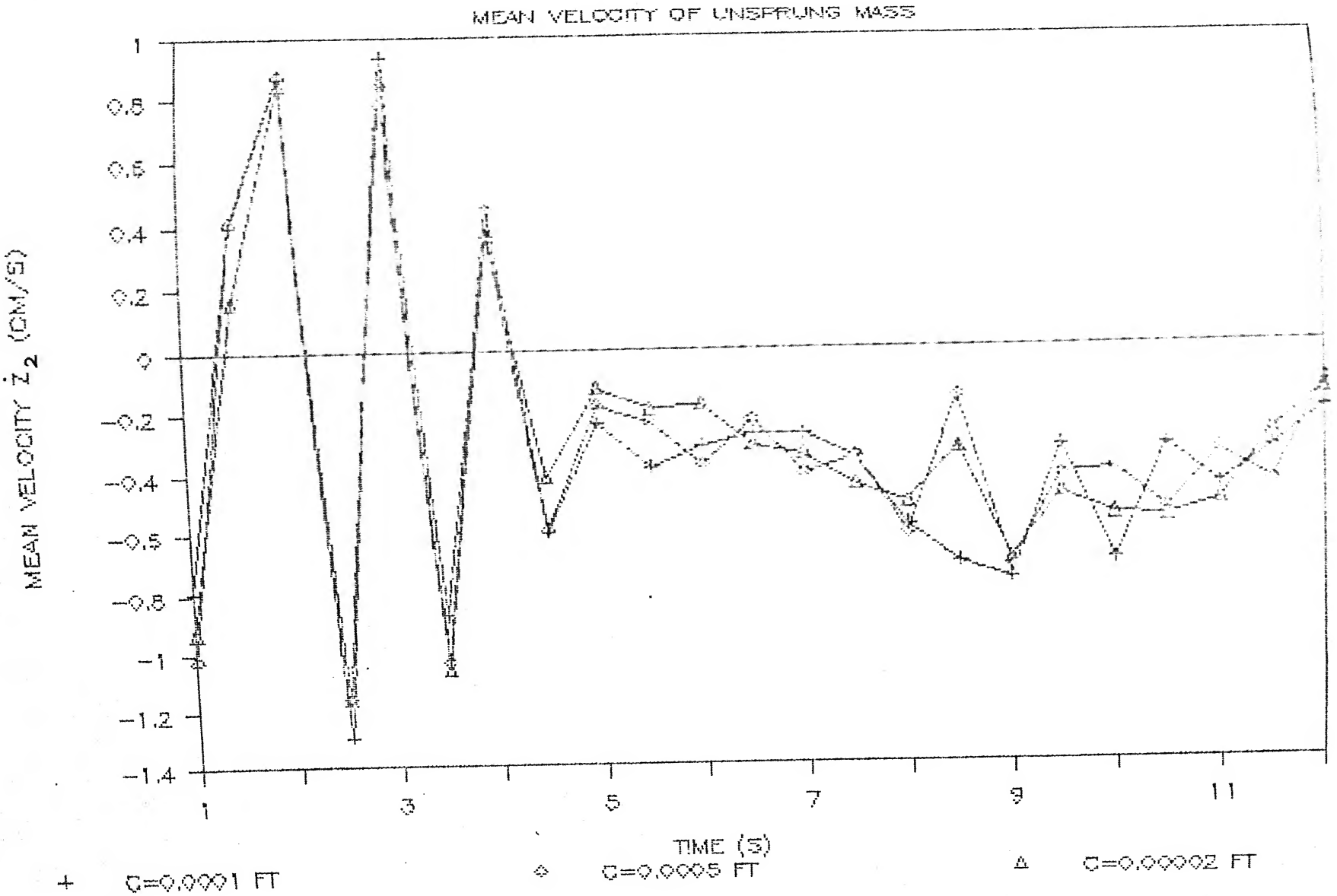

Fig. 4.15b Take-off run,Roughness variation; Mean Velocity Response.

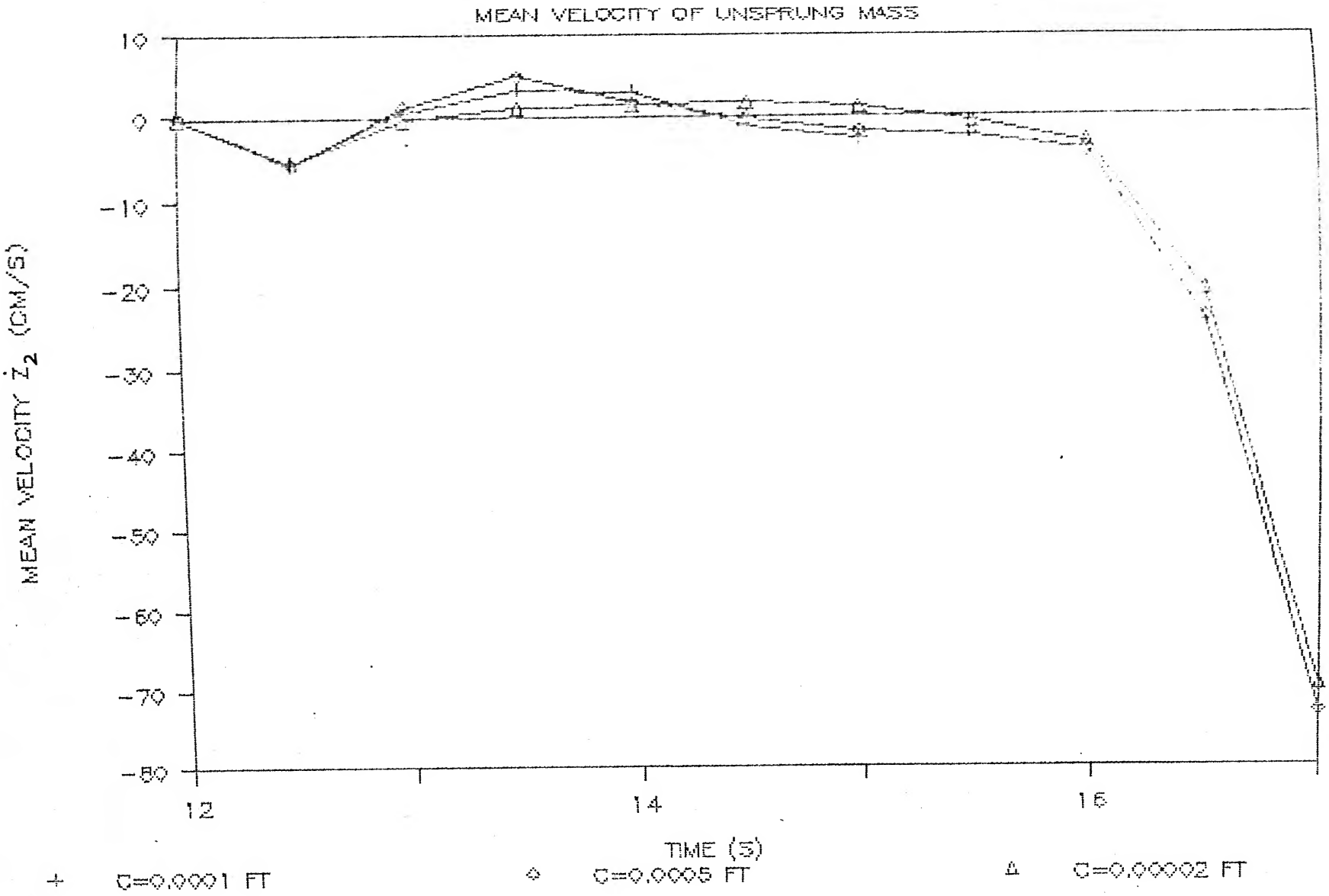

Fig. 4.15c Take-off run,Roughness variation; Mean Velocity Response.

ii) After the initial heavy fluctuations the mean velocity has very small fluctuations upto 12 seconds, but after that time the fluctuations again increase to a certain extent.

iii) Once take-off point is attained the velocity drops off very sharply.

4.4.6 Mean Velocity of the Sprung mass

The response of the mean velocity of the sprung mass is presented in Figure 4.15d. The observations made are :

i) Effect of the variation of the track roughness is not very predominantly seen.

ii) After about 2 seconds the mean velocity is seen fluctuating near the zero level.

iii) Once the take-off point is reached there is a sharp decline in the velocity.

4.4.7 Standard Deviation of Velocity of Unsprung mass

The response of the standard deviation of velocity of unsprung mass is shown in Figures 4.16a and 4.16b. The salient points noted are :

i) The effect of variation of track roughness is clearly visible in both the figures.

ii) Two resonances are observed at around 0.5 and 0.75 seconds after the start of the run.

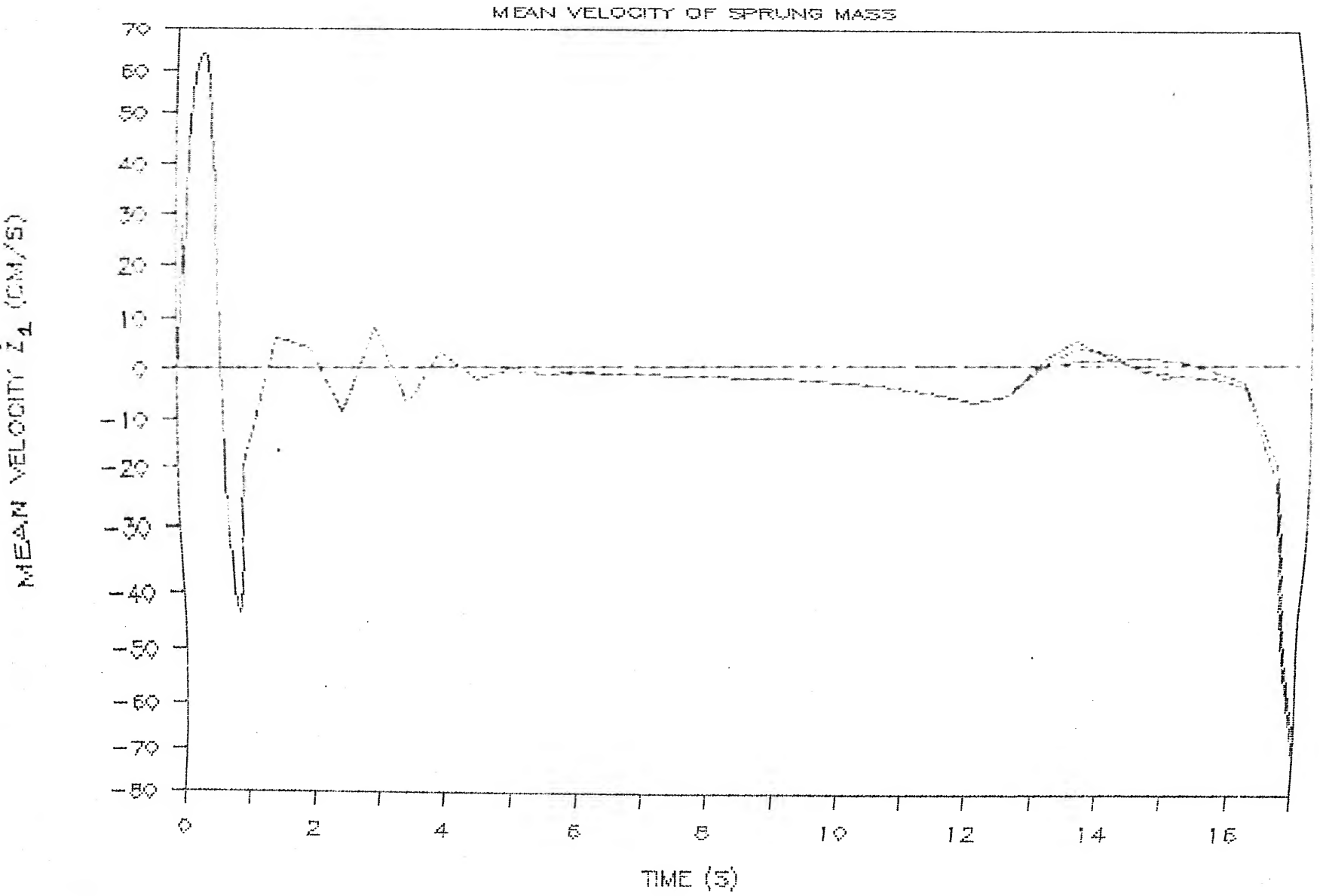

Fig. 4.15d Take-off run,Roughness variation; Mean Velocity Response.

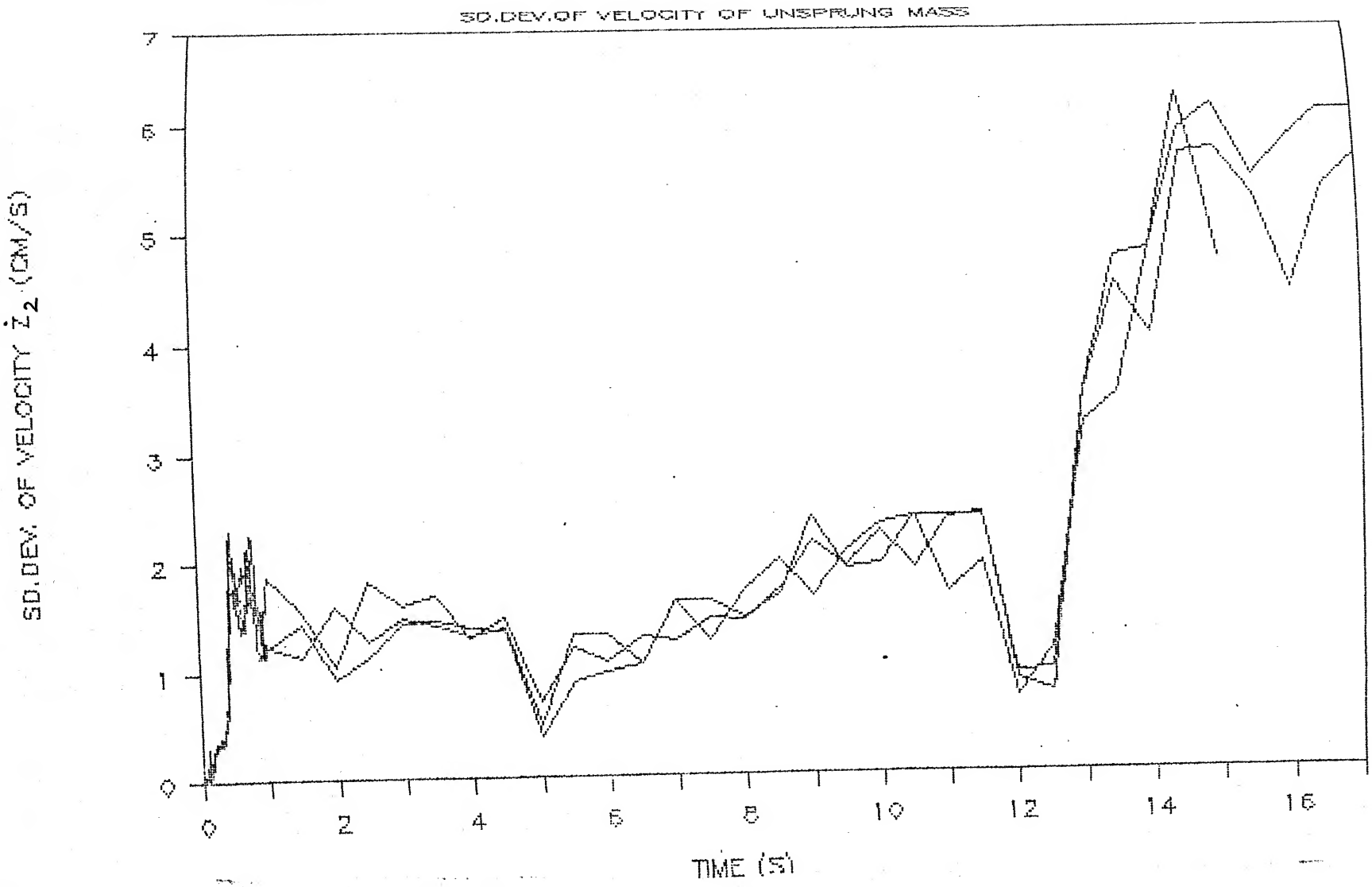

Fig. 4.16a Take-off run,Roughness variation;Standard Deviation of Velocity Response.

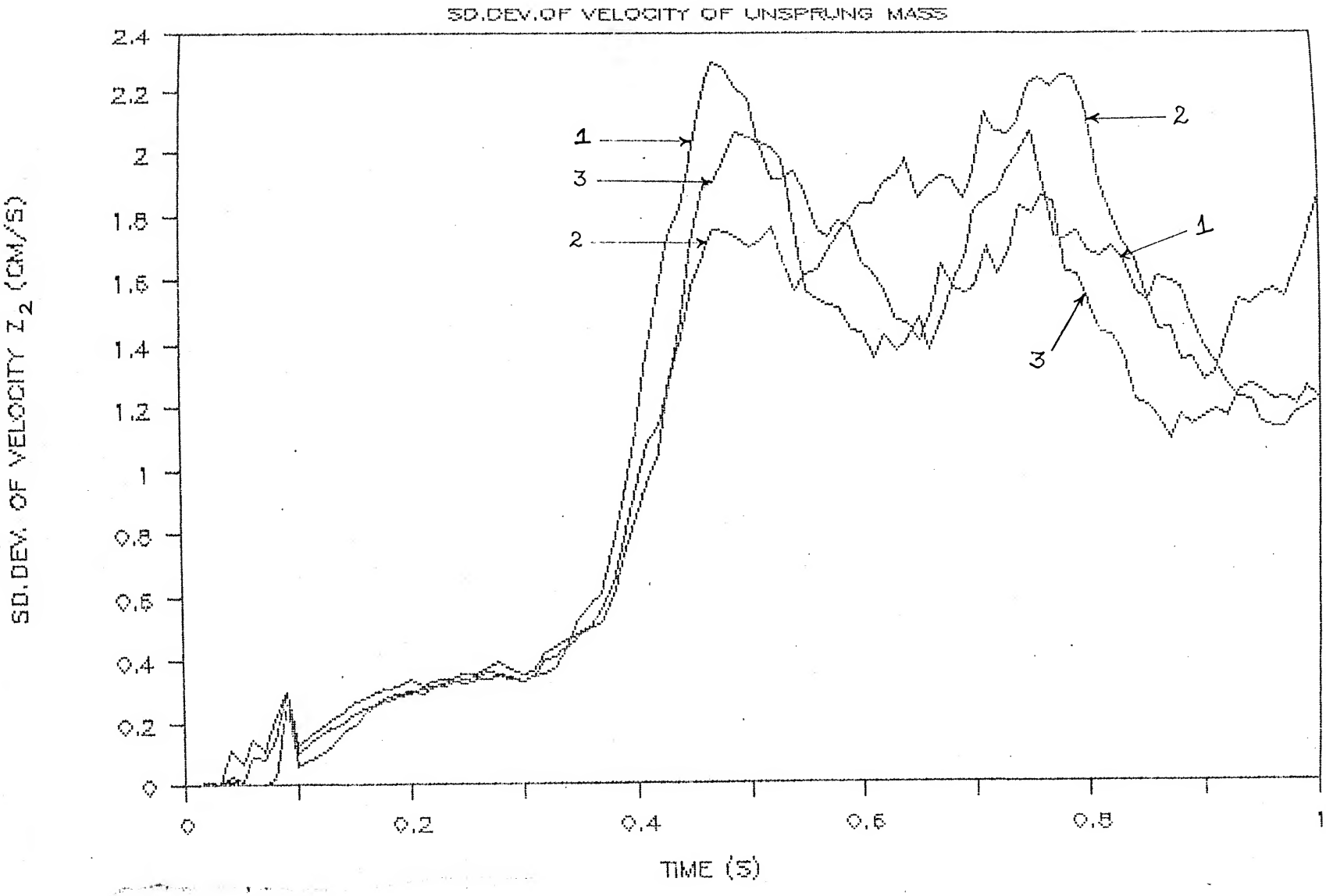

Fig. 4.16b Take-off run, Roughness variation; Standard Deviation of Velocity Response.

iii) After a time duration of 12 seconds there is one more resonance at around 14.5 seconds.

4.4.8 Standard Deviation of Velocity of Sprung mass

The response of the standard deviation of velocity of sprung mass is shown in Figures 4.16c to 4.16e. The interesting observations are :

i) Effect of the variation of the track roughness is clearly visible, but it fails to indicate a set pattern of influence.

ii) Resonances are observed at 0.5, 0.8 and 3.5 seconds for all the values of track roughness considered.

iii) The trend of the standard deviation shows a decrease upto 12 seconds, but after 12 seconds there is again a large increase in the value.

4.4.9 Mean Acceleration of the Unsprung mass

The response of the mean acceleration of the unsprung mass is shown in Figures 4.17a and 4.17b. The noteworthy points are :

i) The effect of the variation of track roughness is clearly visible after 0.3 second.

ii) A resonance occurs at around 0.1 second after which there is a sharp decline in the mean acceleration.

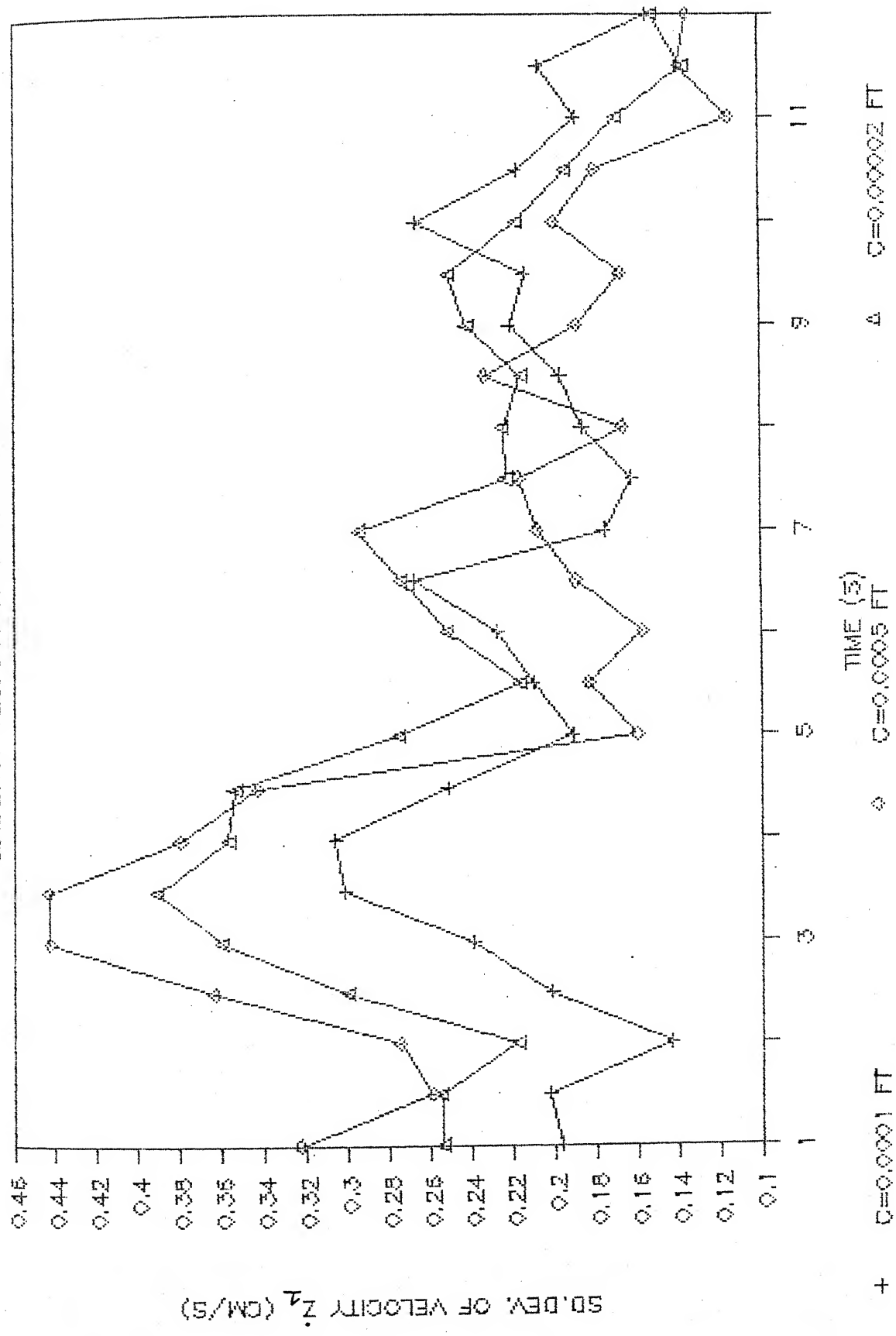

Fig. 4.16d Take-off run, Roughness variation; Standard Deviation of Velocity Response.

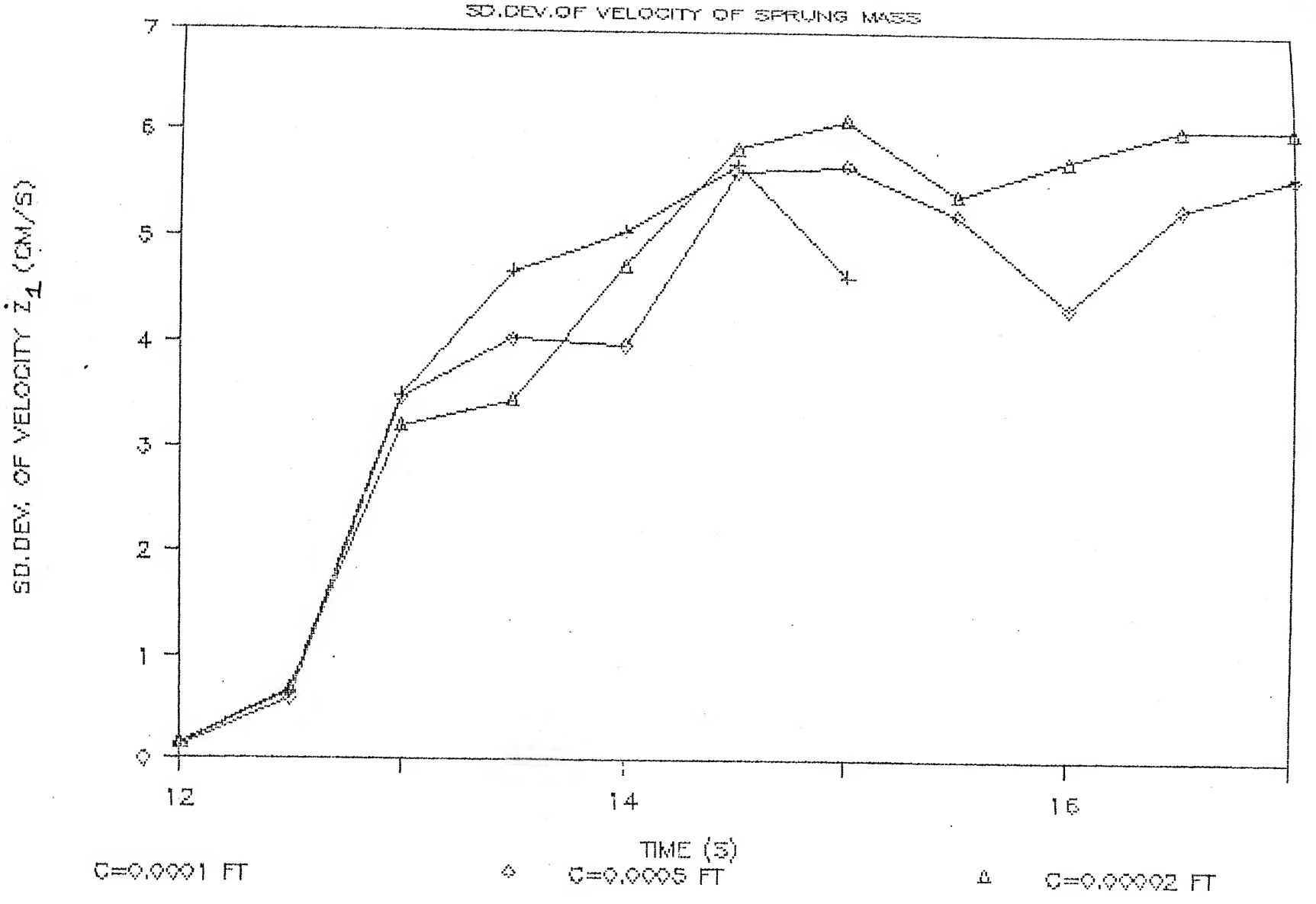

Fig. 4.16e Take-off run,Roughness variation;Standard Deviation of Velocity Response.

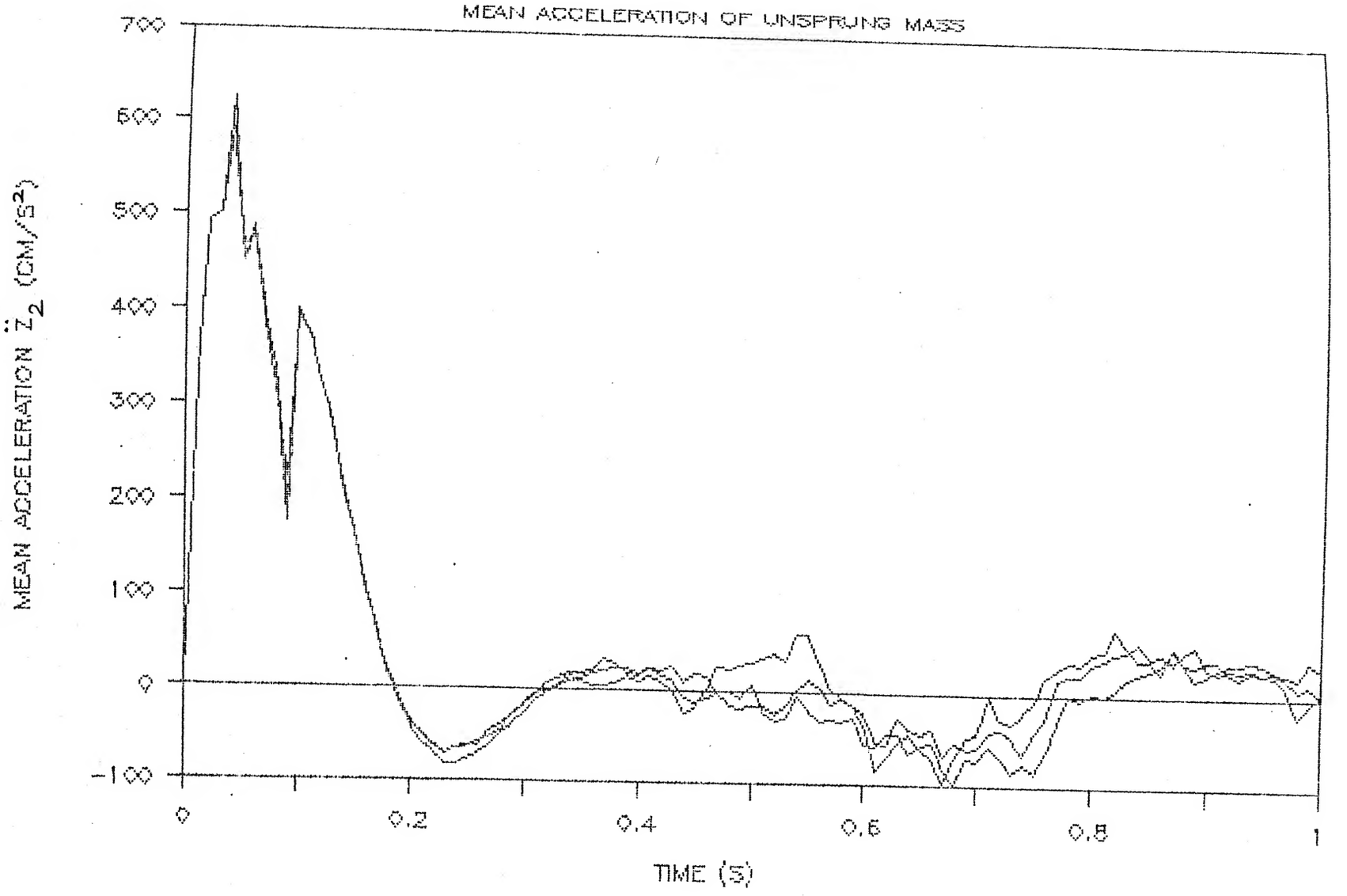

Fig. 4.17a Take-off run,Roughness variation;Mean Acceleration Response.

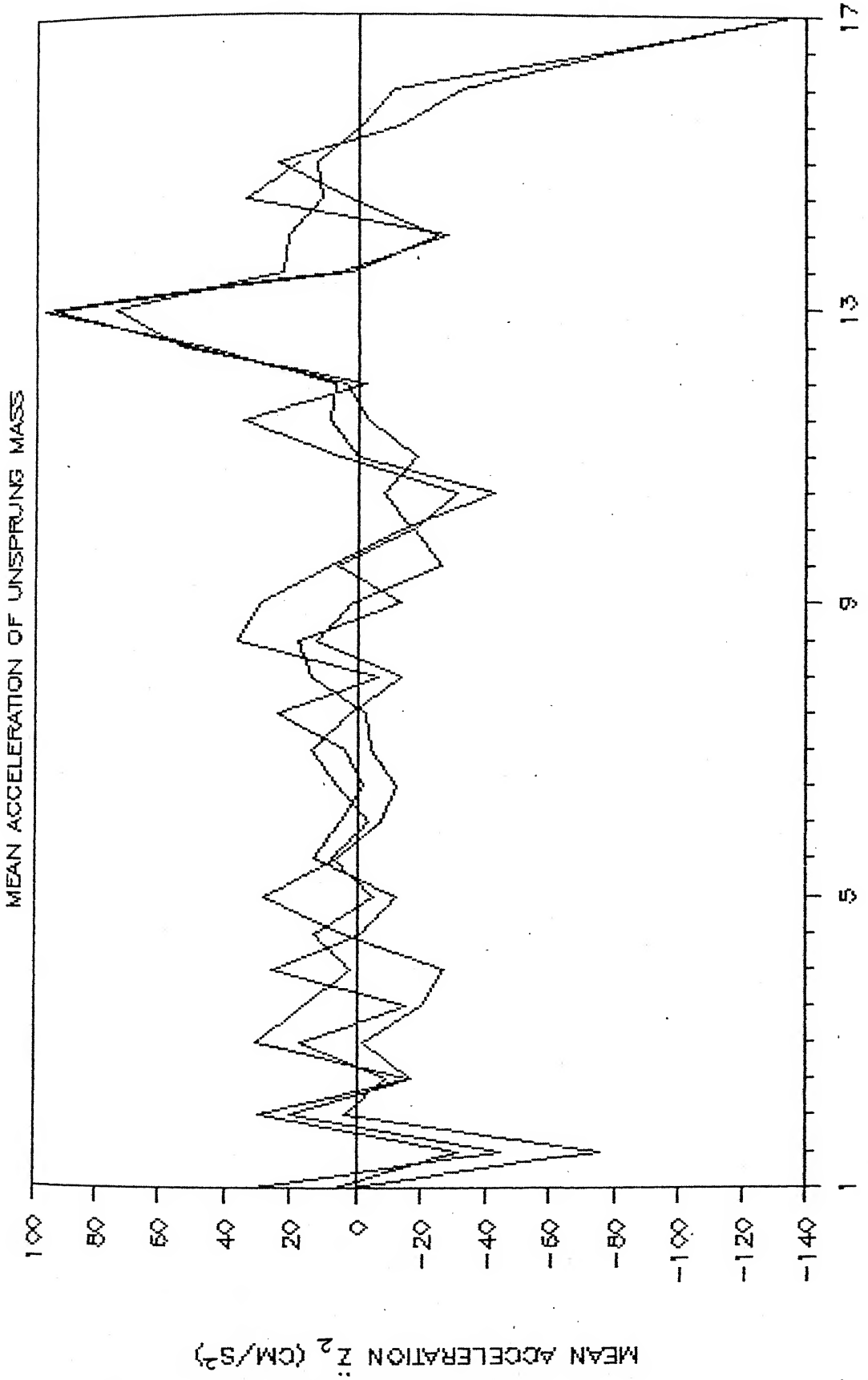

Fig. 4.17b Take-off run,Roughness variation;Mean Acceleration Response.

iii) The fluctuations in the acceleration after 1 second are centered at the zero level, and at around 13 seconds one more resonance is observed.

iv) After reaching the take-off point the value of the acceleration suddenly shows a sharp drop.

4.4.10 Mean acceleration of Sprung mass

Figures 4.17c and 4.17d show the response of mean acceleration of the sprung mass. The points observed are :

i) The effect of variation of track roughness is not very predominant, only after 12 seconds some variation in response is observed at different values of track roughness.

ii) The trend shows a fluctuation in the mean value upto a time duration of 3 seconds. Afterwards the value remains steady at the zero level upto 12 seconds.

iii) Resonance is observed at around 13 seconds, but after that the value again starts oscillating about the zero level.

iv) Once take-off is established the value shows a sharp decline.

4.4.11 Standard Deviation of Acceleration of Unsprung mass

Figures 4.18a and 4.18b show the response of the standard deviation of acceleration of the unsprung mass. The observations

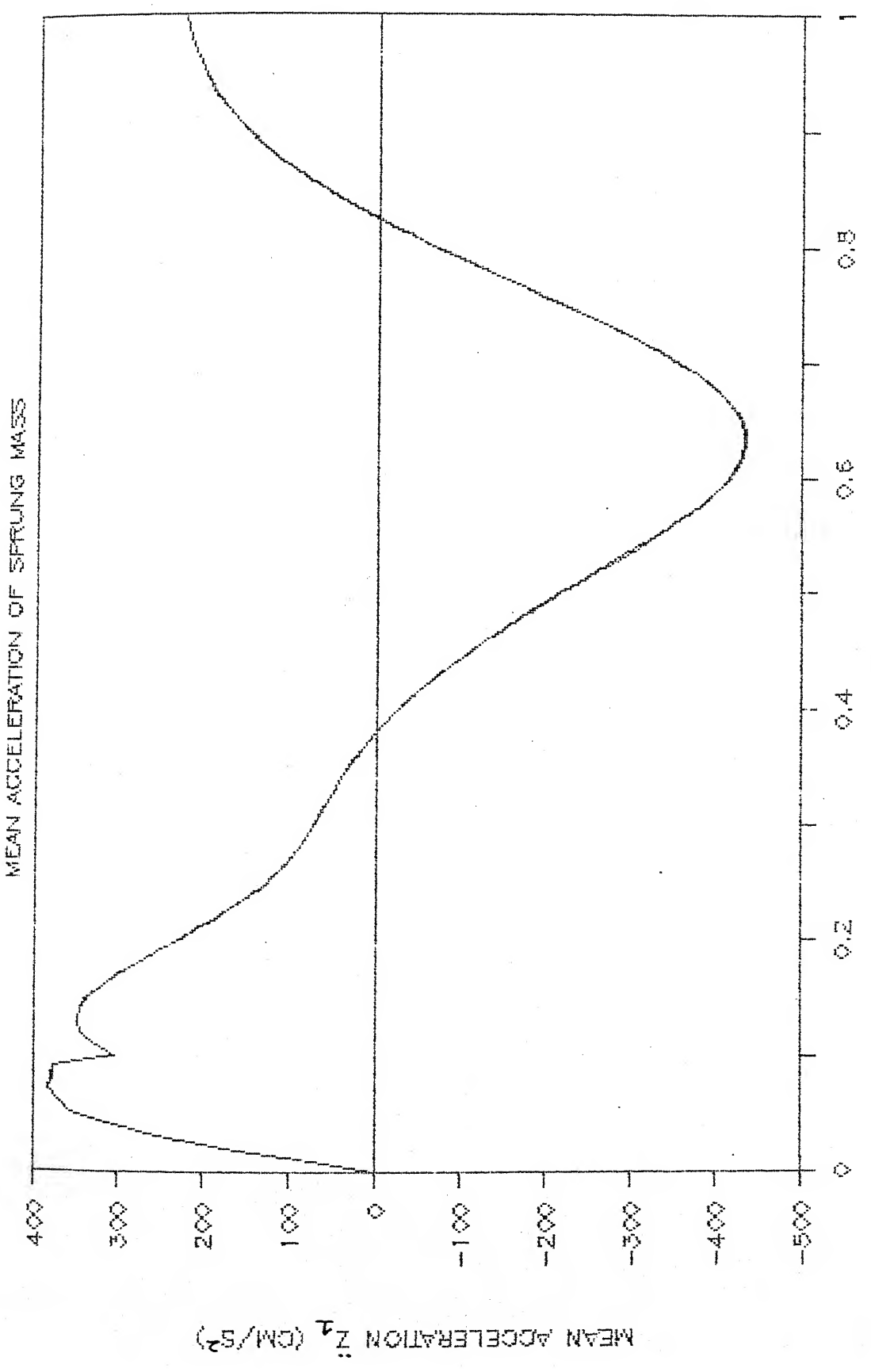

Fig. 4.17c Take-off run, Roughness variation; Mean Acceleration Response.

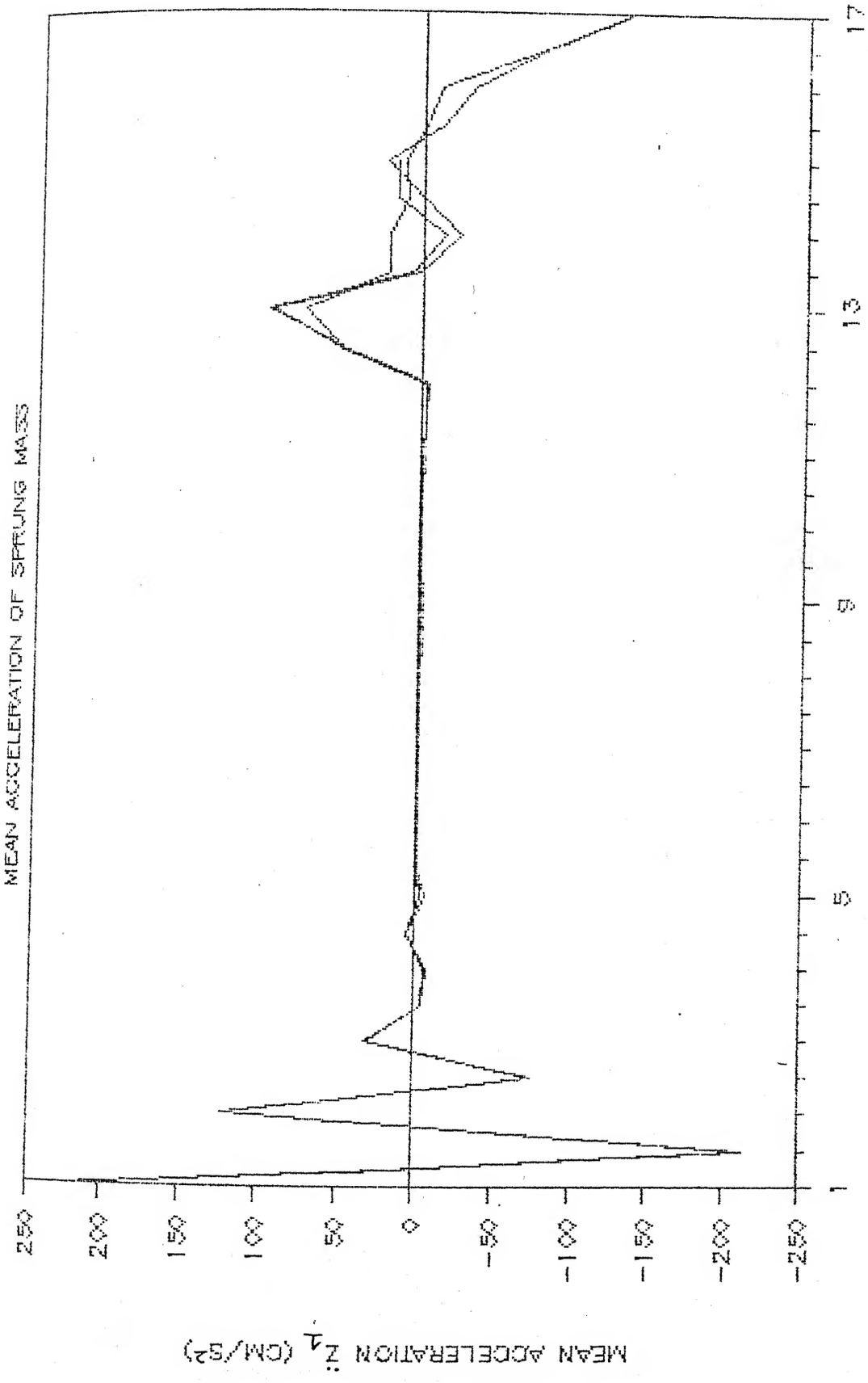

Fig. 4.17d Take-off run, Roughness variation; Mean Acceleration Response.

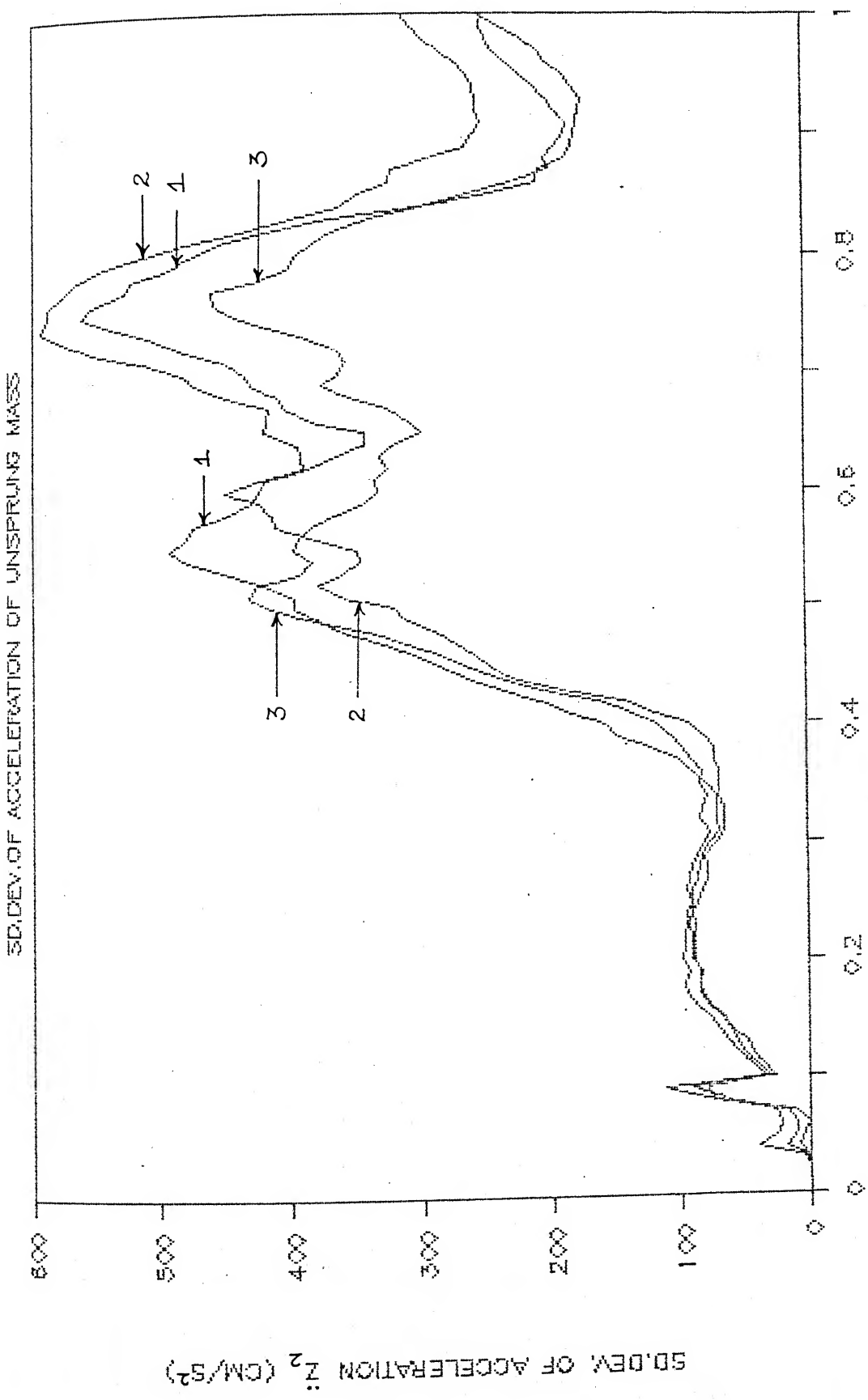

1 C=0.0001 FT 2 C=0.0005 FT 3 C=0.00002 FT

Fig. 4.18a Take-off run,Roughness variation;Standard Deviation of Acceleration Response.

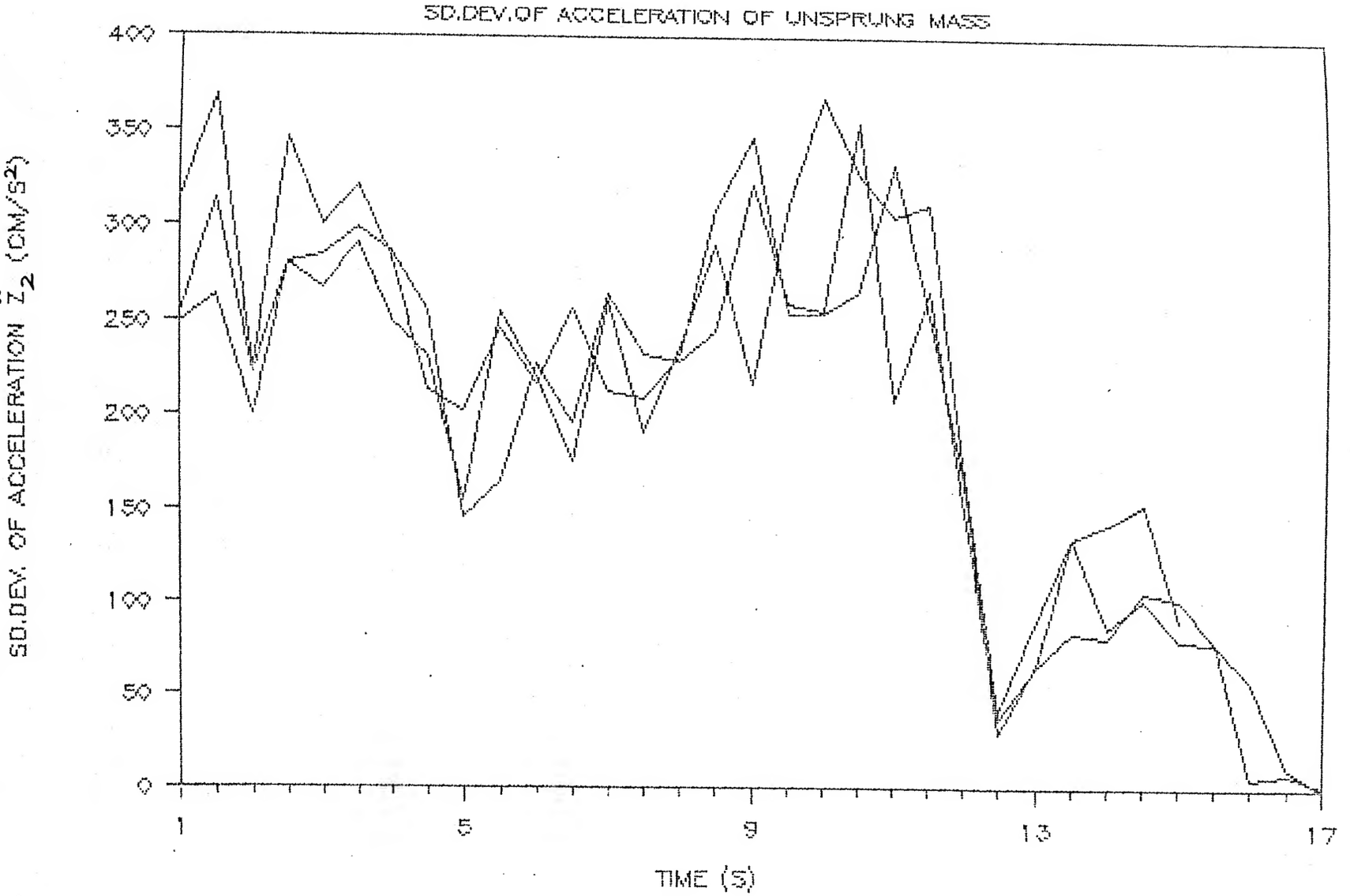

Fig. 4.18b Take-off run,Roughness variation;Standard Deviation of Acceleration Response.

made are :

i) Effect of variation of the track roughness is very clear on the standard deviation of acceleration.

ii) Resonances are observed at 0.45 and 0.55 seconds.

iii) The trend of the graph shows a decreasing pattern after the later resonance has taken place.

4.4.12 Standard Deviation of Acceleration of Sprung mass

The response of the standard deviation of acceleration of sprung mass is shown in Figures 4.18c and 4.18d. The points observed are :

i) The variation in the level of roughness of the track has some effect on the standard deviation of acceleration of the sprung mass.

ii) During the first one second of the take-off run, three resonances at 0.2, 0.5 and 0.8 seconds are observed.

iii) After 1 second the value of standard deviation for all roughness levels considered settles at around 0.01 g. This behaviour continues for about 12 seconds. Then at about 14 seconds after the start a resonance is observed and the value suddenly shoots up to 0.11 g.

iv) After take-off the values are seen to drop sharply.

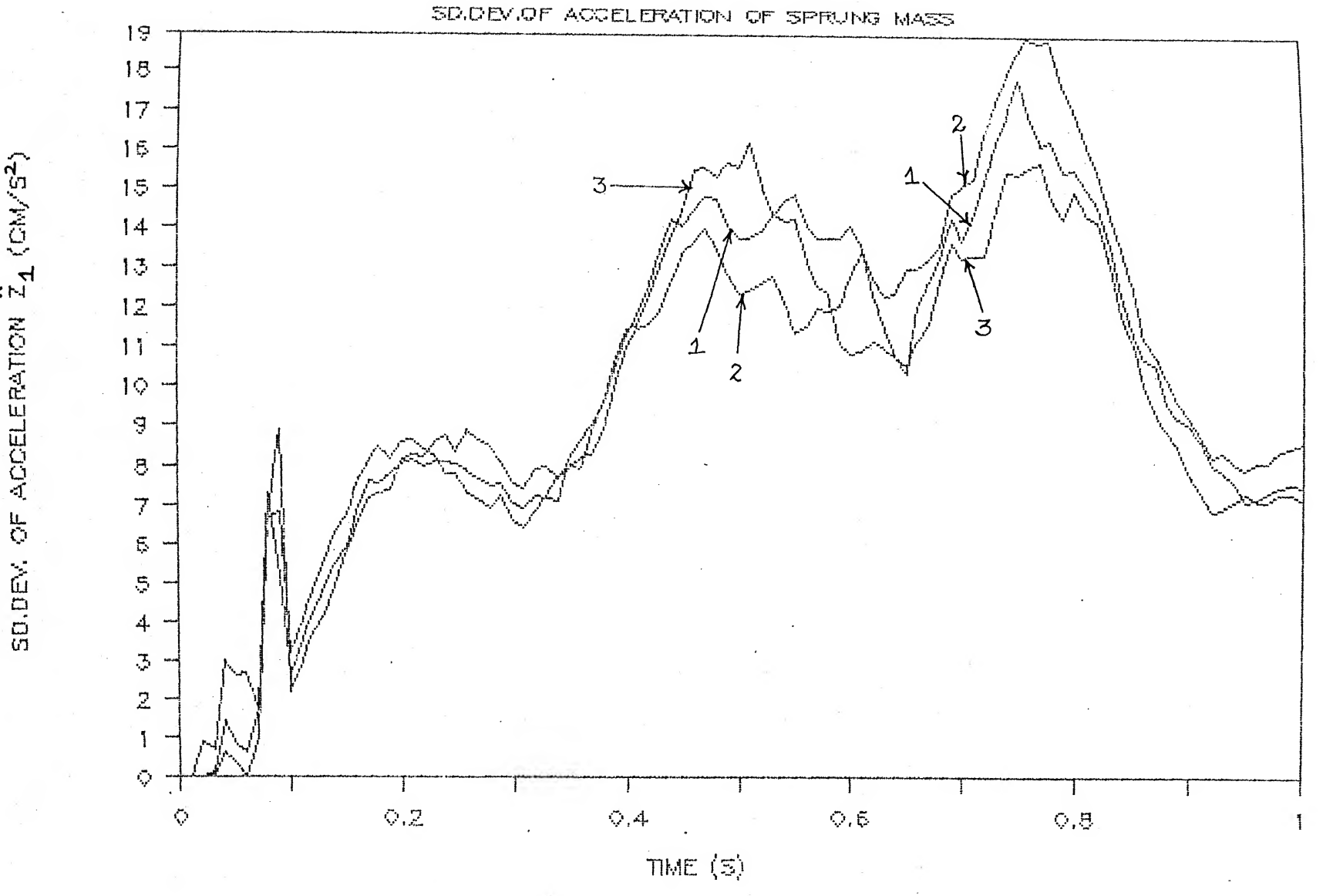

1 C=0.0001 FT 2 C=0.0005 FT 3 C=0.00002 FT

Fig. 4.18c Take-off run,Roughness variation;Standard Deviation of Acceleration Response.

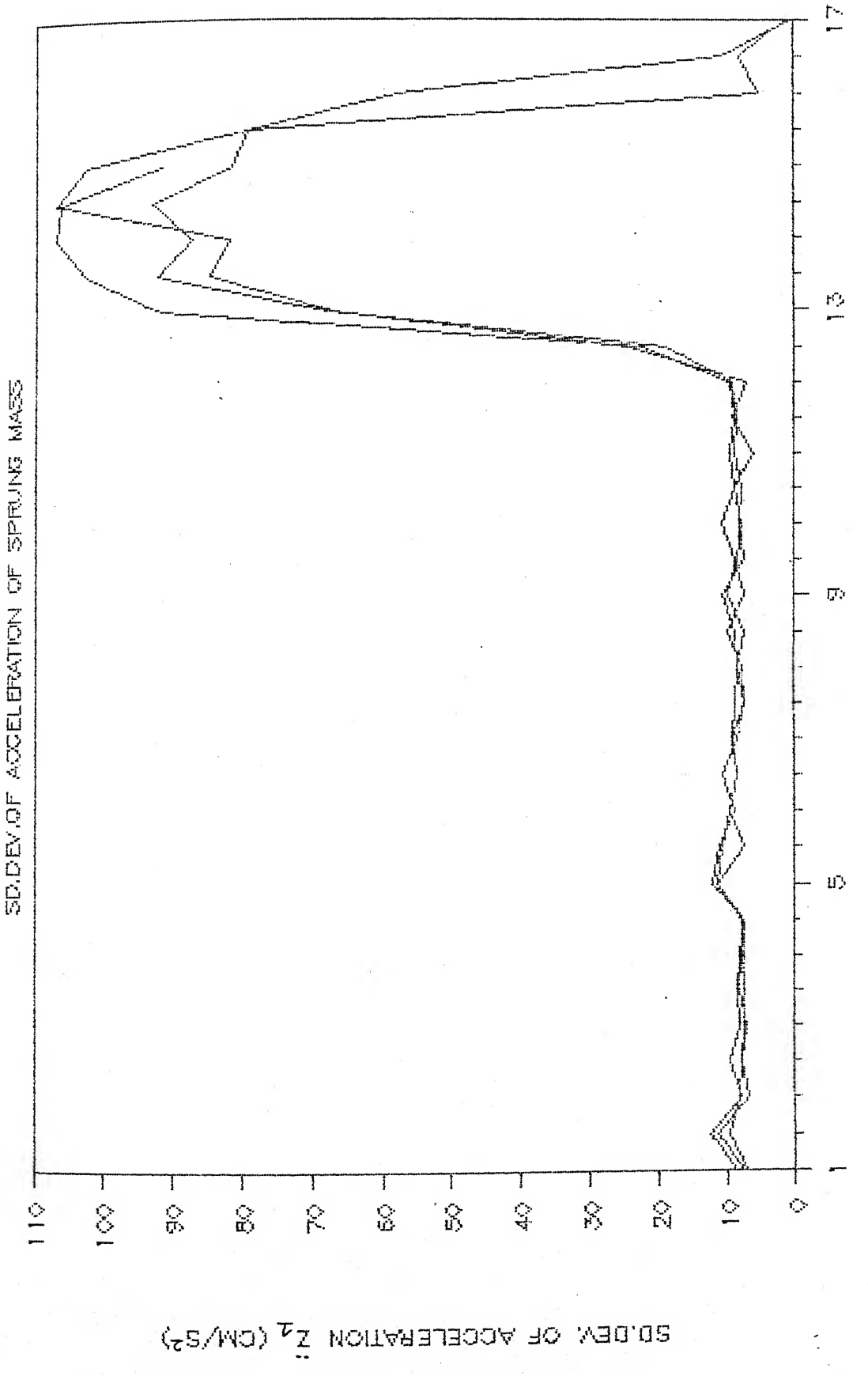

Fig. 4.18d Take-off run,Roughness variation;Standard Deviation of Acceleration Response.

Table 4.1 *Maximum values of Mean and Standard Deviation for roughness variation during Landing.*

	ROUGHNESS CONSTANT (FT)	DISPLACEMENT (CM)		VELOCITY (CM/S)		ACCELERATION (CM/S^2)	
		MEAN	SD.DEV	MEAN	SD.DEV.	MEAN	SD.DEV.
UNSPRUNG MASS	0.0001	13.12	.3282	350.	5.305	-13120	10170.
	0.0005	13.11	.3111	350.	7.107	-12410	13200.
	0.00002	13.12	.3519	350.	4.605	-13060	10870.
SPRUNG MASS	0.0001	19.8	1.1	350.	5.603	-5215	760.2
	0.0005	19.8	0.4732	350.	7.102	-5270	1046.0
	0.00002	19.8	0.6296	350.	4.282	-5233	819.0

Table 4.2 : Maximum values of Mean and Standard Deviation for sink velocity variation during Landing

	SINK VELOCITY (CM/S)	DISPLACEMENT (CM)		VELOCITY (CM/S)		ACCELERATION (CM/S^2)	
		MEAN	SD.DEV.	MEAN	SD.DEV.	MEAN	SD,DEV.
UNSPRUNG MASS	350	13.12	0.3282	350	5.305	-13120	10170
	250	9.913	0.3097	250	4.965	8705	5936
	100	5.596	0.3299	102.1	4.587	-3024	1764
SPRUNG MASS	350	19.8	1.10	350	5.603	-5215	760.2
	250	14.91	0.6125	250	4.801	-4417	460.5
	100	8.774	0.4488	102.1	4.611	-1293	137.0

Table 4.3 : Maximum values of Mean and Standard Deviation for roughness variation during Take-off

	ROUGHNESS CONSTANT (FT)	DISPLACEMENT (CM)		VELOCITY (CM/S)		ACCELERATION (CM/S)	
		MEAN	SD.DEV	MEAN	SD.DEV.	MEAN	SD.DEV.
UNSPRUNG MASS	.0001 *	4.562	0.4252	-30.31	6.207	621.8	558.2
	.0005	4.557	5.469	-72.86	5.668	588.8	593.5
	.00002	4.565	7.000	-69.46	6.105	620.3	455.8
SPRUNG MASS	.0001*	31.93	0.4397	-63.93	5.676	-433.5	106.9
	.0005	31.92	5.469	-72.86	5.668	-432.2	92.6
	.00002	31.94	7.000	-69.46	6.105	-435.4	107.0

* Data for 15 secs only.

CHAPTER V

Conclusions

In the present study the numerical data for the aircraft and the landing gear parameters contained in the appendix, are used to find the response of the aircraft. The aircraft is considered to be a rigid lumped mass with only heave degree of freedom and a single point input from the track. The response study is carried out for the variation in the roughness level of the track for the variable velocity runs - landing and take-off, and for the variation of the sink velocity during landing run. The response samples are then analysed to obtain the second order statistics of the response. The results and discussion for this study have been presented in Chapter - IV.

5.1 *Concluding Remarks*

The salient conclusions drawn from the present study are listed below.

i) Franklin's method of numerical simulation of the random profile fits very well with the prescribed power spectral density (p.s.d.) of the track, for the entire frequency range.

ii) The unsprung mass is subjected to much more severe forces than the sprung mass, as indicated by the higher values of accelerations for the unsprung mass.

iii) During the study of the landing run, it is observed that the response values shoot up rapidly during the impact

phase, but with the passage of time, a decreasing trend is observed.

iv) During landing, the effect of varying the roughness level of the runway track on the mean and standard deviation response is not very significant.

v) Even for the small effect that roughness has on the response, a set pattern is not realised. The reason which can be attributed to this behaviour are the inherent nonlinearity of the system considered, nonstationarity of the track profile and the variable velocity runs of the aircraft. Only for the time duration of initial one second, in most cases, an increase in response with an increase in roughness level is observed.

vi) During landing, the effect of the variation of sink velocity of the aircraft is predominantly observed in the heave displacements of the sprung and the unsprung masses. At higher values of sink velocities, the impact is more and as a consequence the masses are subjected to more heaving displacements. The acceleration response also indicates the same effect of sink velocity. Once the impact phase has passed, the definitive pattern of response due to sink velocity variation is not discernible.

vii) During take-off the maximum values of mean and standard deviation response are lower than the values for landing.

viii) During take-off, the effect of varying the roughness level of the track does not affect the mean response predominantly. The response standard deviation shows some effect, but a consistent pattern is not observable.

ix) The response standard deviation of both the sprung and the unsprung masses show signs of resonance in many cases of landing and take-off runs.

5.2 *Suggestions for Future Work*

Extension of the present study could be carried out keeping in consideration one or more of the following.

(1) Both the drag and and the main shock strut should be made to function simultaneously.

(2) During the landing run, for the present study, lift was considered to be constant. Variation in the lift due to the variation in velocity must be considered.

(3) Variations in the mean profile of the track can be studied.

(4) Pilot's inputs can also be incorporated.

(5) The ensemble size should be increased.

(6) The differential equation solver should be such that during the process of discrete step-by-step solving, there is no back tracking, because this creates lot of computational complexities.

Besides these, extensions can be made in the actual system modelling. Instead of the single point input from the track, multi point input can be studied. In that case the system model will be a heave-pitch or a heave-pitch-roll model. Other variations may include unsymmetric landing, effect of side wind during landing and take-off, flexible aircraft structure (both the wing and the fuselage) and flexible runway pavement.

REFRENCES

1. MORRIS, G.J.,Response of a Turbojet and a Piston-Engine Transport Airplane to Runnway Roughness, *NASA* Tech. Note D-3161, December 1965.

2. STOWELL,E.Z.,HOUBOLT, J.C., and BATDORF, S.B., An Evaluation of Some Approximate Methods of Computing Landing Stresses in Aircraft, *NACA* Tech. Note No. 1584, 1948.

3. COOK,F.E. and MILWITZKY,B.,Effects of Interaction on Landing-Gear Behaviour and Dynamic Loads in a Flexible Airplane Structure, *NACA* Tech. Note 3467, August 1955.

4. RAGHAVAN, K.S.,Analysis of Aircraft Landing Impact, *M.Tech. Thesis, I I T KANPUR*, 1971.

5. MILWITZKY, B.and COOK, F.E., Analysis of Landing Gear Behaviour. *NACA* Report. 1154, 1953.

6. WAHI, M.K., Oleopneumatic Shock Strut Dynamic Analysis and Real Time Simulation, *Journal of Aircraft*, Vol. 13, April 1976, pp. 303-308.

7. WAHI, M.K., Oil Compressibility and Polytropic Air Compression Analysis of Oleopneumatic Shock Struts, *Journal of Aircraft*, Vol.13, July 1976, pp.527-530.

8. JAYARAMI REDDY, P., NAGARAJ, V.T. and RAMAMURTI, V., Analysis of a Semi-levered Suspension Landing Gear with Some Parametric Study. *Journal of Dynamic Systems, Measurement and Control, Trans. of ASME*, Vol. 106, September 1984, pp.218-224.

9. JAYARAMI REDDY, P., NAGARAJ, V.T., and RAMAMURTI, V., Analysis of articulated landing gear behaviour *Sixth IFTOMM Congress on theory of Machines and Mechanisms*, New Delhi, December 1983, pp 391-394.

10. SILSBY, N.S., An analytical study of Effects of some Airplane Landing Gear Factor on the Response to Runway Roughness with Application to Supersonic Transports, *NASA* Tech. Note D-1492, December 1962.

11. TUNG, C.C., PENZIEN, J., and HORONJEFF, R., The Effect of Runway Unevenness on the Dynamic Response of Supersonic Transports, *NASA* CR-119, October, 1964.

12. KIRK., C.L. and PERRY,P.J., Analysis of Taxiing Induced Vibrations in Aircraft by the Power Spectral Density Method, *The Aeronautical Journal*, Vol. 75, No. 723, March, 1971, pp.182-194.

13. VIRCHIS, V.J. and ROBSON, J.D. Response of an Accelerating Vehicle to Random Road Undulations *Journal of Sound and Vibration*, Vol. 18, No. 3, 1971, pp. 423-427.

14. SOBCZYK, K., and MACVEAN, D.B., Non stationary Random Vibrations of systems Travelling with Variable Velocity. *Symposium on Stochastic Problems in Dyanamics*, University of Southampton, ed., Clarkson, B.L., 1976, pp. 412-434.

15. YADAV, D., and NIGAM, N.C., Ground Induced Non Stationary response of Vehicles. *Journal of Sound and Vibration*, Vol. 61, No.1, 1978, pp. 117-126.

16. HAMMOND, J.K. and HARRISON, R.F., Non stationary response of Vehicles on Rough Ground - A State Space Approach. *Journal of Dynamic Systems, Measurement and Control.,Trans. of ASME*. Vol. 103, September, 1981, pp. 245-250.

17. HARRISON, R.F., and HAMMOND, J.K., Approximate, Time Domain, Non stationary Analysis of Stochastically Excited, Non Linear Systems with Particular Refrence to the Motion of Vehicles on Rough Ground, *Journal of sound and Vibration*, Vol.105, No.3, 1986, pp. 361-371

18. FRANKLIN, J.N., Numerical Simulation of Stationary and Non stationary Gaussian Random Processes. *SIAM Review*, Vol. 7, No.1, January, 1965, pp. 68-80.

19. BENDAT, J.S. and PIERSOL, A.G., *Random data: Analysis and measurement procedures*, 2d rev. ed., 1986.

20. BOX, G.E.P. and MULLER, M.E., A note on the generation of random normal deviates, Annals of Mathematical Statistics, Vol. 29, 1958, pp. 610-611.

APPENDIX

AIRCRAFT DATA

I. GENERAL

1. Gross weight of the aircraft	= 4154.0 Kg_f
2. Weight of the main wheels	= 100.0 Kg_f
3. Wheel base	= 345.0 cm
4. Distance of aircraft c.g from main wheels	= 126.2 cm
5. Distance of aircraft c.g from nose wheel	= 218.8 cm
6. Landing velocity of aircraft	= 5400.0 cm/s
7. Take-off velocity of aircraft	= 5900.0 cm/s

II. CHARECTERISTICS OF THE SHOCK STRUT OF THE MAIN GEAR

1. Coefficient of discharge	= 0.6
2. Coefficient of seal friction	= 0.01
3. Mass density of fluid	= 0.85 gm/c.c
4. Orifice area	= 2.405 sq.cm
5. Hydraulic area	= 63.6 sq.cm
6. Pneumatic area	= 49.5 sq.cm
7. Extended air pressure	= 9.5 kg/cm^2
8. Extended air volume	= 1462.0 c.c
9. Index for air compression	= 1.3

10. Initial oil volume = 1950.0 c.c

11. Full stroke = 26.4 cm

12. Coefficient of friction at bearings = 0.1

13. Axial distance between bearings = 20.0 cm

14. Coulomb friction = 0

15. Preload = 470.25 Kg_f

III. MAIN TYRES

1. Radius = 25.0 cm

2. Spin-up time = 0.038 secs

3. Polar moment of inertia = 3217 $kg\text{-}cm^2$

4. Load-deflection curve given

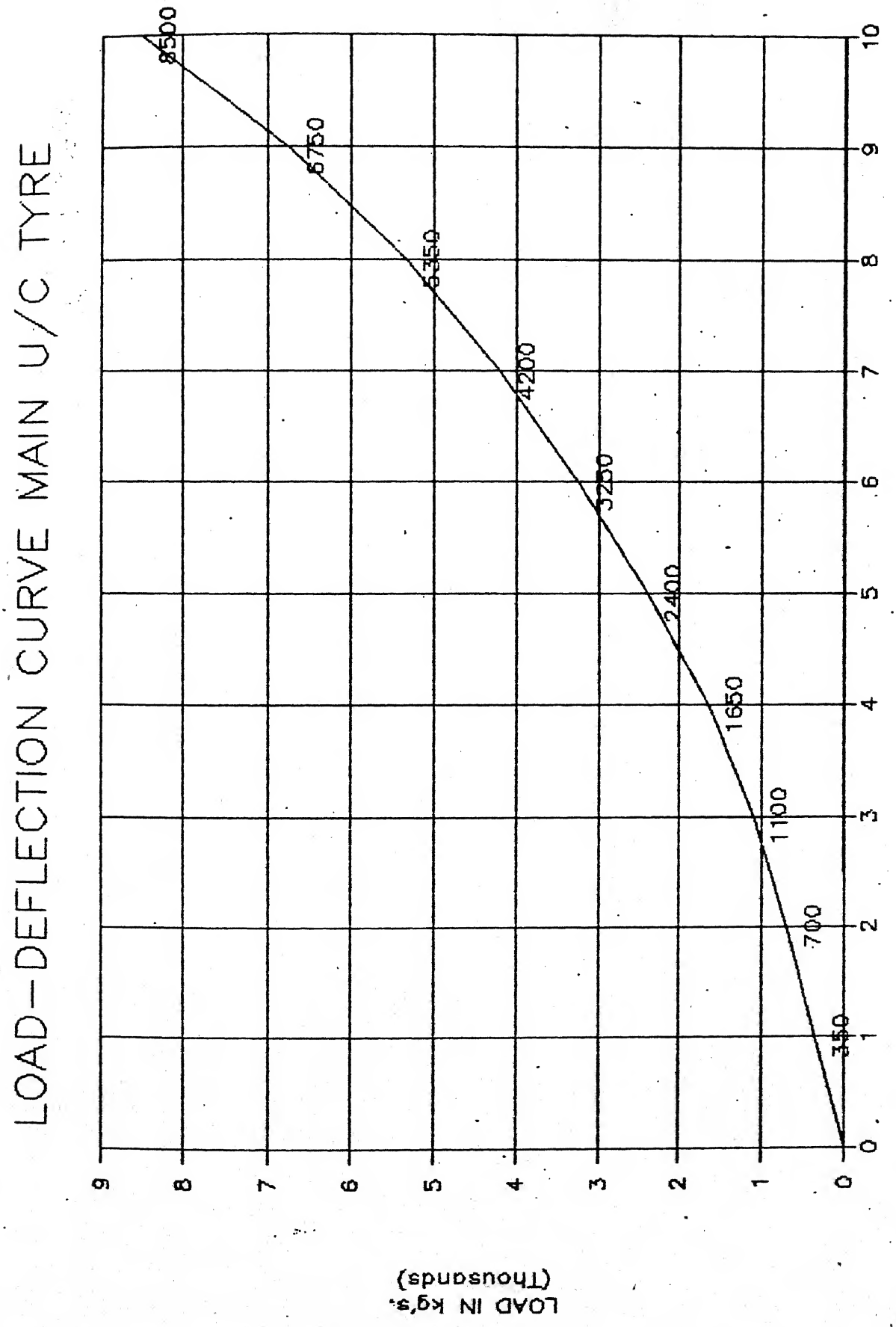
LOAD–DEFLECTION CURVE MAIN U/C TYRE
8500
6750
5350
4200
3250
2400
1650
1100
700
350
0
1
2
3
4
5
6
7
8
9
10
DEFLECTION IN cm.
LOAD IN kg's
(Thousands)